Proceedings of the 111th Annual Meeting of The American Association of Variable Star Observers

December 2022

ISBN 978-1-939538-64-2

The American Association of Variable Star Observers
185 Alewife Brook Parkway, Suite 410, Cambridge, MA 02138, USA

Proceedings of the AAVSO 111th Annual Meeting

Editor

Joyce A. Guzik

Los Alamos National Laboratory

Los Alamos, NM 87545, USA

The American Association of Variable Star Observers
185 Alewife Brook Parkway, Suite 410, Cambridge, MA 02138, USA

Proceedings of the AAVSO 111th Annual Meeting

Editor's Note

This collection of articles was submitted as optional conference proceedings papers by participants of the 111th Annual AAVSO meeting held November 4-7, 2022, at the Omni Tucson National Resort in Tucson, Arizona.

Fifteen articles were received, representing both contributed oral and poster presentations. These articles have remarkable variety of content and are not necessarily the type of articles that would be found in standard astrophysical research journals.

These articles have been edited/curated, but not peer-reviewed. Extended abstracts were reviewed by a committee with members Joyce Guzik (chair), Tom Maccarone, Sebastián Otero, and Elizabeth Waagen before being accepted for presentation at the meeting.

The full meeting schedule with links to abstracts can be found at https://www.aavso.org/111#schedule. The online posters can be found at https://www.aavso.org/111-poster-hall.

AAVSO 111th Annual Meeting Group Photo. Credit: Robert Stephens

The American Association of Variable Star Observers
185 Alewife Brook Parkway, Suite 410, Cambridge, MA 02138, USA

Proceedings of the AAVSO 111th Annual Meeting

Table of Contents

The American Association of Variable Star Observers
185 Alewife Brook Parkway, Suite 410, Cambridge, MA 02138, USA

Work by AAVSO Ambassadors: The Outreach

Teja Begari

The American Association of Variable Star Observers; begariteja@gmail.com

Subject Keywords

AAVSO; Ambassadors; Volunteers; Educating; Promoting

Abstract

The American Association of Variable Star Observers, a truly international organization, has a very diverse community. There are observers, educators, researchers, and a dedicated team of volunteer ambassadors. The AAVSO ambassadors have been doing many outreach activities that help students and the general public understand Variable Star Astronomy and the resources available at the AAVSO to be a part of real science.

1. The Vision of the Ambassador Program

The ambassadors have created a united vision for themselves, which is to be involved, love what they do, and showcase the AAVSO. To be involved is one of the most important factors of the AAVSO ambassador program, to participate in the AAVSO's activities in different ways. AAVSO ambassadors, being astronomy enthusiasts, have always been loving what they do, i.e., popularizing astronomy and showcasing the AAVSO, the resources available at the AAVSO, and the rich history of the esteemed organisation.

2. Our Goal

The goal of the AAVSO ambassadors is to get diverse people interested and capable of beginning variable star astronomy with AAVSO. This helps AAVSO as an organisation as a whole to achieve its mission to "enable anyone, anywhere to participate in scientific discovery through variable star astronomy"

3. Primary Mission: Outreach and Education

Our mission is primarily outreach and education by conducting astronomy outreach to schools, clubs, and communities, creating astronomy education videos for online distribution, presenting on variable stars, and representing the AAVSO at conferences. We also conduct outreach by maintaining an Astro-blog or other online presence and/or engaging with AAVSO's social media content.

3.1 Remote outreach

Remote outreach of course not as effective and hands-on as in-person is, but the best part of remote outreach, in the form of online webinars, is that an individual can get connected to people from different parts of the planet. A few ways the AAVSO ambassadors are utilising the online way of education is by giving talks at international conferences and Universities, submitting abstracts to global meetings, and also speaking at online radio shows.

Figure 1. Left: AAVSO Ambassador Teja Begari at an online talk show along with the former AAVSO director, Dr. Stella Kafka. Right: Teja presenting at the 25th annual conference of Global Hands-on Universe.

3.2 In-Person outreach

In-person outreach is definitely hands-on and does attract people of different age groups while showing what Amateur Astronomers are doing and ways their observations help professional astronomers to continue their research. The use of AAVSO resources is shown by demonstrating the actual way variable star observers do their estimations worldwide.

Figure 2. AAVSO ambassador Teja Begari doing in-person activities such as showing variable star observation methods and explaining different types of variable stars.

Figure 3. AAVSO Ambassador Teja Begari talking at the Indian Central government-initiated All India Radio about Variable Stars and AAVSO.

4. Writing for Magazines

Magazines are one of the amazing ways of promoting astronomy, and AAVSO ambassadors have been writing about different topics and have been successful in publishing them in well-known magazines.

5. Regional Talks

AAVSO ambassadors believe that giving talks in regional languages really helps those people who are studying in their regional language and with no proper English knowledge and are really interested in doing real science. Linguistic problems should never be a barrier and, as AAVSO ambassadors from different parts of the world, each one of them is trying to do outreach even in the regional language.

Figure 4. AAVSO ambassador Teja Begari participating in a regional language talk/radio show.

6. Celestial Events

Getting people together during celestial events is definitely a fun-filled experience and the best part is all is to learn while enjoying the drama in the sky such as eclipses, meteor showers, planetary conjunctions, etc..

7. Conclusion

Astronomy is for all and the AAVSO ambassadors are doing it to their fullest by contributing to science, society, and a non-profit research-based organisation in many different ways, sharing and gaining knowledge and making sure AAVSO achieves its mission.

No Longer Eclipsing —The Strange Case of RS Crateris

Stephen P. Cook

Project Worldview, 910 Oak Terrace Dr., Prescott, AZ 86301 USA; scook@projectworldview.org

Subject Keywords

AAVSO International Database; Eclipsing Binaries; Photometry, CCD; Period Analysis; Data Mining; Constant / Non-Variable Stars; RS Crt

Abstract

Long classified as a (solar) G0 type Algol eclipsing binary, recently AAVSO VSX administrator Sebastián Otero listed RS Crt as constant at V magnitude 10.62. My 2020 differential photometry covering 13 nights in May and June supports this reclassification, showing RS Crt to be constant (with 0.042 V mag. scatter). Probing when its light variation ceased, I analyze data (including my own) from several observers obtained between 1972 and 1995 and find no evidence of periodic variation. Citing the poor quality of the 1930-1944 data upon which its previous classification was based, one could argue RS Crt never was an eclipsing binary. Using data from the digitized Harvard Plate Collection (DASCH), I refute that contention to some extent.

Initially seeing two 0.6 to 0.7 magnitude deep new minima and "noise" associated with constant brightness in a light curve spanning years from 1900 to 1990, after finer probing I rejected one of those minima. But then I found what appear to be seven new shallow minima with 0.2 to 0.3 magnitude dimming—the first in 1929. The best deep minima were used to derive a period of 0.8272 days, which represents all the data significantly better than the older period of 0.8168 days did. After speculating RS Crt's eclipses stopped (between 1950 and 1970?) as system orbital inclination changed, behavior well-documented for V907 Sco and HS Hya, I briefly consider alternate explanations and cite a need for high-resolution spectra to either confirm its binary status or reject it. I also encourage exploring pulsating star explanations for its long-ago periodic light variation.

1. Introduction: Problem Statement and RS Crt Observational History

The problem we'll consider can be stated as a question: "Is it more likely that RS Crt never was an eclipsing binary, or should it be included in the list of stars known to have quit eclipsing?" If eclipsing, has RS Crt ceased exhibiting periodic light variation of some other nature?

Saying RS Crt has quit eclipsing puts it in a special category. Ten years ago, one could assert "About 15,000 eclipsing binaries have been discovered" (Guinan 2012); today the number is many times larger. Only six had been convincingly established to have stopped eclipsing: QX Cas, SV Cen, SV Gem, SS Lac, AY Mus, and V907 Sco. Recently. HS Hya has been added to that list. For V907 Sco, Lacy et al. (1999) report: "The earliest observations of the system in the year 1899

show eclipses; the eclipses stopped around 1918, started again around 1963, and stopped again in about 1986. We predict that the eclipses should start occurring again in the year 2030 ± 5." For HS Hya, Davenport et al. (2021) report "With a total baseline of over 125 yr, this unique combination of data sets—from photographic plates to precision space-based photometry—allows us to trace the emergence and decay of eclipses from HS Hydrae…Recent TESS observations…confirm that eclipses have ceased …we estimate they will begin again in 2195."

V907 Sco once exhibited eclipses of amplitude 0.6 V magnitude or so with a period of 3.7753 days; HS Hya had eclipses of amplitude 0.5 V magnitude or so with a period of 1.5680 days. Perhaps, similarly, one might conclude that RS Crt once exhibited eclipses of amplitude 0.7 magnitude with a period of 0.8168 days. Similar data mining could probe what happened.

RS Crt was discovered in 1930 and was initially observed by European and Soviet observers. On 36 photographic plates taken between March 1929 and April 1934, RS Crt stayed more-or-less constant at photographic magnitude 10.8, with typical plus or minus 0.2 magnitude uncertainty. But on one plate taken on April 23, 1930, it had seemingly dimmed to magnitude 11.5. To my knowledge, that single report of a 0.7 magnitude drop would be linked with RS Crt's eclipse amplitude for the next nine decades. For the record, based on what was also reported with that first time of minimum (Sandig, 1948), had skeptics prevailed from the start, this dimming might have been dismissed as being recorded on an old and worn plate.

Lange (1935) reported an amplitude of 0.4 magnitude and two times of minima. From 51 visual estimates made in 1944, Tsesevich (1947) determined three times of minima and reported amplitude of 0.5 magnitude. This was noted in the University of Pennsylvania (later University of Florida) Eclipsing Binary (EB) Card Catalogue and subsequent editions of "A Finding List for Observers of Interacting Binary Stars" (Wood et al., 1980). There, along with noting Tsesevich provided a light curve and Algol-type classification, RS Crt was said to vary from visual magnitude 10.0 to 10.5 with period of 0.8168 days, and to have six-hour long eclipses. In a later publication, Tsesevich (1954) provided two additional times of minima, also based on 1944 visual observations. Table 1 lists these times of minima for RS Crt.

Where did the period of 0.8168 days come from? Most likely a provisional value was derived from times of minima. Combined with an initial epoch, the period goes into an equation for computing times of minima for future eclipses:

JD TOM = 2431211.39 + 0.8168 N, where N=number of eclipse cycle Equation (1)

The period can be refined using such an equation to compute time of eclipse and O-C, the observed time of minimum minus the computed time. The last column in Table 1 provides these. They can be plotted vs. number N of eclipse cycle as in Figure 1, along with the line defined by Equation (1). The distance above or below the line provides a measure of how good the period is. Note: the plot also includes a point for the mathematically determined initial epoch.

Table 1. Times of Minima for RS Crt used to determine Equation (1)

Source	Type	TOM, JD	method	N	O-C, days
Sandig 1948	II	2426090.336	pg	-6269.5	-0.1264
Lange 1935	I	2427842.25	vis	-4125	0.16
Lange 1935	I	2427890.23	vis	-4066	-0.0512
Tsesevich 1954	I	2431211.35	vis	0	-0.04
Tsesevich 1954	I	2431212.27	vis	1	0.0632
Tsesevich 1954	I	2431252.2	vis	50	-0.03
Tsesevich 1954	I	2431256.25	vis	55	-0.064
Tsesevich 1954	I	2431266.19	vis	67	0.0744

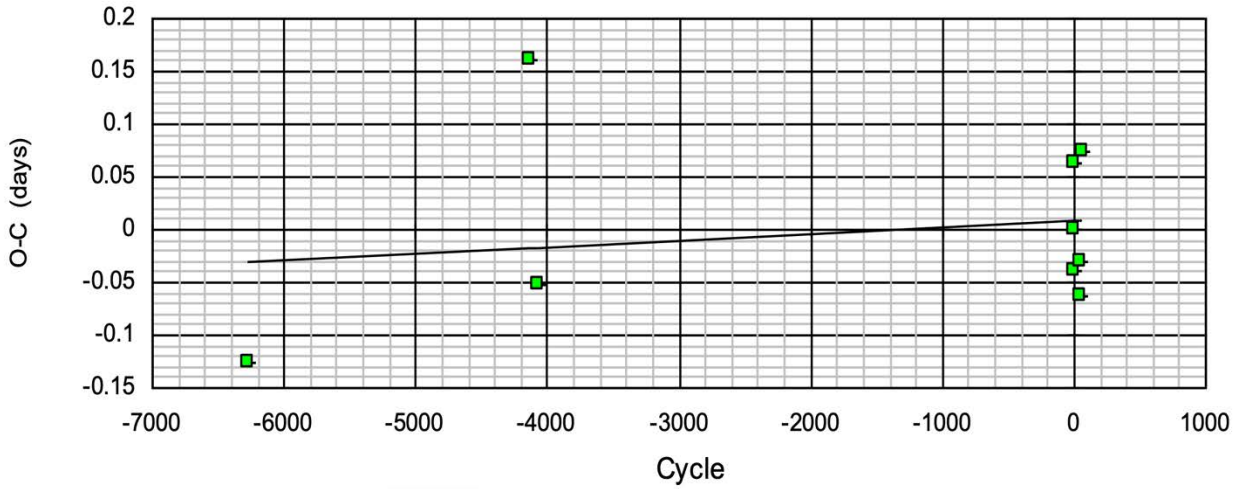

Figure 1. Observed – Computed (O-C) diagram for RS Crt (from Nelson, 2016)

It should be mentioned that the first minimum listed in Table 1 only fits nicely into the Figure 1 plot if it is assumed to have a ½ whole number N (= minus 6269.5) commonly associated with a secondary minimum—even though its associated amplitude (0.7 magnitude drop) is the greatest of the eight. Accepting this implies RS Crt exhibited noticeable brightness changes not every 0.8168 days, or about every twenty hours, but every ten hours. That, combined with the roughly six-hour eclipse duration, apparently from Tsesevich's light curve, implies that much of the time RS Crt will not be at maximum brightness. It is very difficult to reconcile these implications with Sandig's report that RS Crt was constant on 36 of 37 plates in the 1929 to 1934 era!

I suspect Tsesevich, more than anyone else, was responsible for the characterization of RS Crt in catalogs, like the third edition of the General Catalog of Variable Stars (GCVS) published in 1968, that lasted so long. V.P. Tsesevich was born in 1907 and died in 1983. According to the man in charge of the most recent editions of the GCVS, Nicolas Samus, Tsesevich was "a famous man" in the top tier of renown amongst Russian variable star observers (Samus, 2007). In 1971 Tsesevich published what proved to be a great resource for observers: "An Atlas of Finding Charts of Variable Stars." That same year, as an undergraduate astronomy major at UCLA, I first learned about RS Crt from a list of eclipsing stars Daniel Popper gave me.

Popper, another highly respected astronomer, first instilled in me the importance of eclipsing binaries, given their key role in enabling us to get basic information about stars, most notably their mass and diameter. When he later learned that I had found from visual observations over 100 times of minimum for such objects, he solicited my help in getting him that information for stars he was working on. RS Crt was on that list of solar-type eclipsing binary stars. He hoped to get high-resolution spectra of them to use in establishing their fundamental properties.

Popper used the 1968 edition of the GCVS for information on the stars in his list, but the information it contained on RS Crt had problems. Consider three areas: Photometrically, it depicted RS Crt as an eclipsing binary. Astrometrically, the position it provided was believed accurate to better than 1 second in RA, and 0.1 arc minute in DEC. Spectroscopically, RS Crt was assigned spectral class G0. I now believe the information about RS Crt in all three of these areas was wrong to some extent. Photometrically, it contained three erroneous conclusions: 1) RS Crt is an Algol type eclipsing binary; 2) its primary amplitude is 0.7 magnitude; and 3) its eclipses last six hours.

Early on, RS Crt's reported six-hour eclipse duration, representing 30% of its 20-hour (=0.8168 day) period, should have raised suspicions as being too long for an Algol-type eclipser. Algol itself has eclipse duration that is 14% of its period. Back then, V Crt, another eclipsing star with short (0.7020 day) period and 0.6 magnitude amplitude, was similarly listed as having five-hour eclipses. (Decades later V Crt's eclipse duration was revised to three hours.) While I was very slow in getting around to observing RS Crt, Popper got UCLA grad student Phil Dumont to do that. Problems in using Equation (1) to predict times of its eclipses soon became evident.

Dumont was looking for eclipses of RS Crt as part of a "U, B, V photometric program on eclipsing binaries at Palomar and Kitt Peak observatories" during 1972-1973 (Popper and Dumont, 1977). With observations spanning three nights, he failed to see any eclipse and reported the star to be at 10.67 V magnitude (with 0.01 error) and having B-V = +0.54. In March 1976 Swiss visual observer Kurt Locher (BBSAG, 1976) reported "The results of my survey at all phases during the past 13 months show [constant magnitude and] …estimated brightnesses scatter (RMS) less than [0.1 magnitude]." Locher used two comparison stars differing by 0.8 magnitudes in brightness, the brighter one most likely being GSC 005520-00393.

Over a decade later, then AAVSO Eclipsing Binary Committee Chair Marvin Baldwin likewise made visual observations of RS Crt. Unfortunately, no record exists of comparison stars he used. After devising his own step sequence, Baldwin made 151 observations on thirty-six nights between March 1987 and May 1988, with variation ranging from the brightest at 27 on his scale to the faintest at 46. His data can be found in the AAVSO International Database (AID, AAVSO, 2022.) Baldwin tells me 0.03 magnitude might be a good estimate for the value of each of his steps. Despite large scatter, discussed in section 2.2, no evidence for eclipses was found.

The 1990s brought spectroscopic data that challenged RS Crt's previous classification, based on low-resolution objective prism spectra, as a solar-type, spectral class G0 star. After getting three high-resolution spectra of it at Lick Observatory, Popper (1996) both reclassified it, based on

sodium D lines, as a late F (F5-F8) star and, based on its narrow lines, ruled out its published short period. His three spectra showed no variation in radial velocity. The current accepted value (Gaia Collaboration DR2, 2018) is –3.66 km/sec ± 0.40.

In the astrometric realm, in 2004, Dvorak (2004) pointed out that the position of RS Crt listed in the 1968 GCVS as RA: $11^h49^m06^s$, DEC –10°37'12" was slightly off: more accurately it is RA: $11^h49^m03.13^s$, DEC –10°37'14.9" for the 2000 epoch. Note, GCVS editors admit (Kholopov, 1985) RA "error may reach + or – 3 sec." Finally, in 2020, based on data from the European Space Agency's Gaia space observatory gathered in the 2014-2017 era, a highly accurate parallax for RS Crt of 5.8463 milliarcsec ± 0.0268 was published (Gaia Collaboration DR3, 2020) along with proper motion data: -25.429 milliarcsec / yr in RA, and 0.428 milliarcsec / yr in DEC. Its parallax tells us RS Crt is 171 parsecs distant.

Despite all of these observations—astrometric, photometric, spectral and radial velocity data—there is insufficient data to say with 100% certainty that RS Crt not a member of a binary star system.

2. My Work on RS Crt: Methods and Results

2.1 Photometry

My first observations of RS Crt came on two nights in 1995 using an ST6 CCD imager attached to a small (50 mm diameter) wide-angle lens. Fifteen data points, put together from 42 images obtained on two nights in April 1995, showed roughly constant V magnitude of 10.65 with no variation beyond 0.082 magnitude (standard deviation-based) scatter. The comparison "star" used was actually an average of stars A and B in Table 2 (see the AID for these observations). Although I failed to see the eclipse predicted by Equation (1), given poor signal /noise ratio for this nearly 11th magnitude object, I decided I needed a more capable system to better tackle it in the future.

Table 2. Comparison stars used for Cook's differential CCD photometry of RS Crt

Star	GSC #	RA (2000) h m s	DEC (2000) ° ' "	V mag Tycho2	V mag APASS DR3	B - V
A	5520-0303	11 47 19	-10 45 57	10.075	9.998	+0.655
B	5520-0628	11 48 32.40	-10 43 06	10.383	10.361	+0.41
C	5520-0393	11 48 42.30	-10 32 39	10.818	10.589	+1.11

By 2015 I was using a better system, though hardly state of the art! With the ST6 CCD now attached to a 130 mm f/5 reflector, photons are still under-sampled, although not as badly. Given this issue, and with less than perfect tracking, experience suggests that flat fielding does not noticeably improve differential photometry results, in which variable star magnitudes are obtained by subtracting instrumental variable (VAR) and comparison (COMP) magnitudes and then adding the result to an assumed catalog-based comparison-star magnitude. To compensate

for not taking flats, I typically average many images to produce individual (normal) data points, reduced with SBIG CCDOPS software and custom spreadsheet, which also computes associated uncertainties.

The product of my 2020 photometry of RS Crt, based on 13 nights of observing between May 8 and June 15, 2020, was 198 data points distilled from 720 V filter images, each with typical 15-second exposures. This time the comparison "star" used was an average of stars B and C in Table 2 (again see the AID for these observations). This differential, comparison-star magnitude-dependent photometry showed RS Crt to be constant at 10.582 V magnitude with 0.042 V magnitude scatter. Note this magnitude is somewhat brighter than my 1995 value. While averaging my 1995 and 2020 V magnitudes for RS Crt gives a value of 10.62 V magnitude, the differences between them are no doubt due to different comparison stars used. For comparison, the (absolute photometry) APASS DR3-listed value for RS Crt is 10.622 V magnitude with mean error 0.0482 V mag; its Tycho Catalogue-listed value is 10.625 V magnitude with mean error 0.060 V mag.

2.2 Searching RS Crt 1987-1988 visual data and 2020 CCD data for periodicity

While Baldwin's 1987-1988 151 visual data points and my spring 2020 198 CCD data points show no sign of eclipses based on elements in Equation (1), do they show any signs of periodicity? If so, for what period value? I analyzed both data sets using a discrete Fourier transform (DFT) based method (Belserene, 1988) to search for periodicity in time-series photometric observations. I probed for signals associated with a wide range of possible periods from 0.1 to 10 days, with 0.01 day (or better) resolution.

To facilitate this periodicity search using Baldwin's data, I first converted his step values to magnitudes assuming one step = 0.03 mag. The resulting standard-deviation based scatter is large, 0.154 magnitude. One explanation for this scatter is that, after RS Crt's eclipses had stopped, they started again. Another explanation involves possible use of an inappropriate comparison star. It turns out that RR Lyr star X Crt, with magnitude range 11.1 to 11.75 V magnitudes and period 0.7328 days, is in the same one-half degree square field as RS Crt. There is no evidence Baldwin used X Crt as a comparison star, but it certainly represents a possible pitfall all observers of RS Crt must avoid.

DFT analysis of Baldwin's data provided no evidence in support of the published period of 0.8168 days. The analysis showed greatest relative strength (at 20.0) for a period of 7.395 days. The DFT analysis of my data offered no support for that 7.395-day period, and likewise provided no evidence for the published period of 0.8168 days. The analysis of my data showed greatest relative strength (at 12.1) for a period of 3.16 days, a value the DFT analysis of Baldwin data also roughly flagged. In the analysis of the Balwin data, a similar period of 3.14 days showed relative strength of 10.9. Note: relative strengths in the 4 to 6 range were recorded for many possible periods in each data set.

2.3 Data mining supposedly finds two additional times of minima for RS Crt

My expectations were very low when I began searching the digitized Harvard Plate Collection (DASCH project) for images of RS Crt at minimum light. I was skeptical that roughly 0.5 magnitude eclipses would stand out against the expected at least 0.2 magnitude (peak to peak) or so noise associated with photographic magnitude, with uncertainty of at least plus or minus 0.1. My expectations got even lower when I realized that sometimes two-hour exposures were needed for these photographic glass plates to attain a limiting magnitude of around 12.5 that offered some chance of recording RS Crt at its 11.5 magnitude minimum. It seemed such exposures would have to be perfectly centered on time of minimum to record something more than a very small dip in its brightness.

I was thus pleased when, after filtering out flagged (indicating potential problematic) data points, two definite minima stood out in the light curve of RS Crt produced by DASCH software (Figure 2) spanning years 1900 to 1990, with a gap between 1955 and 1975 when no plates were taken. Even then I doubted those two data points represented anything significant. Imagine my delight when it seemed they represented times of minima in 1938 and 1944 (Table 3) consistent with the eclipse elements of Equation (1), as plotting them in the O-C diagram (Figure 3) showed. While the point for plate ai38813 plotted a bit far below the best fit, initially it seemed acceptable.

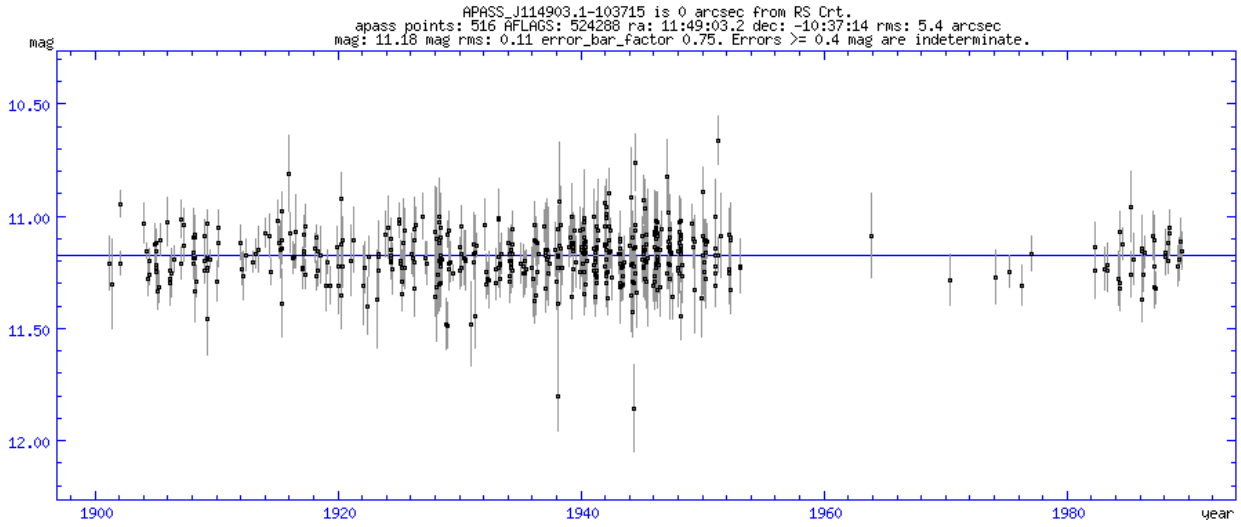

Figure 2. Light curve of RS Crt extracted from Harvard Plate Collection (DASCH project)

Table 3. Data for two times of minima of RS Crt from Harvard Plate Collection (DASCH)

Harvard plate #	Heliocentric time = O	Mag of RS Crt	Limiting Magnitude	Cycle, N Equation (1)	Computed Time for eclipse=C	O – C, days
ai33793	2428926.77019	11.80	12.37	-2797	28926.8004	-0.0302
ai38813	2431200.67009	11.86	12.66	-13	31200.7716	-0.1015

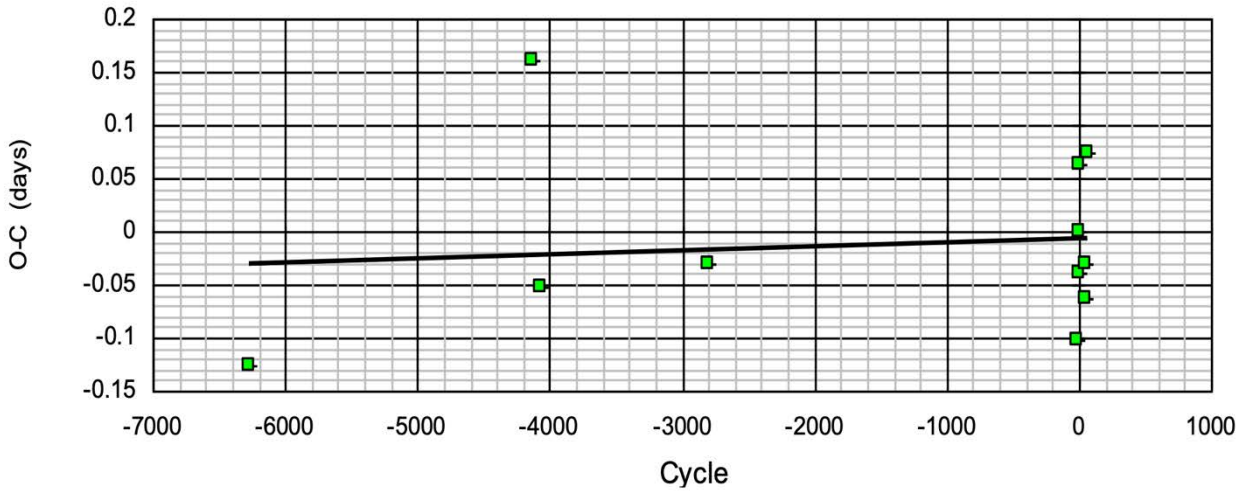

Figure 3. The O-C Diagram of Figure 1 with the two additional minima from Table 3 added

2.4 Questioning those DASCH-derived two additional times of minima for RS Crt

Alas, I now believe that the minimum from plate ai38813 more likely is due to a plate defect rather than RS Crt truly being at minimum brightness. Consultation with LSU professor Brad Schafer, a top expert in using the Harvard Plate Collection in both original glass plate and its digitized (DASCH) form, prompted that conclusion. It opened my eyes to many things: plate defects; weird star image shapes; points resulting simply from outliers associated with noise (some are to be expected in three-sigma level statistical terms); that low probability coincidences can occur; and misplaced faith in DASCH's ability to flag all the data points that it needs to.

Specifically, close examination of the image of RS Crt on plate ai38813 shows a bright, jagged elongated blob and not a fainter, nicely circular stellar image. To his experienced eye, Schafer feels RS Crt doesn't look faint on plate ai33793, despite the magnitude DASCH provides. I do have experience with stars on CCD images looking brighter than they are measured, so I trusted the measurement and kept this point. Note: in Figure 3 this point plotted much closer to the best-fit line than the point for plate ai33813 did.

3. Hypothesis testing: Was RS Crt Once an Eclipsing Binary Star System?

3.1 The O-C diagram in Figure 3 does not inspire confidence. Can we improve on it?

The regression lines in the O-C diagrams shown in Figures 1 and 3 for the period historically connected with RS Crt, 0.8168 days, don't fit the data well. Indeed, their Pearson R^2 correlation coefficients of 0.03 and 0.01 respectively are laughably low. The point for the first time of minima (TOM) in Table 1 contributes to this problem—it lies considerably below the best-fit line. This point also corresponds to a supposed secondary minimum, the only one plotted, observed in 1930. Can we construct an O-C diagram with a better fitting regression line without assuming any of the TOM used are for secondary minima?

We can do this by using a slightly longer period of P=0.8272 days and doing the following: using the first three of the Table 1 minima, replace the last five in that table with the time of minimum that served as the initial epoch in Equation (1), and the best one from Table 3 from the ai33793 plate, omitting the questionable one on the ai38813 plate. The regression line we draw (see Figure 4) fits the data much better: it has R^2 correlation coefficient of 0.58. The equation associated with new period and initial epoch (from time of ai33793 plate) is:

JD TOM = 2428926.77 + 0.8272 N, where=N is number of eclipse cycle Equation (2)

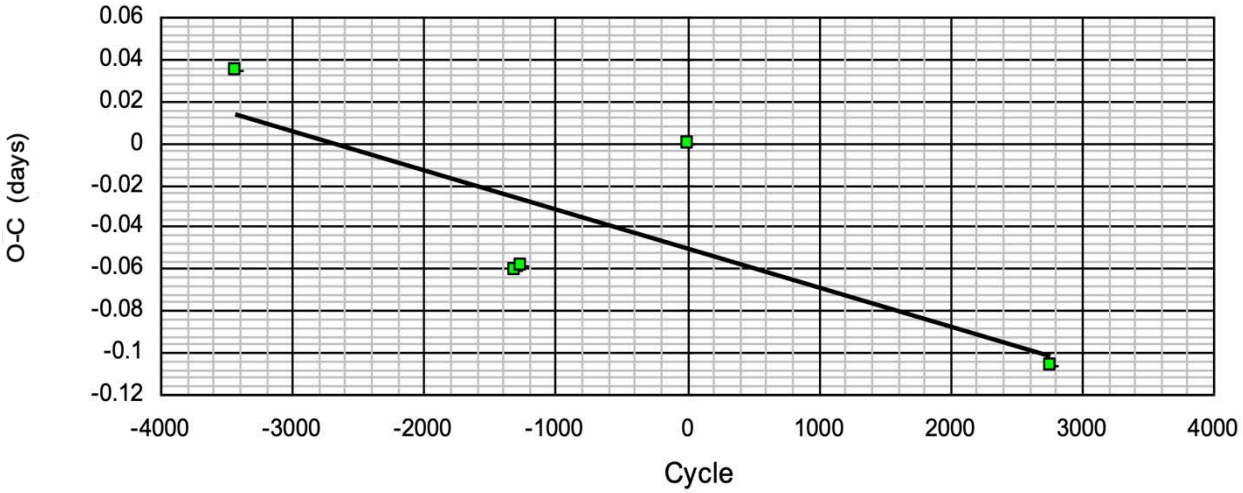

Figure 4. The O-C Diagram for the five "best minima" and period of 0.8272 days

3.2 If RS Crt was once eclipsing, shouldn't the RS Crt historical light curve look like it was?

The Figure 2 light curve for RS Crt can be compared with similar DASCH-derived light curves for two other nearby objects: 1) V Crt, an eclipsing binary with similar period and amplitude as RS Crt may have once had, and 2) the supposedly constant comparison star B (GSC5520-0628) from Table 2. While showing a bit more variation than this comparison star, the RS Crt light curve seemingly looks more like that of comparison star B than it resembles V Crt's light curve.

If RS Crt was once eclipsing, this is not what we expect to see, but can it nonetheless be explained without shelving that hypothesis? I believe so, for two reasons. First, V Crt, at DASCH-reported average magnitude 10.72, is brighter than RS Crt, with its similarly reported 11.18 average magnitude. Thus, it's more likely that more minima of RS Crt were flagged by DASCH, something DASCH does if the measured magnitude is not at least 0.5 magnitude brighter than the limiting plate magnitude. Second, and more importantly, I believe RS Crt's eclipses were shallower than V Crt's. What if RS Crt eclipses were typically just 0.4 magnitude or less in amplitude, as reported for the pair observed in 1934? I suspect, in looking at its light curve, many such eclipses would be lost in "noise," whereas the deeper 0.6-magnitude eclipses of V Crt would rise up out of it.

I did not think the above argument was strong until I started finding such shallow minima for RS Crt. Using Figure 2 and DASCH, I identified seven TOM for RS Crt between 1929 and 1948

corresponding to not-so-deep drops in its brightness. Whereas the five minima used in constructing the Figure 4 O-C diagram are believed to correspond to 0.4 to 0.7 magnitude brightness drops, these seven additional TOM, shown in Table 4, correspond to magnitudes 0.20 to 0.31 fainter than the 11.18 average magnitude DASCH gives for RS Crt in Figure 2.

Table 4. Additional Times of Minima for RS Crt from DASCH data

Minimum #	Harvard plate #	Time of Minimum (TOM) Heliocentric time	Magnitude of RS Crt	Limiting magnitude of plate
1	rh00931	25633.8588	11.49	12.82
2	ac28893	26341.9434	11.48	12.25
3	ac29159	26443.645	11.44	11.98
4	am17421	28245.4711	11.38	14.2
5	ai33850	28956.8107	11.39	13.82
6	bio1188	31170.5525	11.43	12.37
7	ai41592	32648.612	11.44	13.02

The data in Table 4 can be used to test how good equations like Equation (1), with period 0.8168 days, and Equation (2), with period 0.8272 days, are at predicting times of minima. The second column from the left in Table 5 identifies what is being predicted. The other columns identify the basis for the predicted (or computed) TOM and an O-C value gauges how good the prediction is. Observed (or O) TOM values in Table 4 are used in getting O-C. Note the "Eq 1 Init Epoch" refers to what is used as a representative average of the last 5 minima in Table 1 given the large scatter in the individual values.

Table 5. Predicted Times of Minima for RS Crt using either period 0.8272 days or 0.8168 days

#	TOM being predicted	TOM used Initial epoch	Time elapsed from initial epoch, days	Period / from which equation?	N, cycles	O-C, days
1	#2 in Table 4	#1 in Table 4	708.0846	0.8272 /eqn 2	856	0.0014
2	#2 in Table 4	#1 in Table 4	708.0846	0.8168 /eqn 1	867	-0.081
3	#3 in Table 4	#1 in Table 4	809.7862	0.8272 /eqn 2	979	-0.0426
4	#3 in Table 4	#1 in Table 4	809.7862	0.8168 /eqn 1	991	0.3374
5	#3 in Table 4	#2 in Table 4	101.7016	0.8272 /eqn 2	123	-0.044
6	#3 in Table 4	#2 in Table 4	101.7016	0.8168 /eqn 1	125	-0.3984
7	#5 in Table 4	#4 in Table 4	711.3396	0.8272 /eqn 2	860	-0.0524
8	#5 in Table 4	#4 in Table 4	711.3396	0.8168 /eqn 1	871	-0.0932
9	#7 in Table #4	Eq 1 Init epoch	1437.22	0.8272 /eqn 2	1737.5	-0.018
10	Eq 1 Init epoch	#6 in Table 4	40.8375	0.8168 /eqn 1	50	-0.0025

3.3 Weighing evidence for and against RS Crt once being an eclipsing star

Without carefully studying the predictions in Table 5, one might conclude "RS Crt never was an eclipsing variable" based on comparison of its Figure 2 light curve with those of V Crt and the supposedly constant nearby comparison star. One might also draw the same conclusion based on spectroscopic evidence. Namely, RS Crt has not been observed to have a spectrum with double lines that Doppler shift with orbital motion, either because, if double, the bright star hides the fainter star's spectral lines, or because it is not binary. Also, Popper's three high-resolution spectra indicated a constant radial velocity, seemingly not what you'd expect for an eclipsing binary. Unfortunately, the dates/ times of those spectra were not reported, but unless they were taken at an unlikely sequence of orbital phases, they argue RS Crt is not part of a binary system and is not an eclipsing variable.

But studying Table 5 suggests a different conclusion. Table 5 contrasts predictions, made with a new improved model, with those of the older one. Namely, you see that the new model does a much better job at representing the TOM data using the period of 0.8272 days in Equation (2) than the older Equation (1) based model does. Its first prediction is astoundingly good. The first row in Table 5 documents using (as initial epoch) the supposed eclipse observed O time of minimum associated with the first Harvard plate of Table 4 taken in 1929 and computes the time C an eclipse minimum 856 cycles later will occur. That O-C tells us that our longer-period Equation (2) based model's prediction is a mere 0.0014 days = 2 minutes off in predicting an event occurring two years (actually 708 days = 1.94 years) later!

Other predictions based on that model, #3, #5, and #7 in Table 5, are respectably accurate to within 60 to 75 minutes. Compare those made with the earlier (shorter-period) Equation (1) — #2, #4, #6, and #8 in Table 5, which have much bigger O-C prediction errors, ranging from nearly two hours to nine and a half hours. Note that the longest time-elapsed intervals in this table are typically 800 days (prediction #9 excepted). With periods used in both models given to only four significant figures, uncertainties are magnified with multiplication by larger and larger numbers of cycles, and uncertainties eventually grow so large that the prediction becomes meaningless. For example, after one cycle of 0.8168 day, the uncertainty is 0.0001 days; after 1000 cycles (multiplying by 1000) we have 0.8168 x 1000 = 816.8 days with uncertainty of 0.1 day (=2.4 hours) to the initial epoch.

4. Data that Challenge our Periodic Light Variation Models: Additional Considerations

The last five minima listed in Table 1 present problems, beginning with the strange 0.92-day interval between the N=0 and N=1 consecutive eclipses. Before attributing this to observational error, I tried to account for it by assuming a period double that of 0.8272 days = 1.6544 days and postulating an observable secondary eclipse that was offset from 0.5 phase. That attempt didn't work—one of the assumed secondary minima refused to fit.

In trying to make sense of these data and to reconcile them with the earlier minima and with that best minimum in Table 3, I noted the 0.8272-day period worked better in representing the early

minima (1930 to 1938), whereas the 0.8168 day one worked better for the 1944 minima. Prediction #10 in Table #5 illustrates this. The shorter-period Equation (1) based model makes a prediction (for 1944 data) for 50 cycles, or roughly 41 days later, accurate to 0.0025 days or 3.5 minutes. Our longer-period model worked nicely in making predictions #1, #3, #5, and #7 using 1929-1934 data, whereas by 1944 the shorter-period model works better.

Could the period really have shortened during this time? For eclipsing binary stars, this period change of 0.0104 days = 15 minutes would be totally unprecedented and unbelievably large. Typical period changes for such stars are measured in single-digit seconds. But speculation, based on the previously cited astrometric discrepancy in reported positions, that RS Crt was jolted by a collision with some fast-moving object might conceivably explain that period change.

Prediction #9 presents another problem. Our best effort to fit the observed TOM is achieved by using the longer-period Equation (2) based model, but it only works by invoking that the distant minimum observed almost four years later must be a secondary minimum, given the 1737.5 cycles elapsed since the initial epoch. This contradicts our postulating RS Crt has no observable secondary minimum. But prediction #9 consequences probably should not diminish confidence in our eclipsing-star-based longer-period Equation (2) model. That's because, with only four significant figures in its period, we're using it where we shouldn't in a too long elapsed time situation.

Back to our rejection of RS Crt as an eclipsing binary whose period changed very significantly in a short time, as a way to reconcile the longer-period model generally working well, except with 1944 observations where we needed the shorter-period model. How do we resolve this problem?

Beyond the far-fetched stellar collision speculation, there are two ways out of that problem. The first sticks with RS Crt as eclipsing binary and declares the 1944 TOM data as individually flawed. Indeed, subsequent analysis can be rescued from the internal inconsistency and large scatter these data present by not considering the last five minima in Table 1 individually as five points in an O-C diagram, but rather averaging them to make one good point. Thus Figure 4 includes a minimum at the time of initial epoch in Equation (1). The second way out respects the 1944 TOM data, and abandons eclipsing-binary-based models, as described in the last section.

5. Alternate Explanation: RS Crt Periodic Light Variation as Pulsating and Not Eclipsing

Conceivably one might be uncomfortable explaining RS Crt's behavior in terms of eclipses, but nonetheless feel its past photometric history shows signs of periodic light variation. If future high-resolution spectra firmly establish RS Crt is not binary, then single-star explanations including pulsating star, rotational variable, etc. will be required.

5.1 A simple pulsating-star model of RS Crt

Our Equation (1) and Equation (2) based models, instead of being associated with two periods used to predict times of eclipse minima, could be reinterpreted and used to predict a

characteristic feature (minimum, maximum, inflection point, etc.) in the light curve of a pulsating star. In conceiving of what was physically happening, instead of using periods, the emphasis would shift to pulsation-mode frequencies. RS Crt's changing behavior and light curve might be explained in terms of the dynamic interplay of two fundamental pulsation modes.

5.2 Connecting RS Crt to real types of pulsating stars, and imagining pulsation ceases

Given its late F spectral type, one might speculate RS Crt was once a high amplitude delta Scuti (HADS) star that quit pulsating. Both its half-magnitude amplitude and spectral type are at the extreme, but not implausible, edge of what is typical of HADS stars. A bigger problem is RS Crt's period of 0.82 days, which is much too long. The suggestion of a secondary minimum for this period suggests the real pulsation period might have been one-half of that, around 0.4 days. This is still rather long, and more typical of RRa variables. But RS Crt's low luminosity, with its absolute visual magnitude of +4.45, disqualifies it from fitting into that category. Even if RS Crt were once pulsating, why its pulsation would so quickly, in the blink of an eye compared to typical stellar evolution time scales, diminish and cease, is unknown!

5.3 Is RS Crt strictly constant in brightness today, as its VSX listing suggests?

The short answer is no. The light curve shown in Figure 5 from TESS, the best recent source of photometric data we have, shows that it is not strictly constant in brightness. Admittedly the variations shown are tiny, in the peak-to-peak range of at most 0.01 magnitude, but look to be periodic, with possible signs of damping and beats. I won't speculate on what might be responsible.

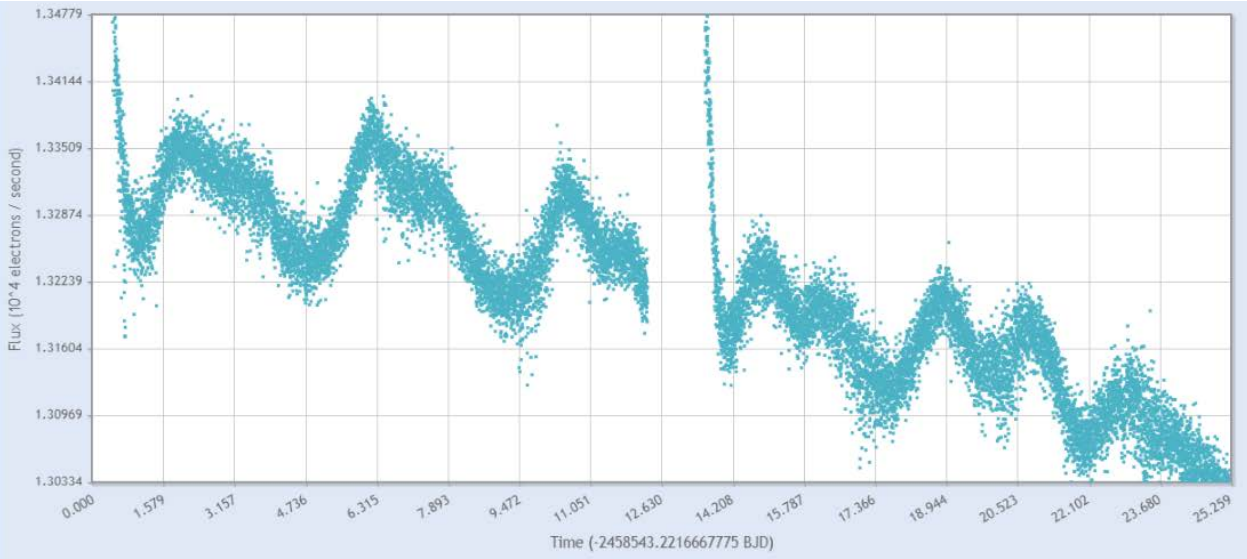

Figure 5. Recent light curve of RS Crt from TESS data

6. Suggestions for Future Work / Conclusion

6.1 Observational Priorities for RS Crt

1) Obtaining high-resolution spectra to definitively establish whether or not RS Crt is a binary star should be a priority. If it is binary, these data could determine its orbital inclination.
2) If established to be binary, finer probing of the Harvard plates could also help in more firmly characterizing its RS Crt eclipsing binary past and inform speculation / predictions as to the possibility of its eclipses resuming at some future date.
3) If binary, searching for a third star in the system, one responsible for changing inclination.
4) If not binary, investigating whether the nature of the variation suggested in Figure 5 might lead to modeling it as a pulsating star that was once more active, but now is seemingly in a quiet state.

6.2 Conclusion

Careful weighing of all data best supports belief that RS Crt once showed a periodic light variation somewhere in the 0.2 to 0.6 magnitude range with a period around 0.82 days, and that eclipses can best account for that variation. However, the author is in no way 100% certain of that conclusion. If its eclipses really ceased, RS Crt belongs to a select group of objects. Giving it that recognition would be bolstered by spectroscopic confirmation of its binary nature.

Even if high-resolution time-series spectroscopy establishes that RS Crt is now a single star, it is still an interesting object. Investigation of its now barely perceptible periodic light variation might point the way to understanding the much higher amplitude periodic light variation this paper has provided evidence of in terms of a pulsating past.

Acknowledgements

I wish to thank 1) Bradley Schafer for critically examining and commenting on what I had on RS Crt from digitized Harvard plates (DASCH); 2) Edward Guinan for copying and sending me the card for RS Crt from The Eclipsing Binary Card Catalogue, now at Villanova University; 3) Marvin Baldwin for answering (via email) my questions regarding his 1987-1988 visual observations of RS Crt; and 4) Gary Billings for his comments. I also wish to honor the memory of Daniel Popper (1913-1999), my teacher long ago at UCLA.

References

AAVSO. 2022, observations from the AAVSO International Database http://www.aavso.org
BBSAG. 1976, *BBSAG Bulletin,* 26, 1976 March
Belserene, E. P. 1988, *Sky & Telescope*, September 1988, page 288
DASCH. 2022, (Digital Access to a Sky Century at Harvard) http://dasch.rc.fas.harvard.edu
Davenport, J. et al. 2021, *Astron. J.* **162**, 189-195
Dvorak, S.W. 2004, *Inf. Bull. Var. Stars*, No. 5549, 1

Gaia Collaboration DR2. 2018, https://gaia.esa
Gaia Collaboration DR3. 2020, https://gaia.esa
Guinan et al. 2012, *JAAVSO*, **40**, 467-480
Kholopov, P. N. et al. 1985, *General Catalogue of Variable Stars*, 4th Ed., Moscow
Kukarikn, B. and Parenago, P. 1968, *General Catalogue of Variable Stars*, 3rd Ed., Moscow
Lacy, C. et al. 1999, *Astron. J.*, **117**, 541-547
Lange, G. 1935, *Tadjik Circular*, **6**, 4
Nelson, B. 2016, http://www.aavso.org/bob-nelsons-o-c-files
Popper, D. and Dumont, P. 1977, *Astron. J.*, **82**, 216-222
Popper, D. 1996 *Astrophys. J. Supp. Series*, **106**, 133-141
Samus, N.N. 2007, *Odessa Astronomical Publications*, **20**, 103
Sandig, von, H.U. 1948, *Astron. Nachr.,* **276**, 175
Tsesevich, V. P. 1947, *Astronomical Circular –Academy of Sciences USSR*, **63**, 11
Tsesevich, V.P. 1954, *Izvestia of the Astronomical Obs. of Odessa*, IV, 242
Wood, F.B. et al. 1980, *A Finding List for Observers of Interacting Binary Stars* 5th Ed., University of Pennsylvania, Philadelphia

A Program for Characterizing Variable Stars Discovered in the MOTESS-GNAT Sky Surveys

Eric R. Craine
Western Research Company/GNAT, 3275 W. Ina Rd., Tucson, AZ 85741; ercraine@wrc-inc.com

Brian L. Craine
Western Research Company/GNAT, Fairfax, CA; blcraine@wrc-inc.com

Roger B. Culver
Colorado State University and GNAT, Fort Collins, CO 80528; Roger.Culver@ColoState.edu

Subject Keywords

Photometry, CCD; variable stars

Abstract

The motivation of this project is two-fold: 1) to help provide quality control over a large, new database of astronomical observations, and 2) to explore details of select, interesting variable stars not previously well characterized. The Moving Object and Transient Event Search System (MOTESS) and the Global Network of Astronomical Telescopes (GNAT) have collaborated from 2001 to 2021 to conduct time series photometric surveys of selected strips of sky along the celestial equator. This project has yielded several million stellar light curves among which are many thousands of newly discovered or previously uncharacterized variable stars. The problem being addressed is to understand nuances of the databases and to provide in-depth analyses of particularly interesting stars within the databases. The methodology is to recruit observers to collaborate with the GNAT research teams to observe, analyze, and publish results for MG Sky Survey stars of interest. The requisite follow-up observations are predominantly small-telescope time series photometry and large telescope spectroscopy. The former observation type, in particular, is a rich area for participation by serious amateur astronomers who are equipped for such photometry in the $14 < R < 18$ mag range. A goal of this presentation is to encourage such observers to productively join our research teams and to share in authorship of the final results.

1. Introduction

The Moving Object and Transient Event Search System (MOTESS) is a time delay integration (TDI) sky survey instrument originally implemented in 2001 as a highly successful asteroid discovery system described in detail by Tucker (2007). It has been subsequently used as a system for discovering and characterizing variable stars through a partnership of the Global Network of Astronomical Telescopes (GNAT) and MOTESS. The first such data product was the MG1 variable star catalog (MG1-VSC) described in detail by Kraus *et al.* (2007).

At this writing the eighth MG survey is underway. The survey strips (48-arcmin high in declination) are described in Table 1. Surveys are typically about two years in duration. MG7P is a survey in polarized light at the same declination as MG1 and MG6. MG8 is a repeat of MG2 in terms of declination. Note that over the duration of each survey the entire 0-24hr right ascension range is covered. Statistics of completed surveys are shown in Table 2 from Craine *et al.* (2021). Note that in Table 2 the "A" suffix to the survey number indicates that the statistics are for the first database reduction for the named survey. Subsequent reductions might be, for example, MG1B.

It should be noted that the MG1-VSC is not the same thing as the MG1 survey but is rather a subset of MG1 data that has been selected for specific thresholds and properties of candidate individual object variability. Depending upon parameters and protocols of data reduction, there can be multiple MG survey databases generated for a single declination, and each such database can likewise produce multiple variable star candidate lists. MG1-VSC is just one such for the MG1 survey strip at the specified MG1 declination.

Table 1. Summary of MG survey strips.

Survey	Declination‡	Start	End
MG1	+03:18:20	2001 Apr	2003 Jul
MG2	+02:05:00	2003 Jul	2005 Jul
MG3	+12:18:20	2005 Jul	2007 Jul
MG4	+05:00:00	2007 Jul	2009 Jun
MG5	+09:56:00	2009 Jul	2011 Jun
MG6	+03:18:20	2011 Aug	2013 Jun
MG7P	+03:18:20	2017 May	2019 Nov
MG8	+02:05:00	2020 Sep	Ongoing

‡Center of 48 arcmin strip

Table 2. MOTESS-GNAT survey comparisons.

Metric	MG1A	MG2A	MG3A	MG4A	MG5A	MG6A
Nights	282	298	233	277	297	232
Images (% reject)	89,354(15.4)	88,837(18.2)	66,308(21.0)	88,266(16.1)	94,829(14.3)	75,394(14.4)
Single Obs	36,295,860	28,142,641	10,644,857	2,838,480	14,514,699	12,777,502
Paired Obs	28,498,119	42,408,209	32,636,334	49,879,379	53,218,750	40,539,506
Coincident reject (%)	13.8	8.4	11.4	13.6	6.2	6.8
Objects	936,764	1,185,506	1,141,170	1,173,723	1,121,111	1,046,732
Mean Nobs	98.2	94.1	66.0	86.6	107.5	89.2
GCVS(%)	248(73.8)	268 (68.0)	202(69.9)	218(80.7)	444 (78.0)	280(83.3)
2MASS (%)	56.0	63.0	65.6	71.1	76.6	68.2

The MG surveys result in serendipitous discovery of a broad range of optically variable celestial objects. Many of these objects are unusual or pathological looking stars that are good candidates for follow-up observation. Thus, one way to think of the MG surveys is as a series of "sieves" for identifying interesting stars for further study.

The purposes of this paper are threefold: 1) to provide a brief status report on the current surveys 2) to provide examples of some of the types of variable stars discovered in the surveys, and 3) to solicit the participation of potential collaborators in follow-up observation and analysis of interesting MG survey discoveries.

2. Typical Follow-up Projects

There are several reasons for conducting follow-up observations of objects discovered in the MG surveys, including 1) determining periods of periodic variable stars whose initial periods may be aliased by survey observing cadences, 2) obtaining higher temporal resolution of object light curves, 3) further characterizing behavior of unusual or interesting stars, or 4) searching for interesting classes or groups of objects. In this section we present a brief overview of the conduct and results for some MG follow-up programs.

2.1 Methods

MG survey follow-up typically involves some combination of 1) identifying stars of interest in the survey database, 2) small telescope time series photometry, 3) light curve analysis, 4) spectroscopy, 5) stellar or system modelling, 6) literature searching and database cross correlations, and 7) discussion and documentation.

Involving multiple small telescopes and observers is potentially an efficient way to collect time series photometry; spectroscopy of the relatively faint stars found in the MG surveys is always a challenge requiring access to 2-m and usually larger telescopes.

2.2. Results from Example Projects

In this section we briefly summarize three MG follow-up projects that are representative of the work that is being done.

2.2.1. Long Period Variables (LPVs)

Long Period Variable stars were identified in the MG1-VSC primarily by visual examination of light curves for which tentative periods had been determined by periodogram analysis. An initial collection of candidates was identified (47 stars) and the light curves were re-analyzed using multiple periodogram analyses. Because of potential aliasing around P ~ 360d (due to the observing cadence imposed by time delay integration (TDI) imaging) some of the stars in the sample were found to have uncertain periods (Craine *et al.* 2015).

As seen in Table 1, the MG6 survey was a ten year later follow-up of the MG1 survey. A new reduction of the MG1 and MG6 surveys was performed and screened for candidate LPVs. The refined data and screening protocols yielded a total of 138 LPVs in the 48.3'-wide equatorial strip. The follow-up data allowed for refinement of the period determinations for most of the LPVs

(Craine *et al*. 2022). This study has identified 9 unique LPVs, bringing the total number of new LPV identifications from the MG1 survey strip to 56.

2.2.2. Short Period Variables (SPVs)

Short period variable stars proliferate in the MG1-VSC, as well as in all of the MG survey databases. Many of these stars exhibit near sinusoidal light curves and are thought to be contact binary stars, however, because of the TDI-induced observing cadence the initial periods reported for the SPVs are often in error.

It should be noted that in preparation of the MG1-VSC, after much deliberation, it was decided to retain the likely aliased periods and to publish the associated phased light curves in conjunction with a false alarm probability of the correctness of the period. The rationale was that, even though the period was likely incorrect, the phased light curve itself would nonetheless provide a strong visual impression of a sinusoidal light curve, thus drawing attention to the star for purposes of follow-up observation. Indeed, it was this very practice that led to discovery of MG1-688432 (see Section 2.2.3.).

Follow-up observation of SPVs is an example of a productive program for collaboration with serious operators of small, private observatories. The typical observing protocol is to conduct time-series photometry, generally observing a program star with multiple observations per night (or per hour) for many nights in a row. It is an activity well suited for automated or semi-automated telescopes equipped with digital cameras.

These data can often resolve an aliased period in a matter of just a few nights of observation, thus helping to determine how to proceed in subsequent observation and analysis.

2.2.3. Unusual Stars

Some MG survey stars exhibit unusual behavior that triggers an interest in follow-up observation. A good example is MG1-688432 (Tucker *et al.* 2021). This star was found in MG1-VSC and MG6 to exhibit a sinusoidal light curve of about a 6.6d period and became a candidate for further observation in an effort to confirm the period. Very shortly after pointed time series observations with a small telescope were initiated the light curve of the star revealed a very high energy outburst of several hours in duration. The observing campaign continued and more high energy outbursts with multiple peaks over several hours in duration were seen.

After several years of photometric observations, it became necessary to obtain spectroscopy to help characterize the star. These observations confirmed that the star was a binary with an unseen companion, and that it was not an eclipsing system. Photometric observations have now shown light curve features that look like classical stellar flares as well as the energetic outbursts that may result from mass transfer or large body collisions.

This star is now the target for a collaborative effort involving the original research team and a small group of collaborators who operate small telescopes. Their job is to help collect time series photometry and to assist in the analysis of the system. The goal of the photometry is to monitor the flare and outburst activity in the hope of improving the statistics of those events and to look for evolution in the nature of the outbursts.

3. Conclusions

The MG survey databases are a rich source of interesting stars worthy of follow-up observing and analysis programs. It is apparent that collaborative programs with small telescope operators can be very productive in helping to accelerate the study of these stars. To that end the authors of this paper are making an appeal to the amateur and small telescope user community to consider participating in one or more of the GNAT MG follow-up programs.

The most productive such collaboration is likely to be time series photometry which would be coordinated through GNAT in communication with a geographically distributed group of observers. Productive work in the past has involved the use of telescopes as small as 8-in aperture, though most telescopes used for these photometric programs have been in the 10- to 24-in range. The key is that they are well-mounted and calibrated for stellar astrophotography.

Observers interested in collaborating with one or more of the GNAT projects should contact the primary author of this paper and we can discuss areas of interest and details of working together. These are voluntary collaborations, but some tangible reward will be in the form of co-authorship for everyone who makes a material, coordinated contribution to the program.

There are other rewards as well. This is a good group with which to work, it is a chance to learn more about astrophysics, it is a good opportunity to meet people with similar interests, and for the right persons it can be a lot of fun.

Acknowledgements

We acknowledge with thanks the contributions to the overall GNAT program of our colleagues Chris Corbally, Adam Kraus, Andy Kulessa, and Doug Walker. The long-term contributions of our friend and colleague Roy Tucker, now deceased, transcend a simple thank you.

References

Craine, B.L., Craine, E.R., Tucker, R.A., Culver, R.B., and Anderson, R. 2021, in *Proceedings for the 40th Annual Symposium of the Society for Astronomical Sciences SAS-2021,* eds. J.C. Martin, R.K. Buchheim, R.M. Gill, W. Green, R. Stephens, SAS, Rancho Cucamonga, CA, 31.

Craine, B.L., Kulessa, A.S., Craine, E.R., Culver, R.B., Kraus, A.L., Tucker, R.A., and Walker, D.K. 2022, *J. Amer. Assoc. Var. Star Obs.,* **50**, 233.

Craine, E.R., Culver, R.B., Eykholt, R., Flurchick, K.M., Kraus, A.L., Tucker, R.A., and Walker, D.K.

2015, *J. Amer. Assoc. Var. Star Obs.,* **43**, 131.

Kraus, A.L., Craine, E.R., Giampapa, M.S., Scharlach, W.W.G., and Tucker, R.A. 2007, *Astron.J.*, **134**, 1488.

Tucker, R. 2007, *Astron.J.,* **134**, 1483.

Tucker, R., Craine, E.R., Craine, B.L., Kulessa, A.S., Corbally, C.J. and Kraus, A.L. 2021, *Astrophys. J. Suppl.*, **256**:1 (17pp).

Reference Set of Mira Variables for the World to Share and Explore

Michelle J. Creech-Eakman[1], Gerard T. van Belle[2], and Dana K. Baylis-Aguirre[1]

[1]New Mexico Institute of Mining and Technology, 801 Leroy Place Socorro, NM 87801, USA; Michelle.CreechEakman@nmt.edu
[2]Lowell Observatory, 1400 West Mars Hill Road, Flagstaff, AZ 86001, USA

Subject Keywords

Stars: Mira variables; techniques: interferometry; instrument: Palomar Testbed Interferometer (PTI); stellar evolution

Abstract

Our team has recently been awarded an NSF grant to create a *Reference Data Set* of Mira variables based on nearly a decade of optical interferometry observations undertaken with the Palomar Testbed Interferometer (PTI). Miras are in some respects the most enigmatic regular pulsators, while also being potentially the most important galactic recycling factories, given their high luminosities, period-luminosity relationships, complex circumstellar environments, and broad distribution throughout the galaxy. The dataset from PTI contains almost 100 Miras periodically changing size during their year-long pulsations with resolutions at the sub-milliarcsecond level. The dataset covers a full range of oxygen-rich to carbon-rich chemistries and includes objects that are likely within about 2 kiloparsecs of the Sun, making them ideal for detailed studies of their atmospheres and mass-loss processes. Our team will supplement the PTI data with archival and contemporaneous data from missions/databases such as 2MASS, COBE, IRAS, Spitzer, SOFIA, TESS, WISE, and NRAO, as well as attempting to improve distance estimations with a novel approach using *Gaia/Hipparcos* data. We present a few examples of science that will be enabled using data on Miras from this set. We provide a list of all the Miras in the set for anyone who would like to add them to their observing programs. All the data we produce and collate for this *Reference Data Set* will be hosted on a website open to the public so that other researchers and citizen scientists can participate in expanding the utility and body of knowledge on this set of "wonderful" stars.

1. Introduction

Asymptotic Giant Branch (AGB) stars are the most prolific dust and molecule factories in the Universe and are foremost sources of chemical enrichment of the ISM. These highly evolved stars are characterized by alternate shell burning atop a degenerate C/O core with extremely extended and complex circumstellar environments (CSE). Chemical subclasses for these stars, as derived from their spectra, progress from oxygen-rich (M-type) to "intermediate" (S-type) to carbon-rich (C-type) as dredge-up activity of the stellar interior alters the stellar makeup over time (van Belle et al. 1997; Herwig 2005). For contemporary galaxies, AGB stars are the primary producers of interstellar dust and, at cosmological distances, they compete with supernovae ejecta in dust

production (Valiante et al. 2009). Mira variables are a subset of AGBs with large amplitude pulsations ($\Delta m_V > 3$) and regular periods longer that 100 days. These pulsations help loft material into the atmosphere and drive impressive mass-loss rates of up to 10^{-4} $M_\odot$/yr (Habing 1996; Ruiz-Velasco et al. 2011); these mass-loss rates, combined with prolific dust and molecule production driven by these pulsations, result in Miras becoming enshrouded in thick circumstellar envelopes.

Despite considerable efforts expended in theoretical studies of AGB stars and Miras (Höfner 1999; Herwig 2005), many of the physical processes related to dust production, such as the interplay between pulsation and dust formation, remain poorly understood. This limited understanding encourages astronomers to exploit the pulsation-driven time-dependent behavior of the Mira variable as it presents the perfect laboratory in which to study the late stages of stellar evolution and the physics of mass-loss processes within CSEs. One key obstacle to advancing our understanding of these processes is having access to sufficiently detailed data about the stars themselves, chiefly across a range of wavelengths and spatial resolutions, which can be used to unveil how the pulsations help create such chemically complex and dynamic atmospheres in Mira variables. The ultimate goal of this new NSF-funded effort is to assemble a detailed, time-variable and complex dataset on a relatively large group of Miras such that significant progress can be made on models and theory in the coming years.

1.1 Period-Luminosity relationship

Miras, like their more famous cousins the Cepheids, also have a period-luminosity (P-L) relationship (e.g., Glass & Evans 1981; Feast et al. 1989) which means they can also be utilized as standard candles to provide rungs on the distance ladder (Nowotny et al. 2003). In order to fully exploit their P-L relationship, providing another independent distance ladder within the galaxy or to other galaxies, we need to understand fundamental properties of Miras at a very detailed level. One of the most basic measures about the pulsation mechanisms concerns the physical size of both the star and its surrounding CSE and how much motion or change each star experiences over the course of a pulsation. A full calibration of the Mira P-L relationship is currently limited by many things, including our knowledge of the pulsation mode(s) of each individual star, which has been an ongoing debate in the community for many years (Iben & Renzini 1983). Some studies indicate that Miras pulsate purely in the fundamental mode (Whitelock et al. 2008) while others show evidence the fundamental mode can mix with the first overtone (Lebzelter & Wood 2005; Soszyński et al. 2013).

1.2 Fundamental stellar properties

A star has five main fundamental properties that can be used to describe its physical state and thus its evolution: luminosity (L), effective temperature (T_{eff}), radius ($R_\star$), mass (M) and chemical composition (Z). Obtaining direct measurements of any of these fundamental properties is exceedingly difficult for most stars. Miras, however, provide some distinct advantages toward arriving at these fundamental measures. Their large

angular sizes, θ ≥1 milli-arcsec (mas), for targets in the galaxy (within about 1 kpc) make them excellent candidates for direct angular size measurements with near-infrared optical interferometry. Their intrinsic luminosities mean that these measurements can be made quickly and repeatedly over a pulsation cycle. And, over the course of the pulsation cycle, this angular size has been found to vary an astonishing 10- 30% (van Belle et al. 1997; Thompson et al. 2002; Haubois et al. 2015).

2. Historical Insights from Infrared Interferometry

Infrared, radio, and interferometric techniques are currently making important contributions to the studies of Mira variables' dynamic atmospheres, their circumstellar environment, and the relationships of measurable quantities to the pulsations themselves. Nobel Prize laureate Charles H. Townes and his collaborators from UC-Berkeley conducted pioneering work beginning in the 1970s using the Infrared Spatial Interferometer (ISI) to measure the size of circumstellar dust shells surrounding Mira variables (Sutton et al. 1977), as well as finding evidence for departure from spherical symmetry and episodes of dust formation and destruction (Tatebe et al. 2006).

Measured angular diameters were found with investigations at Harvard-CfA's Infrared-Optical Telescope (IOTA) facility to be in the range of 350−600 $R_{\odot}$ and varying in size during the pulsation cycle from 13-30% (van Belle et al. 1996, 1997, 2002). In general, the wavelength dependence of angular size progresses across the near-IR, with θ(J) < θ(H) < θ(K) (Millan-Gabet et al. 2005). At finer steps across these broadband windows, other features become evident; for example, the prominent CO band longwards of 2.29 μm shows angular sizes that are systematically larger than those in the middle of the K-band, typically associated with continuum emission for these stars as seen in Figure 1 (Lançon & Wood 2000). This increase in angular size is associated with an increase in opacity at the CO wavelengths (Thompson et al. 2002).

2.1 PTI–The Palomar Testbed Interferometer

In 1999, the Caltech-JPL's Palomar Testbed Interferometer (PTI) (Colavita et al. 1999) began a long-term monitoring program of nearly 100 Mira variables, collecting data until its decommissioning in 2008. The goal of this extensive program was to observe changes in apparent angular size with respect to pulsation phase and wide/narrow-band wavelengths in the infrared, correlating these measurements with chemical abundances, pulsation mode, and spatial geometry. Initial broad-band and narrow-band results were studied by Thompson et al. (2002) for RZ Peg and S Lac, based on only 3 years of observations. Today the entire broad-band dataset for these Miras has undergone an initial analysis and is being prepared for publication; the more spectrally rich, narrow-band data set awaits full analysis, yet tantalizing details are already apparent.

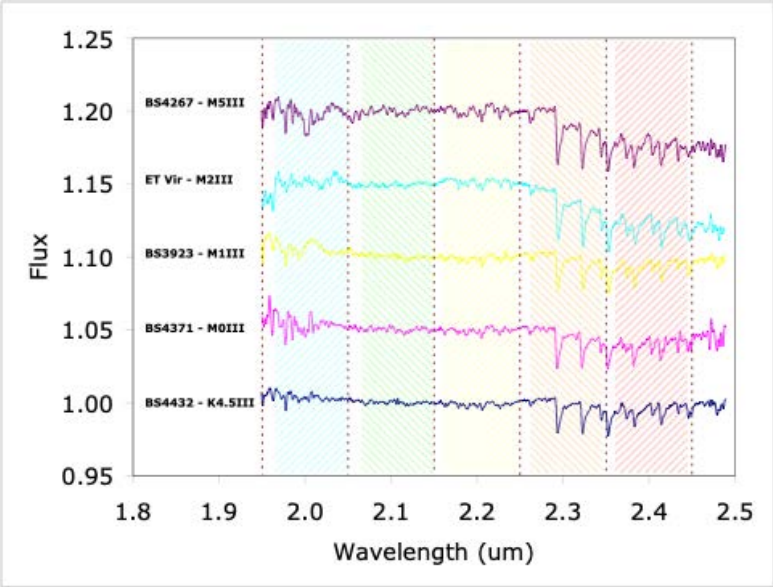

Figure 1. Representative normalized spectra in the K-band for spectral types from K4.5III (bottom) up to M5III (top), from (Lançon & Wood 2000). The coverage of the PTI 5 narrow-band pixels is shown at centers λ_0 = 2.0, 2.1, 2.2, 2.3, 2.4 μm. The carbon monoxide feature redward of 2.3μm can be seen to be increasing in strength for the redder spectral types; the reddest of these stars is representative of spectra expected from Miras. These absorption features appear more resolved in interferometric measurements.

One intriguing aspect of this data set which is of direct relevance to the question of pulsation modes in these stars regards the nature of what the interferometric spectral measurements, especially in the narrow-band data, are actually 'seeing'. Given that the spectral details seen in these objects are related to molecular features in the CSE, the varying opacity as a function of wavelength effectively means the interferometric data are probing different layers within the star. Simply put (and not entirely inaccurately) is the notion that the different PTI narrow-band pixels see different radii of the photospheric environment because of opacity effects (see Figure 1). Studies using the VLT interferometer in Chile have attempted to tease out some of these details (Haubois et al. 2015; Zhao-Geisler et al. 2015; Wittkowski et al. 2018). Yet these studies rarely followed more than a few Miras for even one complete pulsation cycle. Following the time-dependent behavior of these radii relative to each other is expected to reveal the detailed nature of the stellar pulsations.

Using the measured angular diameters at K-band with phase taken from databases like the AAVSO, we are able to create plots of angular diameter versus phase for the stars in the database. Using a distance estimate, typically taken from a database like *Hipparcos* or *Gaia*, the angular diameter can be easily converted into a physical diameter. Using archival photometry over a broad range of wavelengths, an estimate of the luminosity and temperature can be made for each star. If this information is now used to plot the physical diameter versus temperature, unwrapping the phase information and just using

time, one finds that the stars appear to 'loop' in the plots. While this in itself is interestingly reminiscent of plots one might see in a thermodynamics course, the real power of the technique makes itself evident when the stars are separated by chemical subclass. We believe that the nature of these plots can be used to reveal the pulsation mode for individual stars. In Figure 2 we show an example for several dozen stars plotted in this way from this Mira *Reference Data Set*.

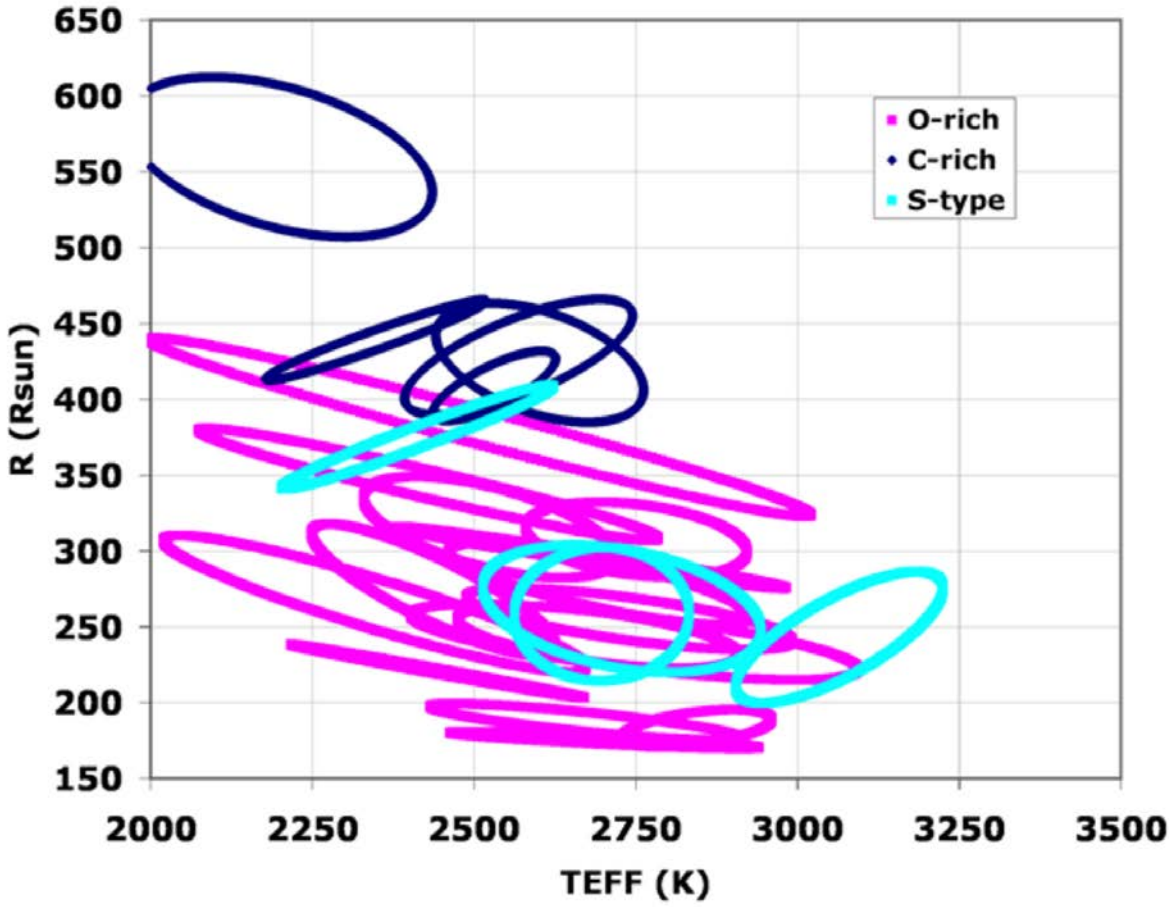

Figure 2. Plots of temperature versus radius for a few dozen Miras using the interferometric and archival data. The stars are separated by chemical subclass (dark blue are C-rich, pink are O-rich, and cyan are S-types with C/O ratios close to 1). The description of how these plots are created and what we believe they represent is detailed in the text.

3. A Reference Data Set

We will use the PTI archival data to directly extract two of the five fundamental parameters (Section 1.2), T_{eff} and $R_{\star}$, over many epochs (pulsation periods) for the stars listed in Table 1. These particular Miras have a large spread across chemistry and pulsation period, making them statistically representative of the general population of Galactic Miras (see Table 1). Archival interferometric and photometric measurements

provide us with a direct measurement of the angular size and bolometric flux of the stars.

Table 1. Inventory of Mira observations in NASA's PTI Archive by chemical type and period bin. Each table cell notes the number of Miras in each category, followed in parentheses by maximum and median number of epochs for individual objects in that category. For example, for O-type Miras with 100-200d periods, the 13 stars in this category have a median number of 12 observing epochs, and one of these Miras has 97 epochs of observing. Observing was typically spread throughout the 11-year life of PTI, meaning phase coverage is typically homogeneously spread throughout a given Mira's cycle.

Mira Type	**Period Range (d)**				**N**
	100-200	**200-300**	**300-400**	**400-600**	
O-type	13 (97, 12)	30 (93, 9.5)	25 (65, 10)	7 (48, 10)	75
S-type	0	4 (46, 24.5)	4 (54, 28.5)	4 (12, 9)	12
C-type	0	1 (21, 21)	6 (51, 13.5)	5 (81, 14)	12
Totals	13	35	35	16	99

When we combine these properties with a distance estimate we can directly determine the physical stellar radius and the effective temperature. Additionally, the wavelength-dependent nature of the interferometric data can be utilized to determine relative proportions of molecular features to their distribution throughout the stellar atmosphere, essentially creating a molecular distribution "map" of the atmosphere which will help build our understanding of the material that is lofted into the surrounding CSE. In Figure 2 we present a conceptualization of the interplay of data and modeling that this dataset will underpin.

Establishing a more precise method of determining the radii, effective temperature and atmospheric composition of Mira variables will benefit the whole astrophysical community. These remarkable stars provide a unique laboratory to perform numerous experiments that will help us better understand topics from stellar evolution and dust formation to galactic chemical enrichment and composition of future exoplanets. For this reason, we refer to this project as developing a *Reference Data Set* of Miras with the PTI dataset at the core in order to provide those fundamental stellar parameters the community needs. We then will build outward using additional datasets from a variety of studies across multiple wavelengths and observational techniques as shown in Figure 3. The full *Reference Data Set* can then be used to reinforce a variety of observational and theoretical studies in pulsation, and circumstellar chemistry and how the interplay of these affects dust production in the CSE.

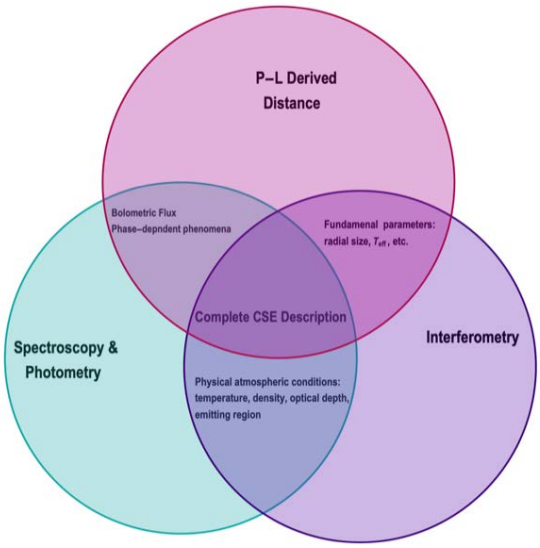

Figure 3. A Venn diagram showing a conceptualization of how observables and modeling interplay for Mira variables; overlapping regions show that feedback between these areas impacts our overall understanding of the physical processes involved. These overlapping regions also demonstrate how sets of detailed information feed our knowledge of a particular physical parameter space for the Mira variables. At the center, the result is a more complete understanding of the star's circumstellar envelope.

Table 2. List of target Mira variables with their respective chemistries and periods.

Constellation	Star	Chemistry	Period[1] (days)	Constellation	Star	Chemistry	Period[1] (days)
	RW And	S-type	430		RW CVn	M-type	NA
	ST And	C-type	326.6	Canes Venatici	U CVn	M-type	342.9
	SV And	M-type	313		V CVn	M-type	194.0
Andromeda	T And	M-type	281.0	Delphinus	X Del	M-type	281.0
	TU And	M-type	316.8		Y Del	S-type	468.4
	X And	S-type	343.4	Draco	WZ Dra	M-type	401.7
	Y And	M-type	220.5		R Gem	S-type	369.9
	OW Aql	C-type	416.6		S Gem	M-type	293.2
	RT Aql	M-type	326.4		T Gem	S-type	287.8
	S Aql	M-type	147	Gemini	V Gem	M-type	274.8
Aquila	SY Aql	M-type	359.65		VX Gem	C-type	379.4
	X Aql	M-type	347.67		X Gem	M-type	264.2
	Z Aql	M-type	128.40		ZZ Gem	C-type	317.0
Aquarius	T Aqr	M-type	201.1		R Her	M-type	318.1
Aries	RU Ari	M-type	353.5		RS Her	M-type	219.7 s
	U Ari	M-type	371.1		RV Her	M-type	205.2
	RU Aur	M-type	463.0		RZ Her	M-type	329.1
Auriga	V Aur	C-type	349.0	Hercules	S Her	M-type	307.3
	W Aur	M-type	271.3		SV Her	M-type	239.0
	X Aur	M -type	165.5		SY Her	M-type	116.9
Böotes	R Boo	M-type	233.1		T Her	M-type	164.9

Cont. on next page

Constellation	Star	Chemistry	Period[1] (days)
	RT Boo	M-type	275.5
Cassiopeia	SS Cas	M-type	140.6
	TT Cas	M-type	396.0
	U Cas	S-type	278.9
	V Cas	M-type	230.6
	WY Cas	S-type	481.5
Cetus	R Cet	M-type	166.2
	Z Cet	M-type	184.8
Coma Berenices	R Com	M-type	362.8
Canis Minor	R CMi	C-type	340.0
	U CMi	M-type	412.1
	V CMi	M-type	366.3
Cancer	V Cnc	S-type	269.7
Corona Borealis	V CrB	C-type	357.6
	X CrB	M-type	241.2
Cygnus	R Cyg	S-type	426.5
	RT Cyg	M-type	190.3
	LX Cyg	C-type	465.3
	U Cyg	C-type	463.2
	UX Cyg	M-type	565.0
	WX Cyg	C-type	410.5
	Z Cyg	M-type	263.7
Pegasus	RV Peg	M-type	396.8
	RZ Peg	C-type	438.7
	S Peg	M-type	319.2
	SW Peg	M-type	396.3
	SX Peg	S-type	303.6
	V Peg	M-type	302.4
	X Peg	M-type	201.2
Perseus	R Per	M-type	209.9
	Y Per	C-type	248.6
Serpens	S Ser	M-type	371.8
Taurus	S Tau	M-type	374.5
	V Tau	M-type	168.7
Hydra	W Her	M-type	280.3
	S Hya	M-type	256.6
Lacerta	S Lac	M-type	241.5
Leo	V Leo	M-type	273.4
Libra	Y Lib	M-type	275.7
Lynx	T Lyn	C-type	406.0
Lyra	RU Lyr	M-type	371.8
	RY Lyr	M-type	325.8
	S Lyr	S-type	438.4
	U Lyr	C-type	451.7
Monoceros	RR Mon	S-type	394.7
	V Mon	M-type	340.5
Ophiuchus	RT Oph	M-type	426.3
	RU Oph	M-type	202.3
	RY Oph	M-type	150.4
	SS Oph	M-type	180.6
	Z Oph	M-type	348.7
Orion	R Ori	C-type	377.1
Pisces	R Psc	M-type	344.5
	S Psc	M-type	404.6
	X Psc	M-type	349.6
Triangulum	R Tri	M-type	266.9
Ursa Major	RS UMa	M-type	259.0
	S UMa	S-type	225.9
	T UMa	M-type	256.6
	X UMa	M-type	249.0
Virgo	R Vir	M-type	145.6
	RU Vir	C-type	433.2
	U Vir	M-type	206.6
	Y Vir	M-type	218.4
End of Table			

[1]Samus' et al. (2017)

4. Citizen Science Contributions

This project has multiple exciting opportunities for citizen science contributions and collaboration. This *Reference Data Set* will benefit greatly from contributions to AAVSO. In particular, while accurate and regular monitoring of the pulsations at multiple wavelengths (ideally in the optical and infrared) is fundamental for variable stars, finding anomalies, such as dimming events, double-pulsations, glitches in the light curves, or period switching, is absolutely crucial to our understanding of how these stars are

evolving. This type of detailed, long-term monitoring is not well-suited to professional telescope facilities which require individual observers managing projects totaling typically hours to days and resubmitted for approval two or more times per year. Contributing photometric or spectroscopic observations from the citizen science astronomical community to AAVSO on these targets in particular can render this *Reference Data Set* all the more valuable for the community of observers, theorists and modelers who care about the types of questions that Miras are well-posed to help answer. Table 2 provides the list of Miras in this dataset for observation. Our team is open and eager for further scientific collaboration on any of these targets.

4. Conclusion

Mira variables are excellent laboratories for studying a variety of astrophysical phenomena and stellar evolution. Using interferometric techniques will herald a new era of precision in the experiments we can perform in our "laboratory". We will use interferometric data as the foundation of our *Reference Data Set* to which we will add multi-wavelength observations from throughout the astronomical community, including citizen-science contributions. This will allow us to create an unprecedented and detailed description of the physical properties of the Mira variable star and its surrounding CSE. Additionally, this data set will be made available to the entire astrophysical community to further our exploration of these wonderful stars.

Acknowledgements

The authors wish to acknowledge the variable star observations from the AAVSO International Database contributed by observers worldwide and used in this research effort and to thank the AAVSO organizers for inviting our work for presentation in these proceedings. This work is being supported through the National Science Foundation under grant number: 2206803.

References

Colavita, M. M., Wallace, J. K., Hines, B. E., et al. 1999, *ApJ*, **510**, 505, doi: 10.1086/306579
Feast, M. W., Glass, I. S., Whitelock, P. A., & Catchpole, R. M. 1989, *MNRAS*, **241**, 375
Glass, I. S., & Evans, T. L. 1981, *Nature*, **291**, 303, doi: 10.1038/291303a0
Habing, H. J. 1996, *A&A Rv*, **7**, 97, doi: 10.1007/PL00013287
Haubois, X., Wittkowski, M., Perrin, G., et al. 2015, *A&A*, **582**, A71, doi: 10.1051/0004-6361/201526482
Herwig, F. 2005, *ARA&A*, **43**, 435, doi: 10.1146/annurev.astro.43.072103.150600 Höfner, S. 1999, A&A, 346, L9
Iben, Jr., I., & Renzini, A. 1983, *ARA&A*, **21**, 271, doi: 10.1146/annurev.aa.21.090183.001415
Lançon, A., & Wood, P. R. 2000, *A&AS*, **146**, 217, doi: 10.1051/aas:2000269
Lebzelter, T., & Wood, P. R. 2005, *A&A*, **441**, 1117, doi: 10.1051/0004-6361:20053464
Millan-Gabet, R., Pedretti, E., Monnier, J. D., et al. 2005, *ApJ*, **620**, 961, doi: 10.1086/427163

Nowotny, W., Kerschbaum, F., Olofsson, H., & Schwarz, H. E. 2003, A&A, 403, 93, doi: 10.1051/0004-6361:20030282

Ruiz-Velasco, A. E., Wittkowski, M., Wachter, A., Schröder, K.-P., & Driebe, T. 2011, *A&A*, **535**, A100, doi: 10.1051/0004-6361/201117994

Samus', N. N., Kazarovets, E. V., Durlevich, O. V., Kireeva, N. N., & Pastukhova, E. N. 2017, *Astronomy Reports*, **61**, 80, doi: 10.1134/S1063772917010085

Soszyński, I., Wood, P. R., & Udalski, A. 2013, *ApJ*, **779**, 167, doi: 10.1088/0004-637X/779/2/167

Sutton, E. C., Storey, J. W. V., Betz, A. L., Townes, C. H., & Spears, D. L. 1977, *ApJL*, **217**, L97, doi: 10.1086/182547

Tatebe, K., Chandler, A. A., Hale, D. D. S., & Townes, C. H. 2006, *ApJ*, **652**, 666, doi: 10.1086/507416

Thompson, R. R., Creech-Eakman, M. J., and van Belle, G. T. 2002, *ApJ*, **577**, 447, doi: 10.1086/342147

Valiante, R., Schneider, R., Bianchi, S., and Andersen, A. C. 2009, *MNRAS*, **397**, 1661, doi: 10.1111/j.1365-2966.2009.15076.x

van Belle, G. T., Dyck, H. M., Benson, J. A., & Lacasse, M. G. 1996, *AJ*, **112**, 2147, doi: 10.1086/118170

van Belle, G. T., Dyck, H. M., Thompson, R. R., Benson, J. A., & Kannappan, S. J. 1997, *AJ*, **114**, 2150, doi: 10.1086/118635

van Belle, G. T., Thompson, R. R., & Creech-Eakman, M. J. 2002, *AJ*, **124**, 1706, doi: 10.1086/342282

Whitelock, P. A., Feast, M. W., & van Leeuwen, F. 2008, *MNRAS*, **386**, 313, doi: 10.1111/j.1365-2966.2008.13032.x

Wittkowski, M., Rau, G., Chiavassa, A., et al. 2018, *A&A*, **613**, L7, doi: 10.1051/0004-6361/201833029

Zhao-Geisler, R., Köhler, R., Kemper, F., et al. 2015, *PASP*, **127**, 732, doi: 10.1086/682261

Comparison of the 3D Printed Spectroscopes LowSpec and StarEx: Design, Construction, and Performance

Harry R. (Rick) Diz, PhD, PE

Professor Emeritus of Environmental Engineering, Gannon University, Erie, PA, USA;
hrickdiz@gmail.com

Subject Keywords

Spectroscopy

Abstract

The recent availability of inexpensive 3D printers has made it possible to create precision instruments at home. Two inventors, P. Gerlach in The Netherlands and C. Buil in France, have made it possible to build at home sophisticated spectroscopes that are well within the capabilities of amateur astronomers, and which are comparable in performance to the well-known commercial spectroscope LHires III. Both are of the classical spectroscope design, and both can be completed for a cost (in 2022 dollars) of about $700, not including the cost of cameras. The LowSpec by P. Gerlach has a more complex structure than the StarEx, but has an easily changed slit system and a quickly replaceable grating system. The StarEx by C. Buil, which is an extension of his spectroheliograph, the Solex, has fewer parts and is simpler to assemble with fewer failure possibilities. The LowSpec design results in better performance when using gratings of 1800 or fewer lines/mm, but the StarEx can accommodate a grating of 2400 lines/mm which cannot be used in the LowSpec, and thus can achieve a resolution (R) as high as 30,000. The quality of the guide image in the StarEx appears to be of higher quality than the LowSpec, but both provide adequate guide images for good function using a simple 'mini' guide camera. The choice of which instrument to build and use may well be an arbitrary one.

1. Introduction

Modern-day amateur astronomy is not a cheap hobby, and cost can present a significant hurdle to entry. Some amateur astronomers choose to move into spectroscopy in order to obtain and study the spectra from distant objects. However, commercial slit spectroscopes (those capable of achieving high resolution) are expensive. For example, the well-known French-manufactured spectroscope LHires III sells for about $4,000 depending on currency exchange rates (Shelyak.com). Thus there is considerable interest in finding a lower cost alternative. The advent of at-home 3D printers has provided such an alternative, and innovative amateur designers have generously shared their inventions with the public. Thus a motivated amateur astronomer can build their own device. The instrument must incorporate the necessary optics as well as a guiding module to maintain the target object on the slit for extended periods of time. It is possible to create such a device with performance equivalent to the LHires III for under $1,000, not including the cost of cameras.

Two inventors have offered their designs to the public free of royalties or other consideration. The LowSpec was invented by Paul Gerlach of The Netherlands, who has provided a detailed assembly manual and computer files on the public website 'Thingiverse.com'. The other device considered here, the StarEx, invented by the French amateur spectroscopist Christian Buil is an extension of his spectroheliograph referred to as the Solex. The main difference is the addition of a guide module. Buil has his own website which includes extensive information on design theory, construction guidance, and operational performance (astrosurf.com/solex).

2. Spectroscope Design and Construction

2.1 Spectroscope design

Both instruments employ the classical design as described by Trypsteen and Walker (2017). For more detail on spectroscope theory and design the reader is referred to this excellent source. The essential difference between the two devices is the angle of light rays at the diffraction grating, i.e., an angle of 45° for the LowSpec, and 34° for the StarEx. This angle and the ratio of collimation lens focal length to objective lens focal length have implications for performance differences.

2.2 The 3D printing process

An example of a typical low-cost 3D printer is provided in Figure 1. A plastic filament is fed into a moving print head that melts the plastic and deposits it onto the print surface in a very precise pattern with sub-millimeter precision. The most common type of plastic used for homemade spectroscopes is glycol-modified polyethylene terephthalate (PETG), which combines acceptable properties of thermal stability, stiffness, and strength. Opacity to light is enhanced if the PETG is infused with carbon fibers.

The production of plastic parts on a 3D printer requires computer files which carry the information to the printer on how to create a part. Each component part of the device must be designed in a 3D CAD system, and exported as a sterolithography file (file extension "stl"). These files are then processed in a 'slicer' program which produces the instructions (in a 'Gcode' file) for a specific type of printer to create the part. The process is slow, and some larger parts may take a day or more to be produced by the printer.

The LowSpec has twenty-five component parts. Print time and material consumed is highly dependent on the specifications of the slicer program. In this author's experience, it took about 42 hours of print time to produce the LowSpec, with a total mass of about six hundred grams. While the StarEx has fewer parts, it still took about 39 hours to produce a set of parts, which weighed about five hundred grams.

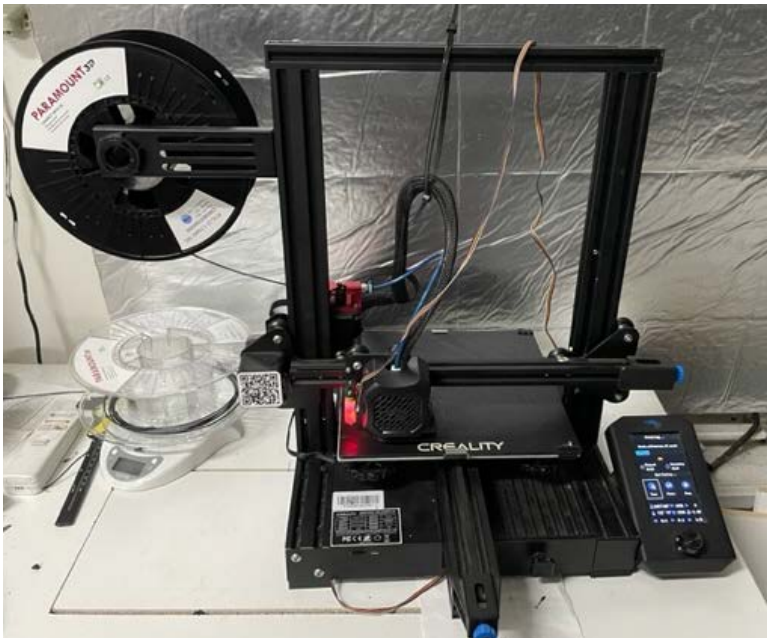

Figure 1. A typical low-cost 3D printer.

2.2 LowSpec design and optical system

The LowSpec (Figure 2) consists of a rectangular box in which light from the target passes through a slit in a reflective slit disc, is reflected off a mirror and passes through the collimator lens, which creates a parallel light beam as it moves towards the diffraction grating. The focal ratio of the collimator lens can be modified to match the focal ratio of the telescope in the range of F/6 to F/10. The beam is diffracted by the grating producing the spectrum which then passes through the main camera lens (FL 100 mm) and on to the sensor in the attached camera. Light from the target that does not pass through the slit reflects off the disc and is routed through a pair of focusing lenses to the guide camera.

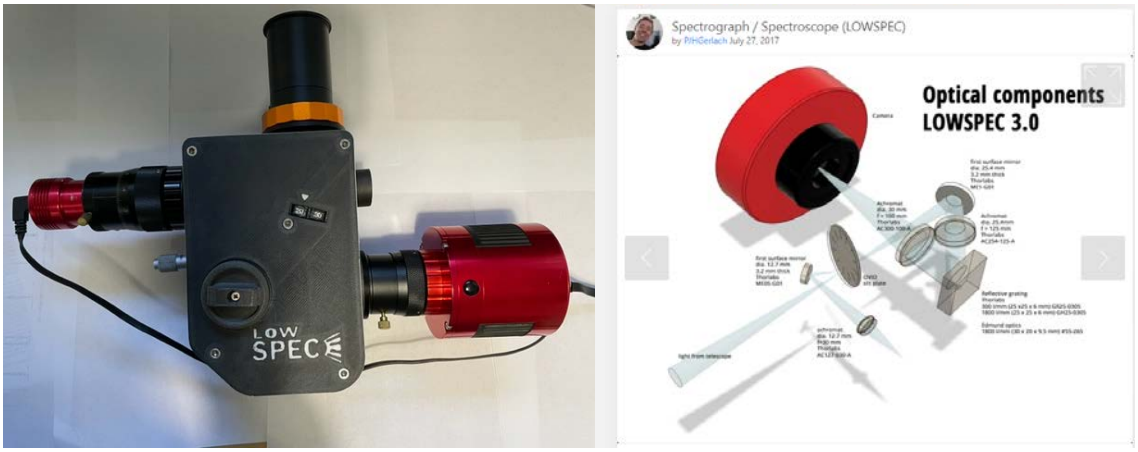

Figure 2. An assembled LowSpec, and a diagram of the optical path from the LowSpec Assembly Manual.

The interior of the LowSpec is complex (

Figure 3). The slit disc, which contains 12 radially arranged slits of varying widths, may be rotated without opening the device to switch from one slit to another. Each mirror and lens in the device has an adjustment feature, and the grating holder sits on a turntable. A micrometer is used to adjust the rotation of the turntable to alter the angle of the grating to the incoming beam, thus allowing the user to select the desired wavelength range that reaches the camera. An illuminator is inserted into the back of the box to help visualize the slit when aligning the guide camera. The grating holder, held in place by a magnet in its base, may be removed without opening the box, making grating changes quick and easy. Mounted on the back (not shown) of the LowSpec is an adjustment mechanism for the camera lens.

Figure 3. Interior of the LowSpec, and an illustration from the assembly manual (Gerlach 2021) showing how the grating is removed and replaced.

2.3 StarEx design and optical system

By comparison with the LowSpec, the StarEx is a simple device (

Figure *4*). It consists of a triangular box with its only moving part being the rotatable grating, adjusted by moving the large red wheel. The light beam from the telescope passes through the slit to the collimator lens located at the end of a tube. The collimator lens (FL 80 mm) is focused by adjusting the position of the tube in the collimator block. The now parallel light beam is diffracted by the grating and enters the camera lens on its way to the camera sensor. The camera lens, which may be either FL 80 or 125 mm, is focused externally by adjusting an add-on helical focuser. To replace the grating, it is necessary to unscrew the red wheel from the main box. The unit may then be lifted out and the grating replaced on that holder, or an alternative holder and wheel can be reinserted. The surface of a diffraction grating is easily ruined if the surface is touched. Therefore, this is a delicate operation and would only be done on a workbench.

Figure 4. A completed StarEx equipped with the same set of cameras as shown above with the LowSpec. The cut-away on the right shows the simplicity of the interior. The cut-away shows the Solex version which does not have a guide module.

Figure 5 is a view of the disassembled slit compartment. Replacing the slit requires great care. Alternative slits are available only from the vendor Shelyak, Inc. The spectroscope must be removed from the telescope, disassembled, and the slit holder either replaced or itself disassembled. This work must be done on the workbench.

Figure 5. Disassembly of the slit holding compartment of the StarEx; on the right, a close-up or the small parts holding the slit in place (no slit is present in this photo).

3. Cost

There are numerous alternative configurations of both devices, and individual builders are frequently reporting enhancements. This analysis therefore only addresses the base condition for both spectroscopes. The cost of labor and the 3D printer is not addressed here.

A typical spool of PETG filament sells for about $25, while the price for PETG with carbon fiber ranges from about $30 to $100, depending on the vendor and performance features. A standard spool of 3D printing filament contains 1 kg of material which is more than sufficient to produce a single device, even considering that misprints do happen and some parts have to be discarded and redone. A factor that may be overlooked by a new builder is that it will be necessary to purchase a larger quantity than needed of each size and type of screw, insert, etc., because of vendor packaging, thus increasing the overall cost of the project. A detailed listing of the hardware required for each device is provided in the Appendix. The cost estimates do not take this excess into account. The cost for hardware for each device is estimated to be about $140, most of which is related to helical focuser(s). For the guide camera on both devices, a helical focuser, which typically costs $50-$60, is not necessary, but users may find one convenient. The StarEx requires a helical focuser for the main camera while the LowSpec has a built-in focuser for the main camera lens.

The required optics and their cost as of this writing are presented in Table 1 and Table 2. The LowSpec's slit disc is only available from the French company Jeulin, Inc. Slits for the StarEx are only available from the French company Shelyak, Inc. Other components may be obtained from Thorlabs, Inc., Edmunds Scientific, or Shelyak, Inc., based on availability, taxes, and shipping costs. In most cases, the parts are equivalent from these sources, but there may be some subtle differences in lenses as described by C. Buil on his website.

Table 1. Optical parts list for the LowSpec. Prices as of Fall, 2022.

Part #	Supplier	Qty	Desc	unit cost	Total
AC127-030-A	Thorlabs	2	GUIDE LENSES 12.7 mm x 30 mm focal length	$ 66.00	$ 132.00
ME05-G01	Thorlabs	1	GUIDE MIRROR 1/2"	$ 18.00	$ 18.00
ME1-G01	Thorlabs	1	Main mirror	$ 34.00	$ 34.00
AC254-125-A	Thorlabs	1	COLLIMATOR LENS 25.4mm x 125 mm FL	$ 87.00	$ 87.00
GH25-18V	Thorlabs	1	HOLOGRAPHIC GRATING 1800 L/mm	$ 156.00	$ 156.00
GH25-0305	Thorlabs	0	ALT GRATING 300 L/mm	$ 126.00	$ -
GH25-0605	Thorlabs	0	ALT GRATING 600 L/mm	$ 126.00	$ -
GH25-1205	Thorlabs	0	ALT GRATING 1200 L/mm	$ 126.00	$ -
AC300-100-A	Thorlabs	1	STD OBJ LENS 30 mm x100 mm focal length	$ 99.00	$ 99.00
204012	Jeulin	1	slit disc (French company Jeulin.com/ovio_en/pr-193206.html)	$30.00	$ 30.00
			GRAND TOTAL, no tax or shipping included		$ 556.00

*Table 2. Optical parts list for StarEx from Shelyak, Inc. Prices as of Fall, 2022**

Part #	Qty	Desc	est. Cost
ES0031	1	STAREX HR OPTICAL KIT -est equiv $ from €485 (no VAT or shipping) includes 10u slit, 2400 L/mm holographic grating, 80 mm collimator lens, 125 mm objective lens, two guide lenses, 15 mm mirror for guide unit, a multi-slit 15-19-23-35	$ 485.00

*Most items can be obtained a la carte from other sources such as Thorlabs.

3. Performance

3.1 Theoretical performance

The theoretical performance of the two instruments may be compared using the so-called SimSpec V4 spreadsheet, developed by C. Buil, translated into English by Ken Harrison. This spreadsheet tool is available for download from C. Buil's web site (http://www.astrosurf.com/buil/us/compute/compute.htm). To create a fair comparison, values for a modest telescope system (8-inch F10 SCT scope, ASI183MM-Pro camera) were used in two arbitrary target scenarios. In the lower resolution case with a 600 L/mm grating (*Table **3***), the target star was of spectral type K5 and magnitude 8.0. In the high-resolution case (*Table **4***), the target star was of spectral type A0 and magnitude 6.0. In both cases, the exposure routine was six 600 second exposures for a total exposure time of 3600 seconds under Bortle 5 skies.

It will be noted that with the lower dispersion grating, the LowSpec outperformed the StarEx with an R value of 2,203 compared to 1,402, but had a corresponding lower signal-noise ratio. The wavelength range was greater for the LowSpec than the StarEx.

Table 3. Theoretical performance of the LowSpec and the StarEx spectroscopes using a low dispersion grating (600 L/mm) and a slit width of 20µm.

Target: VMag 8.0, Type K5	StarEx	LowSpec
Resolving power R	1402	2203
Reference wavelength, Å	5500	5500
Spectral resolution, Å	3.92	2.50
Wavelength range, Å	1745	2145
Grating-Lines/ mm	600	600
Grating-Diffraction order	1	1
Slit width, µm	20	20
Target Mag.	8.0	8.0
Signal/Noise (SNR/pixel)	422	328
Signal/Noise (SNR/$\Delta\lambda$)	1049	586

In the higher dispersion case using an 1800 L/mm grating in each, the LowSpec once again outperformed the StarEx, with an R value of 20,750 compared to 13,152. These effects are primarily the result of the more obtuse angle of incidence at the grating for the LowSpec (45°)

compared to the StarEx (34°). However, that wider angle prevents the use of a yet higher dispersion grating in the LowSpec. Where the StarEx really excels is with the very high dispersion grating with 2400 L/mm, and is capable of reaching a theoretical resolving power of 31,041. Even with the 19 µ slit, the 2400 L/mm grating yields an R of about 20,000.

Table 4. Theoretical maximum performance of the LowSpec and the StarEx spectroscopes using high dispersion gratings (1800 and 2400 L/mm) and a slit width of 10µm.

Target: VMag 6, Type A0	StarEx2400	StarEx1800	LowSpec
Resolving power R	31041	13152	20750
Reference wavelength, Å	6563	6563	6563
Spectral resolution, Å	0.21	0.50	0.32
Wavelength range, Å	344	547	700
Grating-Lines/ mm	2400	1800	1800
Grating-Diffraction order	1	1	1
Slit width, µm	10	10	10
Target Mag.	6.0	6.0	6.0
Signal/Noise (SNR/pixel)	142	195	224
Signal/Noise (SNR/$\Delta\lambda$)	261	436	353

3.2 Actual performance

Since theoretical performance is rarely achieved, several examples are presented to illustrate the actual performance of the two instruments. Two of the many examples provided by C. Buil on his website (http://www.astrosurf.com/solex/sol-ex-etoiles.html) are actual profiles obtained with the StarEx.

Figure 6 shows a profile for the star Deneb, acquired with a 600 L/mm grating and a 23 µm slit. The R value achieved was 1,350 at 4000 A, which was only slightly less that predicted by the spreadsheet.

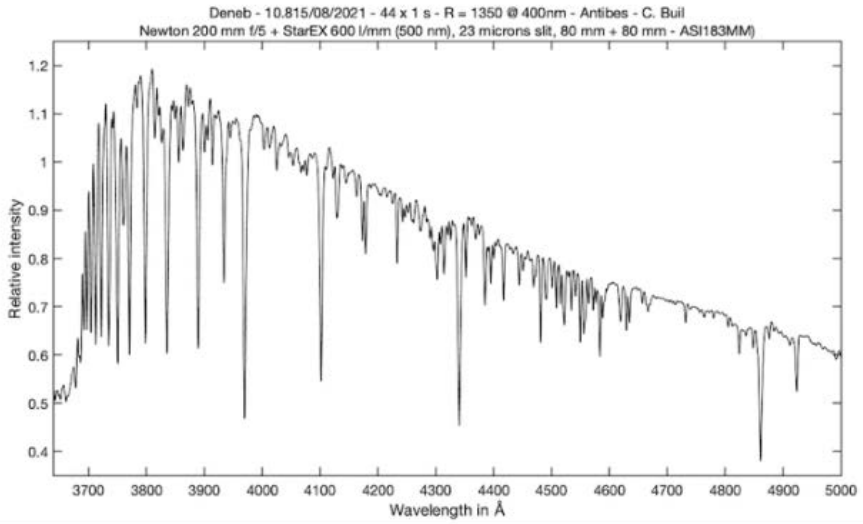

Figure 6. Spectral profile of Deneb using the StarEx with a 600 L/mm grating and a 23 µm slit. Source: http://www.astrosurf.com/solex/sol-ex-etoiles.html

A resolving power of 6,000 was achieved by the StarEx when using a 2400 L/mm grating as shown in

Figure *7* as presented by C. Buil on his website. In this case, the slit width was 23 µm, and the focal length of the objective lens was 80 mm rather than the standard focal length of 125 mm.

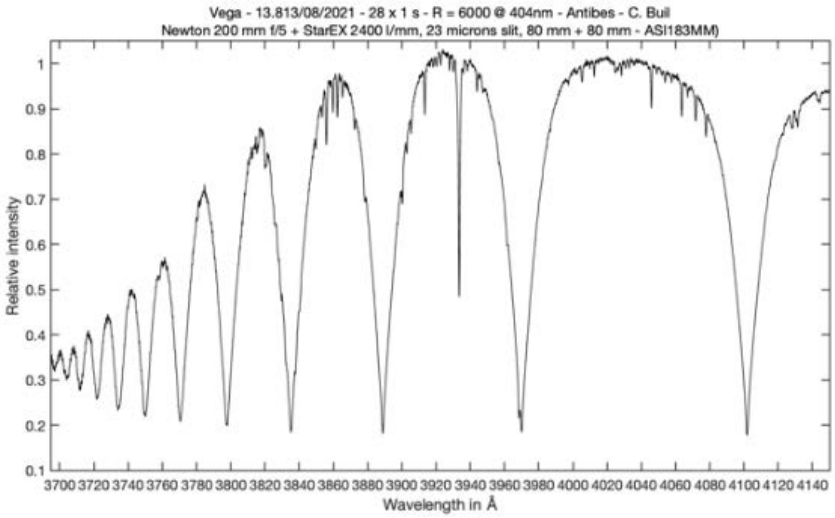

Figure 7. Spectral profile of Vega using the StarEx with a 2400 L/mm grating and a 23 µm slit. Source: http://www.astrosurf.com/solex/sol-ex-etoiles.html

This author acquired profiles of Vega using a C8 telescope on different nights during the second week of October 2022. The line at 4483 Å had an R = 2,318 for the StarEx, while the same line with the LowSpec had an R of 2,764. Figure 8 shows the two profiles using the same 600 L/mm grating and the same telescope. These values could be affected by the focus quality of the camera.

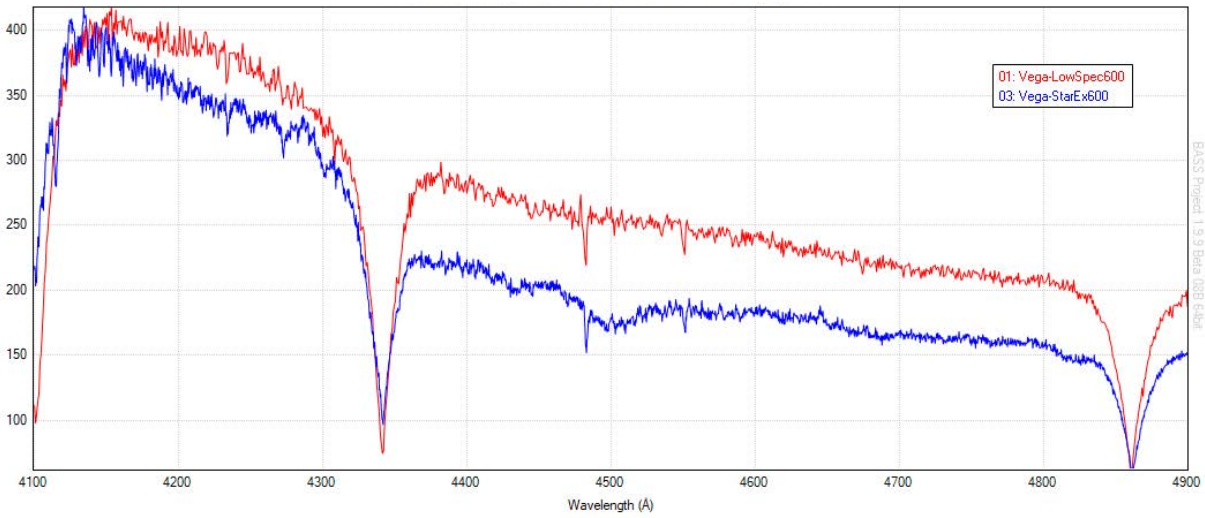

Figure 8. Corresponding profiles acquired using the same telescope system with each of the two spectroscopes and a 600 L/mm grating.

Presented in *Figure 9* are profiles of Vega at a higher level of dispersion, with the LowSpec using a 1800 L/mm grating (20µ slit) and the StarEx using a 2400 L/mm grating (19µm slit). Using neon calibration images (not shown), resolving power was determined for both instruments. For the StarEx-2400, this combination yielded an R of 18,140 (@ 6599 Å), while the LowSpec-1800 had an R of 10,789 (@ 6532 Å). These values could be affected by the focus quality of the camera.

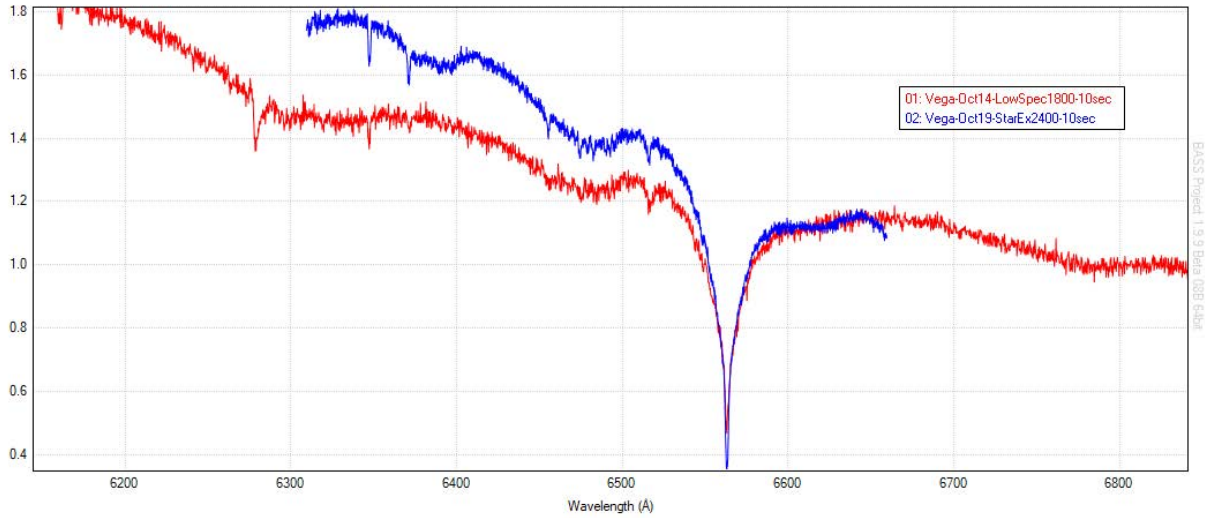

Figure 9. High resolution profiles of Vega acquired using the same scope: the LowSpec with an 1800 L/mm grating (20µm slit) and the StarEx with a 2400 grating (19µm slit).

4. Summary and Conclusions

On first impression, these two devices look quite different. However, upon more thorough examination, they perform the same functions in quite similar fashion. Certain conclusions can be drawn, but the decision to select one design over another will depend on user preferences.

1. 3D Printing (essential components, mass and time dependent on slicer settings):
    - LowSpec: 25 parts, 42 hrs print time, 597g
    - StarEx: 21 parts, 39 hrs print time, 477g
2. Cost: about $600 to $700 in most basic configuration, and depending on VAT and other taxes, shipping costs, etc.
3. Complexity: StarEx is simpler than LowSpec, requires fewer adjustments, therefore fewer failure points.
4. Micrometer adjustment of LowSpec grating gives more precise control than with the StarEx.
5. The LowSpec can be reconfigured quickly and more easily (slit and grating change); the LowSpec also has a built-in illuminator to visualize the slit.
6. Neither device incorporates a calibration lamp. Some users are developing calibration units; good advice is provided by C. Buil at http://www.astrosurf.com/solex/specinti1_en.html for alternative calibration techniques.
7. The guide image appears less distorted in the StarEx guide unit than the guide image in the LowSpec.
8. Performance (resolution):
    - The LowSpec out-performs the StarEx with gratings less than or equal to 1800 L/mm.
    - The StarEx can utilize a 2400 grating which is not possible in the LowSpec, and thus may achieve R > 30,000!
9. Popularity and acceptance:
    - Unknown numbers of each have been built; C. Buil's reputation and extensive website seems to have led to a surge of interest in the Solex/StarEx.

Acknowledgements

Paul Gerlach of The Netherlands provided direct assistance to this author throughout the process of creating the author's LowSpec, and he was very responsive to inquiries and questions.

Christian Buil of France is probably the most energetic, knowledgeable, and creative amateur spectroscopist in the world. He has provided vast reservoirs of knowledge to the public for free on his extensive system of websites, and he has also starred in many instructional videos which are available on YouTube (in French, but most available with English subtitles).

Robin Leadbeater of the United Kingdom provided valuable assistance in evaluating spectra and provided recommendations on how to improve profile quality.

References

Buil, C., 2022. The Solex/StarEx: http://www.astrosurf.com/solex/

Gerlach, P. 2021. LowSpec Assembly Instructions. PDF file available at: https://www.thingiverse.com/thing:2455390

Shelyak, Inc. http://shelyak.com

Trypsteen, M.F.M and Walker, R. 2017. *Spectroscopy for Amateur Astronomers: Recording, Processing, Analysis, and Interpretation*, Cambridge University Press, Cambridge, UK.

Appendix: Parts Lists and Print Times

Table A1. StarEx parts list

	Print time		
StarEx Parts	**hours**	**min**	**mass (g)**
collimator block	4	32	59
lower body	5	54	79
upper body	7	20	100
grating holder		52	10
grating tab		6	1
grating wheel	1	29	21
telescope interface	1	10	12
ring-collimator		13	2
ring-objective		11	2
ring-#13		25	6
slit holder		39	9
stiffener	1		15
tube-collimator	1	26	21
tube-objective	2	8	32
guide box	3	35	39
guide lens holder	1	9	12
mirror support		50	9
guide washer		17	1
guide camera ring		59	15
lens spacer		3	1
Guide camera holder	4	25	31
21 parts	30	523	477
	38.7	=total hours	

	Print time		
LowSpec Parts	**hours**	**min**	**mass (g)**
Lid	6	45	111
body	20	19	291
autoguide tube		59	16
camera T2		25	6
telescope T2		16	4
grating holder	1	30	21
turn table	1	8	14
grating cap		44	10
holder collimator lens		31	5
holder camera lens		19	4
main mirror holder		22	5
focuser railholder-a		38	8
railholder-b		42	9
focuser slider	1	17	16
focuser shield		56	15
holder guide lens a		20	3
holder guide lens b		12	2
juelin guide plat	2	18	31
slit illuminator		6	1
slit disc holder		42	7
lock ring		3	1
lock plate		9	2
guide mirror holder		46	10
guide mirror slider		19	3
backlight adapter ring		10	1
backlight plug		6	1
25 parts	31	662	597
	42.0	=total hours	

Table A2. StarEx hardware parts list

29	**Hardware parts list StarEx**					
30	Part		Qty	Desc	unit cost	Total
31	Guide unit and threaded plate		7	screw-3mm x 10mm Phillips	$0.10	$0.70
32	Grating wheel		3	screw-3mm x 10mm Phillips	$0.05	$0.15
33	slit disc holder		4	screws 2mm x 10 mm	$0.10	$0.40
34	Collimator block		5	screws-4mm x 12mm	$0.10	$0.50
35	Main body		2	screws-4mm x 12mm	$0.10	$0.20
36	Grating wheel		2	screws-4mm x 12mm	$0.10	$0.20
37	Collimator block		1	screws-4mm x 16mm	$0.10	$0.10
38	Main body		5	screws-4mm x 40mm	$0.36	$1.82
39	Main body		2	screws-4mm x 60mm with locking nuts	$0.60	$1.20
40	Guide unit and threaded plate		4	screws-4mm x 60mm	$0.50	$2.00
41	Collimator block		10	threaded inserts - 4mm	$0.06	$0.60
42	Camera focusing tube		2	screws-4mm x 10mm	$0.10	$0.20
43	lock ring-red		1	screws-4mm x 10mm	$0.10	$0.10
44	lock ring-black		1	screws-4mm x 10mm	$0.10	$0.10
45	Main body		11	threaded inserts - 4mm	$0.06	$0.66
46	Guide unit and threaded plate		7	threaded inserts-3mm	$0.06	$0.42
47	Guide camera holder		3	thumb screws-4 mm x 10 mm	$2.00	$6.00
48	Collimator block		6	washers-4mm	$0.05	$0.30
49	Main body		9	washers-4mm	$0.05	$0.45
50	Grating wheel		2	washers-4mm	$0.05	$0.10
51				Fastener sub-total (no shipping or tax)		$16.20
52						
53			1	T adapter-T2 x 1.25"	$12.00	$12.00
54			1	T2 extension ring 10 mm (for guide camera)	$10.00	$10.00
55			1	Helical focuser for science camera	$59.00	$59.00
56			1	PETG-CF filament roll	$40.00	$40.00
57				Hardware and parts total		$137.20

Table A3. LowSpec hardware parts list

Hardware parts list LowSpec					
Supplier		Qty	Desc	unit cost	Total
McMaster Carr		5	hex socket cap screw M4x60mm		
		1	Phillips screw M3x25mm		
		2	Phillips screw M3x20mm		
		4	Phillips screw M3x16mm		
		3	Phillips screw M3x12mm		
		5	Phillips screw M3x10mm		
		4	M4 threaded inserts		
		5	M4 lock nuts		
		5	M3 lock nuts		
		10	M4x10mm Allen grub screws		
		6	M4x6mm Allen grub screws		
		1	M6x6mm Allen grub screw		
		1	Knurled screw M3x30mm		
Amazon			Estimate collective cost for screws and nuts, highly variable		$50.00
		1	ball-point-pen spring		$0.00
		1	Coil spring 7.5x35	$1.00	$1.00
Harbor Freight		1	Extension spring 5x18x0.45mm	$1.00	$1.00
		1	steel ball 5 mm diameter	$0.50	$0.50
		1	Ball bearing 625ZZ	$10.00	$10.00
Lowes		2	8x2mm Neodymium magnets	$2.00	$4.00
		1	M5x25mm round coupling nut	$1.00	$1.00
		1	Aluminum tube 6x55mm	$1.00	$1.00
Amazon		1	Micrometer, travel 1-13mm, diameter 9.5mm	$20.00	$20.00
		1	T adapter-T2 x 1.25"	$12.00	$12.00
ZWO, Agena Astro		0	Helical focuser (optional for either camera)	$59.00	$0.00
various		1	PETG-CF filament roll	$40.00	$40.00
			Hardware and parts total		$140.50

Motivation, Public Health Improvement, Developing Friendly Relations among Nations, and Promotion of Science through Teaching Astronomy and Variable Star Observation by the AAVSO and Volunteers

Mehdi Esmaili

https://www.linkedin.com/in/mehdi-e ; mehdi.esm.4@gmail.com

Keywords

AAVSO; AAVSO 111th Annual Meeting; astronomy; observation; variable star observation; teaching; learning; volunteer; volunteering; school; university; hospital; rehabilitation; cancer, United Nations; UNESCO; Wall Street; motivation; public health; friendly relations among nations.

Abstract

Peace, happiness, and life expectancy are the characteristics of a healthy society. Any life pressure, loneliness, financial problems, depression, and despair can lead to quick and dangerous decisions with very high financial and social costs, both for the individuals and for society. Meanwhile, children, the elderly, the poor, and people with social problems or severe diseases such as cancer are more vulnerable psychologically. At the same time, there are always plenty of talented students in schools and universities who welcome an interesting scientific idea for activity and research as excellent volunteers. During ten years of volunteer teaching basic astronomy concepts with night sky observation sessions publicly in various places including schools, universities, hospitals, rehabilitation centers, and parks, these programs have always been very well received by the audience, and this is a cost-effective care strategy that brings more positive energy into life. People, including patients and the elderly, usually report positive emotions, and higher life expectancy, as well as increasing desire to continue treatment and recovery along with a significant reduction in treatment costs. Usually about five to ten percent of these people will be interested in more advanced levels and more serious activities. The next step is to introduce the AAVSO, and let them know about the variable star observation, and its attractive scientific applications by volunteers as ambassadors for the AAVSO. Observing the night sky is relaxing. Cooperation and community of variable star observers from different countries also develops friendly relations among nations.

1. Introduction

A little above the ground, no border between cities and countries can be seen from the sky. It seems the Earth is a sphere with a unified civilization on it. From space, Earth is a Pale Blue Dot (Image 1).

Variable star observers from different countries around the world are working with great coordination and cooperation to collect and record scientific data in an integrated system that is

created by the AAVSO. Variable star observation is a serious scientific activity by international volunteers, written in the language of peace and love that develops unity and friendly relations among nations.

Image 1. The Pale Blue Dot is a photograph of Earth taken Feb. 14, 1990, by NASA's Voyager 1 at a distance of 3.7 billion miles (6 billion kilometers) from the Sun (Image credit: NASA)

> *"From this distant vantage point, the Earth might not seem of any particular interest. But for us, it's different. Consider again at that dot. That's here. That's home. That's us."*
>
> – Carl Sagan [1]

2. Why Astronomy and Variable Star Observation?

Of all types of motivational activities, night sky observation and astronomy are among the most attractive and influential for all ages. Basic concepts of astronomy are very attractive and easy to learn. Topics include observing the beauty of the night sky, constellations, the solar system, lunar phases, tides, solar eclipses, lunar eclipses, what causes days and nights, what causes Earth's seasons, evidence that the Earth is round, planet Earth, other planets, the stars, nebulae, galaxies, comets, and meteors, are very interesting for all people.

Serious and purposeful people are attracted to serious and purposeful activities. Because a small portion of people want to know more about astronomy, variable star observation is suggested as a good choice because interested people can easily learn and make genuine contributions to scientific research and discovery.

3. Variable Stars and What are Variable Star Observations

"A variable star is a star whose brightness as seen from Earth (its apparent magnitude) changes with time. This variation may be caused by a change in emitted light or by something partly blocking the light, so variable stars are classified as either:

1. Intrinsic variables, whose luminosity actually changes, for example, because the star periodically swells and shrinks.
2. Extrinsic variables, whose apparent changes in brightness are due to changes in the amount of their light that can reach Earth; for example, because the star has an orbiting companion that sometimes eclipses it." (From Wikipedia, [2])

"The most common kinds of variability involve changes in brightness, but other types of variability also occur, specifically, changes in the spectrum. By combining light curve data with observed spectral changes, astronomers are often able to explain why a particular star is variable. Variable stars are generally analysed using photometry, spectrophotometry, and spectroscopy. Measurements of their changes in brightness can be plotted to produce light curves. For regular variables, the period of variation and its amplitude can be very well established. Amateur astronomers can do useful scientific study of variable stars by visually comparing the star with other stars within the same telescopic field of view of which the magnitudes are known and constant. By estimating the variable's magnitude and noting the time of observation a visual light curve can be constructed. The American Association of Variable Star Observers (AAVSO) collects such observations from participants around the world and shares the data with the scientific community." (From Wikipedia, [3])

4. About the AAVSO

Image 2. AAVSO logo (image credit: https://www.aavso.org)

Since its founding in 1911, the American Association of Variable Star Observers (AAVSO) has coordinated, collected, evaluated, analyzed, published, and archived variable star observations made largely by amateur astronomers and makes the records available to professional astronomers, researchers, and educators. These records establish light curves depicting the variation in brightness of a star over time. Since professional astronomers do not have the time or the resources to monitor every variable star, astronomy is one of the few sciences where amateurs can make genuine contributions to scientific research. During 2011, the 100th year of the AAVSO's existence, the 20-millionth variable star observation was received into the database. The AAVSO International Database (AID) stores over 35 million observations as of 2019. The organization receives nearly 1,000,000 observations annually from around 2,000 professional and amateur observers and is quoted regularly in scientific journals. The AAVSO is also very active in education and public outreach. They routinely hold training workshops for citizen science and publish papers with amateurs as coauthors. [4]

The mission of the AAVSO is to enable anyone, anywhere, to participate in scientific discovery through variable star astronomy. [5] After more than a century of successful activity, the AAVSO has developed multilingual educational facilities and content for teaching variable star observation and its data registration; and if they wish and receive enough support, they can lead and manage volunteers for general teaching of astronomy from basic concepts to variable star observation.

The participation and cooperation of scientists and observers from all over the world in the AAVSO and their communication and sharing in the AAVSO's forum and events provide a great opportunity, not only for the development of science and discovery, but also to develop friendly relations among nations.

5. Applications of Variable Star Observation

"The science of variable star astronomy teaches us about one important part of the universe – the stars. Stars are the primary engines of cosmic evolution, particularly in the creation of elements heavier than hydrogen and helium which make up us and the world that we live in. Further, stars and their systems of planets are the only likely places we will find life in the universe; by studying stars (including our own Sun), we are also learning about possible abodes for life. Research on variable stars is important because it provides information about stellar properties, such as mass, radius, luminosity, temperature, internal and external structure, composition, and evolution. Some of this information would be difficult or impossible to obtain any other way. In many cases, it is the nature of the variability that provides the clues to the answers. This information can then be used to understand other stars." (From AAVSO web site, [6])

"Variable stars play a crucial role in our understanding of the universe. Cepheid variables have played a major part in determining distances to far-away galaxies and determining the age of the Universe. Mira variables give us a glimpse into the future evolution of our own star, the Sun. Accretion disks in cataclysmic variables help us to understand larger scale disk behaviour, such as the activity inside active galaxies with supermassive black holes. Supernovae have led us to the surprising realization that the expansion of the Universe is accelerating. Even the search for extra-terrestrial life is illuminated by variable stars. Transiting extrasolar planets provide clues into the processes of planetary formation, and the very stuff life as we know it is made of comes from the hearts of stars that explode in the final stages of their evolution." (From AAVSO web site, [6])

6. Other applications of variable star observation

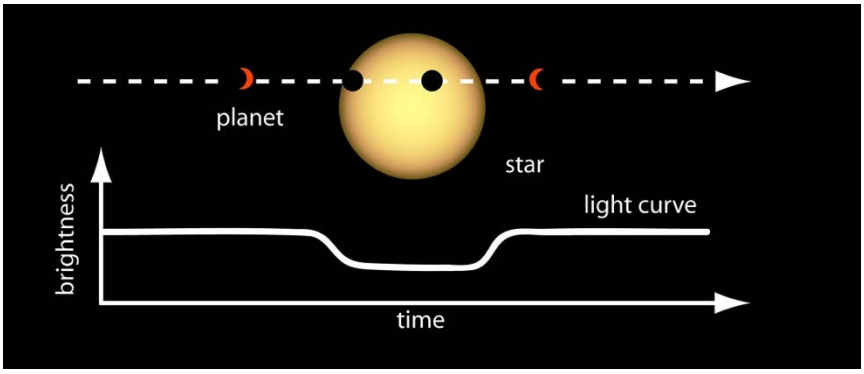

Image 3. Light Curve of a Planet Transiting Its Star (image credit: NASA Kepler and K2)

"Stars with planets may also show brightness variations if their planets pass between Earth and the star. These variations are much smaller than those seen with stellar companions and are only detectable with extremely accurate observations. Examples include HD 209458 and GSC 02652-

01324, and all of the planets and planet candidates detected by the Kepler Mission." (From Wikipedia, [7])

"Transit data are rich with information. By measuring the depth of the dip in brightness and knowing the size of the star, scientists can determine the size or radius of the planet. The orbital period of the planet can be determined by measuring the elapsed time between transits. Once the orbital period is known, Kepler's Third Law of Planetary Motion can be applied to determine the average distance of the planet from its stars." (From NASA Kepler web site, [8])

In addition to the application of variable star observation in the discovery of exoplanets, variable star observers also have the chance to discover phenomena such as new supernovae and comets.

7. Science promotion and public health improvement

7.1. For children

Night sky observation is very amazing for children, especially telescopic observation of the moon, Jupiter, and Saturn. Children are always eager to learn. Learning basic concepts of astronomy helps them to plan for the future, and to have an even better understanding of school subjects and their applications, especially mathematics, physics, chemistry and biology. They may even become interested in variable star observation. In the future, maybe they will decide to study astrophysics, or astrochemistry, or astrobiology in university, or maybe they will choose computer programming, or professional photography and astrophotography as a job, or maybe they will choose something completely different. The truth is that astronomy would be a basis for their familiarity with different sciences and professions, and they will have more opportunities for innovation and creativity.

7.2. For young people

Whether at home, school, university, hospital, rehabilitation center or even in prison, young people either have a lot of free time or they are very busy because they are surrounded by different ideas and plans. In any case, observing the night sky and astronomy is attractive and relaxing for them, and if they get interested in variable star observation, they can be serious and reliable observers and even eager and productive volunteers.

7.3. For the elderly

Having free time and a great desire to feel useful in society is one of the characteristics of most elderly people. Elderly people in hospitals and rehabilitation centers usually have more free time and enthusiasm to do fun and useful things, especially if these activities have a scientific and humanitarian aspect. After learning basic concepts of astronomy and observing the beauty of the night sky, they usually request question-and-answer sessions. Those interested in more advanced levels are good candidates to learn and to start observing variable stars.

7.4. In schools and universities

Schools and universities are the best places to attract serious volunteers, both for holding night sky observation sessions and for teaching astronomy, and as variable star observers. This is a good opportunity for current students and future scientists to improve their social, communication and teamwork skills as well as research, innovation, and creativity.

7.5. In hospitals and rehabilitation centers

Feeling alone, being forgotten or abandoned, illness, despair and depression – This is what most people in hospitals and rehabilitation centers experience more or less. They also have a lot of free time along with a strong desire to feel useful in society.

In addition to many problems for patients with cancer and severe diseases, such as suffering from disease and the high costs of access to appropriate treatment and medicine, which puts pressure on patients and their families, sometimes patients are not able to attend classes in the classroom. Therefore, serious concern about their future and fate after recovery is also formed in their minds.

Participating in night sky observation sessions and learning basic concepts of astronomy, even once, can increase positive emotions and helps patients to use their free time for study and useful scientific activities instead of focusing only on their illness. Moreover, those interested in more advanced levels are good candidates to learn and to start observing variable stars to enjoy its benefits for a long time. These benefits can be associated with more positive energy, reducing death anxiety and increasing happiness, improving quality of life, and more willingness to continue treatment, thereby reducing duration of treatment for patients, less need for medication, and reducing costs.

7.6. Insurance for insurers (and a proposal for a case study)

Any plan related to reduction in healthcare costs is associated with greater profitability for insurance companies. Every dollar they pay to sponsor these plans can save them more dollars in the future.

As mentioned in Section 7.5, participating in night sky observation sessions and learning basic concepts of astronomy, even once, can increase positive emotions and decrease healthcare costs. But by how much? Let's propose a case study. For example, let’s consider Kaiser Permanente.

Kaiser Permanente, commonly known as Kaiser, is an American integrated managed care consortium, based in Oakland, California, United States, founded in 1945. Kaiser Permanente is one of the largest non-profit healthcare plans in the United States, with over 12 million members. It operates 39 hospitals and more than 700 medical offices, with over 300,000 personnel, including more than 87,000 physicians and nurses. [9]

In one of their hospitals, it is possible to hold sessions on observing the beauty of the night sky, teaching the basic concepts of astronomy, and then variable star observation for interested patients, by volunteers. The positive results can be collected, investigated, and compared with other hospitals. Even patients with cancer or cardiovascular diseases can be good candidates to participate and enjoy the benefits of this plan.

7.7. Wall Street

In the case of companies, employees, and their families, they could also participate in teaching sessions by volunteers on the basic concepts of astronomy and observing the beauty of the night sky. As a suggestion, it could be considered as a paid service based on mutual benefits. This would be a low-cost hobby for company employees with a lot of benefits for themselves and their families and would also provide a small amount of financial support for volunteers.

8. Science Promotion and Developing Friendly Relations among Nations

8.1. United Nations

Image 4. Flag of the United Nations (image credit: https://www.un.org)

The United Nations (UN) is an intergovernmental organization whose stated purposes are to maintain international peace and security, develop friendly relations among nations, achieve international co-operation, and be a center for harmonizing the actions of nations. [10]

The United Nations Economic and Social Council (ECOSOC) is one of the six principal organs of the United Nations, responsible for coordinating the economic and social fields of the organization. Over 1,600 nongovernmental organizations have consultative status with the Council to participate in the work of the United Nations. [11] The AAVSO could have consultative status with the Council to participate in the work of the United Nations too, because both have one role in common: to develop friendly relations among nations.

Variable star observation inspires people in peacekeeping and motivates them to international cooperation in promoting science for people of all colors, races, and nationalities.

8.2. UNESCO

Image 5. UNESCO logo (image credit: https://www.unesco.org)

"The United Nations Educational, Scientific and Cultural Organization (UNESCO) is a specialised agency of the United Nations (UN) aimed at promoting world peace and security through international cooperation in education, arts, sciences, and culture. UNESCO's founding mission is to advance peace, sustainable development, and human rights by facilitating collaboration and dialogue among nations. It pursues this objective through five major programme areas: education, natural sciences, social/human sciences, culture, and communication/information. UNESCO sponsors projects that improve literacy, provide technical training and education, advance science, protect independent media and press freedom, preserve regional and cultural history, and promote cultural diversity." (From Wikipedia, [12])

Natural science can be divided into two main branches: life science and physical science. physical science is subdivided into branches: physics, chemistry, Earth science, and astronomy. [13]

AAVSO and UNESCO can cooperate in many fields. UNESCO can also sponsor variable star observation and AAVSO projects.

9. Conclusions

Over the years, the following experimental results have been observed during volunteer holding night sky observation and astronomy teaching sessions in various places such as schools, universities, hospitals, rehabilitation centers and even on the streets for people of all ages:

1. Participating in the night sky observation sessions and learning basic concepts of astronomy, even once, can increase positive emotions, life expectancy, and getting away from sadness.
2. Observing the night sky and astronomy is relaxing and humbling. It is associated with the development of peace and friendship too.
3. Knowing that the universe is so vast and that we are made of stardust comes with a sense of greatness.

4. Understanding the fact that everything in the world has a limited life is associated with a decrease in death anxiety and an increase in happiness.
5. Getting to know that space is a very harsh and dangerous environment for life is inspiring people to resist and bear the hardships of life.
6. At any level, a cell, human body or the planet Earth, life is a complicated phenomenon and understanding it motivates people to appreciate the value of life better.
7. Observing the beauty of the night sky even once (especially using a telescope or binoculars), or variable star observation as a continuous activity, is so relaxing that can be associated with reducing the need to use of sedatives, painkillers and sleeping pills in some people and can reduce the cost of treatment and healthcare. In the case of some elderly, cardiovascular and cancer patients who often have a history of sadness or depression, it may be associated with a decrease in mortality. Note that these are not general rules. Measuring and providing more detailed information requires specialized research.
8. The participation and cooperation of scientists and observers from all over the world in the AAVSO and their communication and sharing in the AAVSO's forum and events is a great opportunity, not only for the development of science and discovery but also to develop friendly relations among nations.

Acknowledgements

Many thanks to my parents, all the volunteers, and those who supported me in various ways over the years. I would also like to express my sincere thanks to all AAVSO's volunteers, members, and staff, especially Lindsay Ward and Joyce Ann Guzik, for their great support in preparing this paper.

References

1. Sagan, Carl. 1997. *Pale Blue Dot*, United States: Random House USA Inc. p. 6-7. ISBN 9780345376596.
2. Wikipedia. *Variable star – Wikipedia*, Accessed October 27, 2022. https://en.wikipedia.org/wiki/Variable_star.
3. Wikipedia. *Variable star – Wikipedia*, Accessed October 27, 2022. https://en.wikipedia.org/wiki/Variable_star#Detecting_variability.
4. Wikipedia. *American Association of Variable Star Observers – Wikipedia.* Accessed October 27, 2022. https://en.wikipedia.org/wiki/American_Association_of_Variable_Star_Observers.
5. AAVSO. *Slogan*, https://www.aavso.org. October 2022.
6. AAVSO. *Variables: What Are They and Why Observe Them? - AAVSO.* Accessed October 27. 2022. https://www.aavso.org/variables-what-are-they-why-observe-them#:~:text=Research%20on%20variable%20stars%20is,to%20obtain%20any%20other%20way.
7. Wikipedia. *Variable star – Wikipedia.* Accessed October 27, 2022. https://en.wikipedia.org/wiki/Variable_star#Planetary_transits.

8. NASA. *Light Curve of a Planet Transiting Its Star*, https://www.nasa.gov/mission_pages/kepler/multimedia/images/transit-light-curve.html. Accessed October 27, 2022.
9. Wikipedia. *Kaiser Permanente – Wikipedia.* Accessed October 28, 2022. https://en.wikipedia.org/wiki/Kaiser_Permanente.
10. Wikipedia. *United Nations – Wikipedia.* Accessed October 28, 2022. https://en.wikipedia.org/wiki/United_Nations.
11. Wikipedia. *United Nations Economic and Social Council – Wikipedia.* Accessed October 28, 2022. https://en.wikipedia.org/wiki/United_Nations_Economic_and_Social_Council.
12. Wikipedia. *UNESCO – Wikipedia.* Accessed October 28, 2022. https://en.wikipedia.org/wiki/UNESCO.
13. Wikipedia. *Natural science – Wikipedia.* Accessed October 28, 2022. https://en.wikipedia.org/wiki/Natural_science.
14. Esmaili, Mehdi (2022). *Announcement of successful completion of one of my volunteer projects*. LinkedIn. Accessed October 30, 2022. https://www.linkedin.com/posts/activity-6941048957850533888-RBK-/

Appendix: About the Author

Because of his father's job, the author has experienced working as a volunteer with the International Committee of the Red Cross since childhood. In 2012, the author started a volunteer project to help treat patients with cancer or severe disorders by motivating and life expectancy. The main goal of this non-profit humanitarian research project is motivation, creating perspective, and hope for the future in the minds of patients to take them away from frustration and depression in order to be stronger in treatment as well as in life.

In order to motivate people, they were given the opportunity to participate in a series of training programs and attractive activities including: Training school lessons, extracurricular activities, sports, astronomy and night sky observation, photography, astrophotography, music, computer programming, robotics, and electronics to create positive energy and even jobs for patients. On a small scale with a limited number of patients with diseases such as cancer, epilepsy, hepatitis and HIV, this program has been tested with positive and satisfactory experimental results. We are ready to start on a large scale.

The author will try to publish the results over time in the form of scientific papers or simple guidelines based on the case studies in each disease and age category. Related organizations, medical and rehabilitation centers, hospitals, volunteers, and patients all over the world should learn about these types of cost-effective motivational activities, details, and their amazing impacts on creating good feeling and positive energy to improve the quality of life as well as faster treatment. [14]

Together stronger.

A Visit to a Few High-Amplitude Delta Scuti Stars

Joyce A. Guzik[1], Richard Wagner[2], Karen Kinemuchi[3], Ebraheem Farag[1,4], Michael S. Soukup[5], Melissa Rasmussen[1], and Philipp V. F. Edelmann[1]

[1] Los Alamos National Laboratory, Los Alamos, NM 87545; joy@lanl.gov
[2] Leeside Observatory, Elgin, ON Canada
[3] New Mexico State U., Las Cruces, NM 88003
[4] Arizona State U., Tempe, AZ 85287
[5] Los Alamos National Laboratory, retired

Subject Keywords

High-Amplitude Delta Scuti Stars (HADS); stars: evolution; stars: pulsation; stars: individual (V1965 Aql, LS Cet, RV Ari, DDE 148)

Abstract

We present results from Johnson B-band photometry of four high-amplitude delta Scuti (HADS) stars--two fundamental-mode pulsators, V1965 Aql and LS Ceti, and two double-mode pulsators, RV Ari and DDE 148. For the latter two stars, the photometry shows additional frequencies, including low frequencies less than 5 cycles per day that may be non-radial gravity-mode pulsations. These stars were also observed as part of the ASAS-SN survey, and three out of four stars have been observed by the *TESS* spacecraft. We are using the MESA code to model the evolution and pulsations of these stars. We hope to contribute to resolving some of the outstanding problems surrounding delta Scuti pulsations, such as mode selection and amplitudes, causes of amplitude and period changes, and the driving mechanism for low-frequency pulsations.

1. Introduction

High-amplitude delta Scuti (HADS) stars are post-main-sequence stars with late-F through early A spectral type and masses 1.5 to 2.5 solar masses which pulsate in the fundamental (F) and/or first overtone (1O) radial modes with amplitudes greater than 0.15 V-band magnitude (Watson et al. 2006). Like other delta Scuti stars, the periods of HADS stars are typically a few hours.

Space-based photometric data from, e.g., the NASA *Kepler* mission (Borucki et al. 2010, Gilliland et al. 2010) have shown that many HADS stars pulsate in additional non-radial modes, and that HADS are located throughout the instability strip at earlier evolutionary stages, so may not be distinct as a class from normal delta Scuti stars[1] (Balona 2016). There are many outstanding questions for delta Scuti stars, such as the reasons for mode selection and amplitudes, causes of

[1] Balona 2016: "there is no physical attribute that defines a HADS apart from some arbitrary amplitude limit."

amplitude and period changes, and the origins of low frequencies (< 5 c/d) associated with non-radial gravity modes seen in many of these stars (see review by Guzik 2021).

HADS stars provide excellent targets for amateur observing because of their high amplitudes and short pulsation periods. Here we visit several delta Scuti stars which are targets of our ground-based observing program: 1) V1965 Aql, which shows a single period of 0.137 d; 2) LS Cet, the brightest and coolest of the four stars, with main period 0.0842 d; 3) RV Ari, a double-mode pulsator with a first-overtone to fundamental-mode amplitude ratio of 30%; and 4) DDE 148, another double-mode pulsator which is also an eclipsing binary candidate.

We use Period04 (Lenz and Breger 2005) to derive pulsation frequencies and amplitudes from the light curves. Taking into account additional constraints from photometry and spectroscopy, we model the evolution and pulsations of these stars using the open-source MESA (Paxton et al. 2019; Jermyn et al. 2022) and GYRE (Townsend and Teitler 2013) codes. We also apply the radial stellar pulsation (RSP) capability in MESA to model the hydrodynamics of radial pulsations of the stellar envelopes.

2. Observational Results

We summarize observational results by R. Wagner in the Johnson B band for these four HADS stars. The targets were observed using a Meade 0.25m Schmidt-Newtonian telescope with camera (field 61 x 46', 1.1"/pixel). All images were reduced for bias, dark, and flats using the AstroPy ccdproc package. Differential magnitudes were obtained using the multi-aperture photometry tool in AstroImageJ. A fixed aperture radius was used for each image equal to 2.5 times the full-width half-maximum (FWHM) of the target star on that image.

For V1965 Aql, photometry was done using an ensemble of 28 stars of approximately the same color as V1965 Aql, constructed from APASS DR9 (https://www.aavso.org/apass). The data set comprised 391 photometric observations, spanning 67 Julian days. The only frequencies found in the light curve were the fundamental mode and four of its harmonics.

For LS Cet, both B and V data were taken, 151 observations in each color spanning 59.8 Julian days. Photometry was performed against an ensemble of 4 stars from AAVSO chart X26893AD, all having similar color to LS Cet. Magnitudes were transformed to Johnson standard B and V magnitudes using previously measured transformation coefficients. This process resulted in somewhat increased scatter in the observations compared with the other stars. Only the fundamental mode and 3 of its harmonics were found in the B data, with a somewhat large remaining residual.

For RV Ari, B-band photometry was done using an ensemble of 5 stars from AAVSO chart X28148CDV, all with roughly the same color as the target. The data set comprised 187 observations spanning 13 Julian days. The Period04 analysis showed 10 frequencies, 6 of which could be identified as the fundamental and first overtone and their harmonics or combinations. However, four other frequencies, including a low frequency at 4.16 c/d, are not associated with

the F or 1O modes, and could be separate modes. The amplitude of the 1O mode is about one third as large as large as the F-mode amplitude, making this an interesting star for modeling as a double-mode pulsator.

For DDE 148, photometry was done using the single comparison star TYC 2218-01320-1, which has B=12.599 from APASS DR9. The data set included 362 observations spanning 67 Julian days. Period04 analysis reveals 8 modes, 7 of which can be associated with either the fundamental or first overtone or harmonics and combinations of these two modes. The 1O/F amplitude ratio is 0.11. The remaining significant mode with frequency 0.61 c/d could be a separate mode. The ATLAS catalog of variables (Heinze et al. 2018) reports this star as an eclipsing binary candidate; however, we have not been able to find the ATLAS photometry to follow up, and don't see evidence of eclipses in our photometric data.

Table 1. Periods and amplitudes from B-band photometry of R. Wagner

Star	V1965 Aql	LS Cet	RV Ari	DDE 148
F Mode Frequency (c/d)	7.3025	11.8627	10.7372	8.8796
F Mode Amplitude (mag)	0.2789	0.116	0.26758	0.2895
1O Mode Frequency (c/d)	N/A	N/A	13.8981	11.4951
1O Mode Amplitude (mag)	N/A	N/A	0.07524	0.0318

Table 1 summarizes the frequencies and amplitudes found from the Wagner B-band data. There are other sources of photometric data for these stars, for example, from the ASAS-SN survey (Jayasinghe et al. 2019, Kochanek et al. 2017, Shappee et al. 2014). Figure 1 shows the ASAS-SN V-magnitude phased light curves for the four stars.

Three of these stars have been observed by the *TESS* (Ricker et al. 2015) spacecraft. We processed a 2-minute cadence *TESS* light curve taken during *TESS* sector 54 observations for 27 days beginning July 9, 2022 using Keaton Bell's Pyriod software (https://github.com/keatonb/Pyriod). Figure 2 shows a portion of the 27-day 2-minute cadence *TESS* light curve and the periodogram. It was a surprise that the *TESS* data revealed only harmonics of the main pulsation period. Although it is possible that continued observations may reveal low-amplitude modes, this star appears truly to be a single-mode pulsator. Analysis of *TESS* light curve products for LS Cet and RV Ari taken during sector 42 and 43 observations, beginning August 21, 2021 and September 16, 2021, respectively, is in progress.

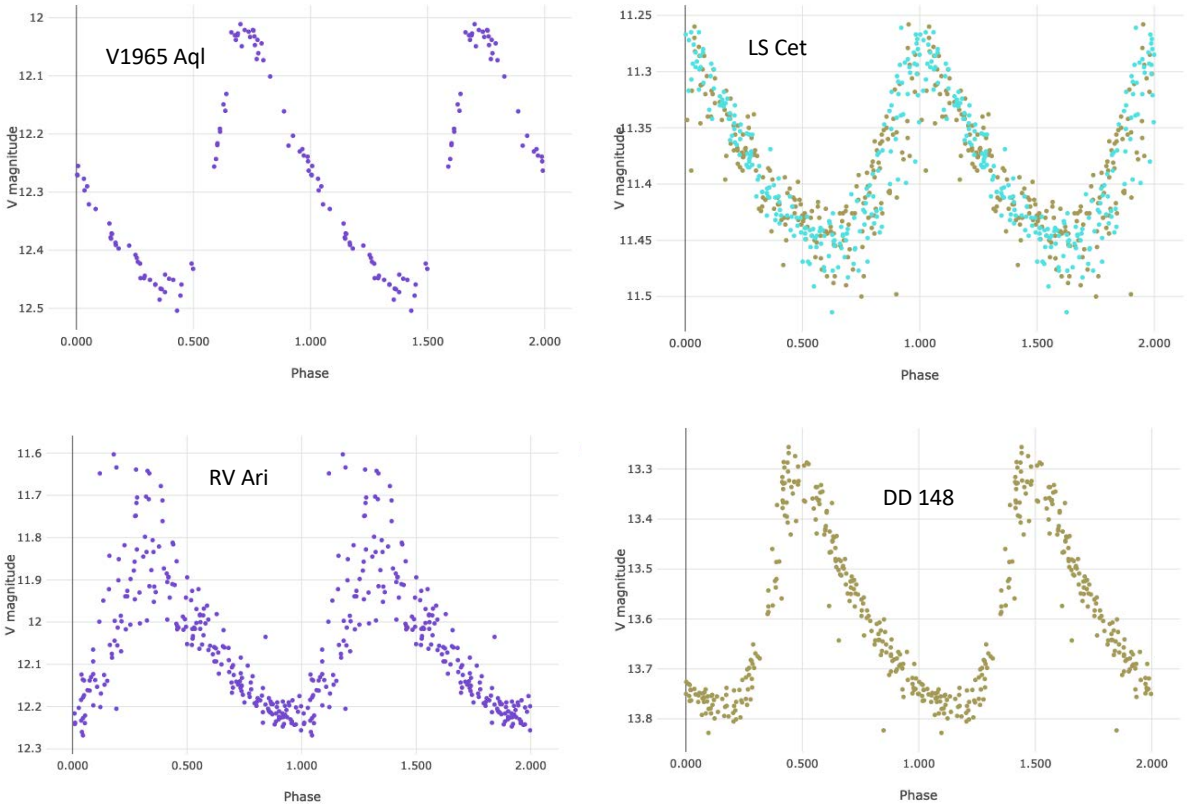

Figure 1. Light curves phased on fundamental mode period for four stars from ASAS-SN database (https://asas-sn.osu.edu/variables).

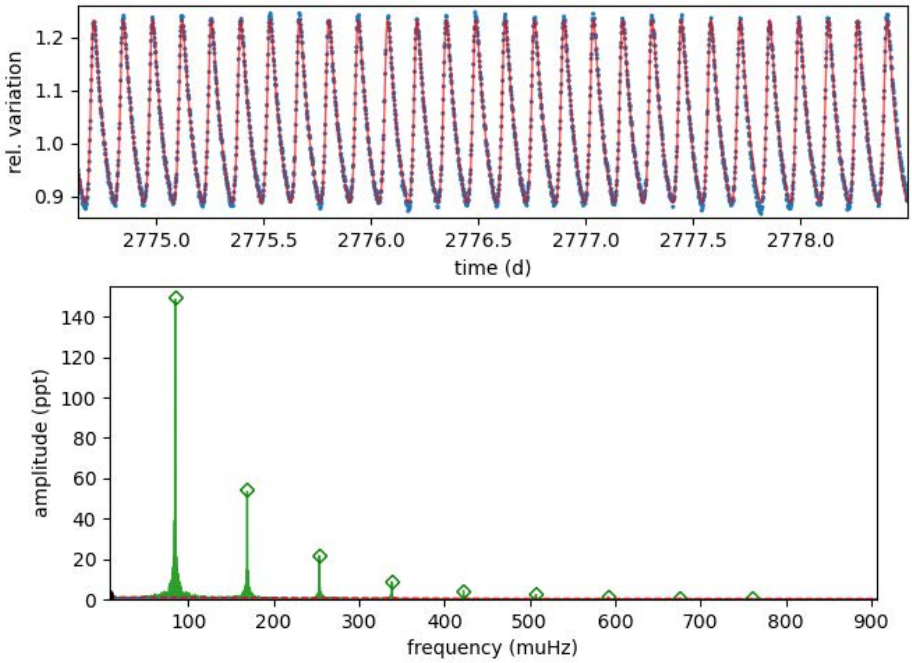

Figure 2. Top: Zoom-in on 2-min portion of V1965 Aql from TESS light curve (blue) and fit to light curve fit by the first nine harmonics of the fundamental mode (red). Bottom: Periodogram showing 9 harmonics. The barely visible red line is the local noise level.

3. Evolution and Pulsation Modeling Results

Obtaining data on pulsations of HADS stars is only a first step in unlocking the potential for asteroseismology of these stars. We would like to predict and explain the behavior of these stars using stellar evolution and pulsation modeling. We apply the MESA/GYRE codes to model the evolution and pulsation of these stars. Constraints for the stellar models are needed as a starting point. Table 2 summarizes properties of the four stars from the TESS Input Catalog 8.2 (Stassun et al. 2019) accessible via MAST (https://mast.stsci.edu). These properties were collected or derived from several observational sources or estimated by interpolating on calibrated model fits, and therefore have large uncertainties. Stellar pulsation properties in conjunction with stellar models can be used to better constrain these quantities.

Table 2. Stellar properties from TESS Input Catalog

Star	V1965 Aql	LS Cet	RV Ari	DDE 148
TIC number	388720888	365227352	306517089	261223010
V mag	12.72 ± 0.034	11.43 ± 0.015	12.16 ± 0.13	13.68 ± 0.08
B mag	12.57 ± 0.29	11.67 ± 0.19	12.33 ± 0.27	13.90 ± 0.31
T_{eff} (K)	6926 ± 205	7017 ± 125	7243 ± 277	7303 ± 208
Mass ($M_\odot$)	1.51 ± 0.26	1.55 ± 0.26	1.63 ± 0.28	1.65 ± N/A
Radius ($R_\odot$)	3.16± 0.26	2.24 ± 0.13	2.44 ± 0.21	2.26 ± N/A
Luminosity ($L_\odot$)	20.70 ± 2.38	10.97 ± 1.01	14.63 ± 1.34	13.05098
Distance (pc)	1290 ± 65	657 ± 26	929 ± 37	2075 ± 118
TESS data	S54	S42	S42 and S43	No

Figure 3 (left) shows a Hertzprung-Russell (H-R) Diagram including the theoretical blue edge and observational red edge of the delta Scuti pulsation instability region from Breger and Pamyatnykh (1998) and theoretical red and blue edges of the gamma Doradus instability region from Warner et al. (2003). The figure also shows the location of the four HADS stars and their uncertainties taken from Table 2. The four stars lie well away from the zero-age main sequence (black border), near the red edge of the delta Scuti instability strip, and not far from the blue edge of the gamma Doradus instability strip, where non-radial gravity-mode pulsators with low frequencies reside.

For our initial stellar model exploration, we adopt metallicity Z =0.02, helium mass fraction Y = 0.28, and opacities based on the Asplund et al. (2009) solar abundances. We calculate evolution models of different stellar masses to identify evolution tracks that pass through the locations of the four stars. We identify models with fundamental mode period that matches the observed period, and examine predictions for other modes, including the first overtone as well as non-radial low-frequency gravity-mode pulsations.

Figure 3 (right) shows the H-R diagram with a calculated 1.9 $M_\odot$ evolution track that passes through the location of V1965 Aql. The model with fundamental mode period most closely

matching that of V1985 Aql is marked by the red x, has T_{eff} = 6881 K, luminosity L = 22 $L_\odot$, radius R = 3.3 $R_\odot$, and age 1.4 billion years. The fundamental mode is pulsationally unstable, with fundamental-mode period 0.1342 d. The first overtone mode, however, actually has a higher linear growth rate, and period 0.1036 d. Comparing the stellar properties to those in the TIC in Table 2, it is clear that the mass estimate found in the TIC, 1.5 $M_\odot$, is low compared to the mass derived using stellar models and the pulsation periods.

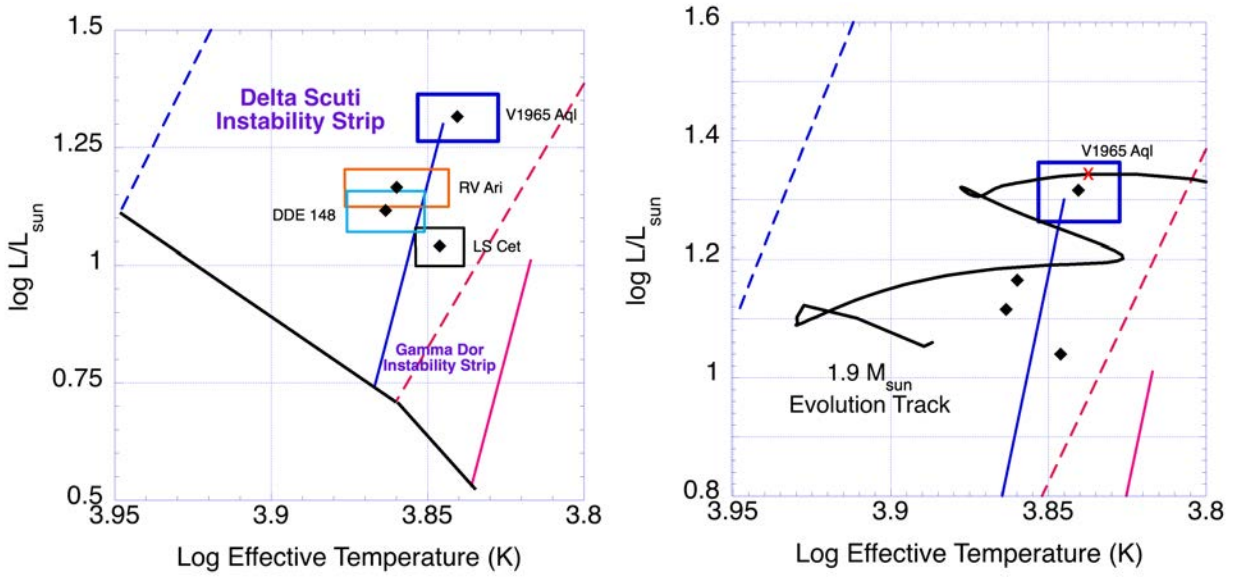

Figure 3. Theoretical Hertzsprung-Russell Diagram showing delta Scuti (dashed blue and red border) and gamma Doradus (solid blue and red border) instability regions and locations of four HADS stars based on TESS Input Catalog L and T_{eff} values. The black border at the bottom of the instability regions is the location of the zero-age main sequence. Right: 1.9 $M_\odot$ evolution track that passes near the location of V1965 Aql. The red x marks the position of a model with fundamental mode period matching the observed period.

We also use the Radial Stellar Pulsation (RSP) package in MESA to model the hydrodynamics of the stellar envelope. Our goal is to compare predicted light curve amplitudes and shapes with the measured ones as seen in Fig. 1. The growth rates of delta Scuti pulsations are two orders of magnitude lower than, e.g., Cepheid pulsations, which makes the calculation challenging, because many hundreds of thousands of pulsation cycles must be run to reach a limiting amplitude. Our RSP model for V1965 Aql, using mass, luminosity, and T_{eff} based on the evolution model has F mode period of 0.1374 d and 1O period of 0.1016 d. However, the growth rate of the F mode is only 4 x 10^{-6} per period and the growth rate of the 1O mode is 5 x 10^{-5} per period, so more than one million pulsation cycles may need to be calculated before the model reaches a limiting amplitude.

Figure 4 shows the first few cycles of the RSP model initialized with radial velocity amplitude 3 km/sec (top), and the resulting absolute visual magnitude (bottom). The first pulsation cycle looks anomalous as the model envelope structure is rearranging to satisfy the input constraints. The amplitude of the model pulsation is around 0.03 V mag, much smaller than the 0.5 mag seen for

V1965 Aql in Fig. 1. Also, the light curve shape is sinusoidal instead of being saw-toothed as in the observations; running additional cycles should result in changes in the light curve shape and amplitude.

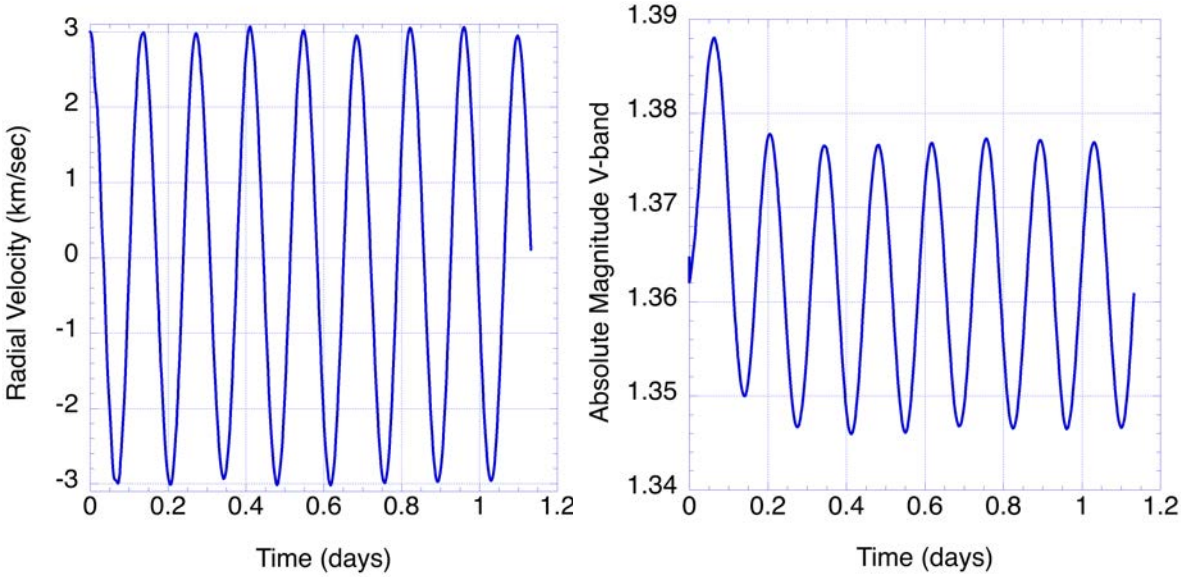

Figure 4. Radial velocity (left) and absolute V magnitude vs. time (right) for first several cycles of V1965 Aql RSP model.

4. Conclusions and Future Work

We have only just begun to analyze and interpret the data for these four stars. We plan to compare our observational results with those of others, and to make use of additional photometric data available for these stars. In future work, we would like to make use of multi-color photometry for mode identification. We will continue to refine evolution and pulsation modeling and comparisons to pulsation frequencies and amplitudes. We hope to constrain stellar properties such as mass, radius, luminosity, age, and metallicity more precisely. We will also compare our asteroseismic results with those available in the literature, in particular for RV Ari (Balona and Evers 1999, Casas et al. 2006).

Acknowledgements

We acknowledge the Mikulski Archive for Space Telescopes (MAST, https://mast.stsci.edu) for obtaining *TESS* data. We made use of the SIMBAD database (https://simbad.u-strasbg.fr/simbad/sim-fid), the ASAS-SN database (https://asas-sn.osu.edu/), AstroPy ccdproc (https://github.com/astropy/ccdproc), AstroImageJ software, (https://www.astro.louisville.edu/software/astroimagej/), Keaton Bell's Pyriod software (https://github.com/keatonb/Pyriod) and AAVSO-sponsored tutorial on facebook (https://www.facebook.com/AAVSO/videos/394253469585766), and Warrick Ball's qpmg plotting package (https://github.com/warrickball/qpmg). We thank the AAVSO for opportunity to present a talk at the 111th AAVSO meeting. JG, EF, MS, and PE acknowledge support from

LANL managed by Triad National Security, LLC, for the U.S. DOE's NNSA, Contract #89233218CNA000001.

References

Asplund, M., et al., The Chemical Composition of the Sun, *ARA&A* **47**, 481 (2009).

Balona, L. A., Combination frequencies in high-amplitude δ Scuti stars, *MNRAS* **459**, 1097 (2016).

Balona, L. A. and Evers, E. A., Mode identification and asteroseismology of δ Scuti stars, *MNRAS* **302**, 349 (1999).

Borucki, W. J., Koch, D., Basri, G., Batalha, N., Brown, T., Caldwell, D., et al., *Kepler* planet-detection mission: Introduction and first results, *Science* **327**, 977–980 (2010).

Breger, M. and Pamyatnykh, A.A., Period changes of δ Scuti stars and stellar evolution, *A&A* **352**, 938 (1998).

Casas, R., Suarez, J. C., Moya, A., and Garrido, R., A comprehensive asteroseismic modelling of the high-amplitude δ Scuti stars RV Arietis, *A&A* **455**, 1019 (2006).

Gilliland, R. L., Brown, T. M., Christensen-Dalsgaard, J., Kjeldsen, H., Aerts, C., Appourchaux, T., et al., *Kepler* asteroseismology program: Introduction and first results, *PASP* **122**, 131–143 (2010).

Guzik, J. A., Highlights of Discoveries for δ Scuti Variable Stars from the *Kepler* Era, *Frontiers in Astronomy and Space Sciences*, Vol. **8**, id.55 (2021).

Heinze, A. N., et al., A First Catalog of Variable Stars Measured by the Asteroid Terrestrial impact Last Alert System (ATLAS), *AJ* **156**, 241 (2018).

Jayasinghe, T., et al., The ASAS-SN catalogue of variable stars – II. Uniform classification of 412000 known variables, *MNRAS* **486**, 1907 (2019).

Jermyn, A. S., et al., Modules for Experiments in Stellar Astrophysics (MESA): Time-Dependent Convection, Energy Conservation, Automatic Differentiation, and Infrastructure, https://arxiv.org/pdf/2208.03651.pdf

Kochanek, C. S., et al., The All-Sky Automated Survey for Supernovae (ASAS-SN) Light Curve Server v1.0, *PASP* **129**, 104502 (2017).

Lenz, P. and Breger, M., *Communications in Asteroseismology* **146**, 53 (2005).

Paxton, B., et al., Modules for Experiments in Stellar Astrophysics (MESA): Pulsating Variable Stars, Rotation, Convective Boundaries, and Energy Conservation, *ApJS* **243**, 10 (2019).

Ricker, G. R., et al., Transiting exoplanet survey satellite (*TESS*), *J. Astron. Telesc. Instr. Syst*. **1**, 014003 (2015).

Shappee, B. J., The man behind the curtain: X-rays drive the UV through NIR variability in the 2013 Active Galactic Nucleus outburst in NGC 2617, *ApJ* **788**, 48 (2014).

Stassun, K. G., et al., The Revised *TESS* Input Catalog and Candidate Target List, *AJ* **158**, 138 (2019).

Townsend, R. H. D. and Teitler, S. A., GYRE: an open-source stellar oscillation code based on a new Magnus Multiple Shooting scheme, *MNRAS* **435**, 3406 (2013).

Warner, P. B., et al., A Theoretical γ Doradus Instability Strip, *ApJ* **593**, 1049 (2003).
Watson, C. L., Henden, A. A. and Price, A., The International Variable Star Index (VSX), *Soc. Astron. Sci. 25th Annu. Symp. Telesc. Sci.*, Vol. **25**, Published by Soc. Astron. Sci. (2006).

Demonstrating Real-Time Photometry

Gary J. Hawkins

San Diego Astronomy Association (SDAA), American Association of Variable Star Observers (AAVSO), ghawkinsall@gmail.com

Subject Keywords

Public Outreach; Real-time Photometry; V796 CAM; American Association of Variable Star Observers; AAVSO International Database, RedDwarf Flare Star Project; EV Lac

Abstract

The demonstration of real-time photometry to amateur astronomers and the public offers a powerful and seldom-seen outreach opportunity. Based on a poster presented at the AAVSO 111th Annual Meeting, this paper describes the equipment and software used to provide such a demonstration at the SDAA Julian StarFest, Julian, CA, in August 2022. It was hoped that outreach of this type would appeal to the public and encourage astrophotographers and those practicing Electronically Assisted Astronomy to expand their interest into photometry. Having demonstrated real-time photometry at the Julian StarFest, the author incorporates real-time photometric display into his regular observing workflow. Further results are presented associated with data collected for the RedDwarf Flare Star Project.

1. Introduction

My interest in public outreach began soon after I looked through a telescope for the first time. It is a highly fulfilling experience to share the beauty of the night sky with others. My outreach journey started with Electronically Assisted Astronomy (EAA), initially face-to-face at public outreach events and then online with the onset of the COVID pandemic. Towards the end of the pandemic, my interest shifted from deep space object live streaming to photometry. As the first face-to-face outreach events post-pandemic became a reality, it was natural to investigate the possibility of demonstrating real-time photometry. Further, since one of my goals was to attract astrophotographers and those practicing EAA to citizen science, it was logical to use an RGB-based system typical of that used in these two branches of astronomy. People are reluctant to spend money on something new when they don't know it is a good fit, so allow them to use what they already have. A color CMOS camera, or monochrome CMOS camera with RGB filters, is just fine for starting photometry.

2. Equipment and Software

Coming into photometry from an EAA background using a CMOS color camera, all I needed to add to my existing setup was a UV/IR cut filter to constrain the camera's spectral response to the visual range. My optical tube assembly for the Julian StarFest demonstration would consist of a Celestron C8 SCT, f/6.3 focal reducer, UV/IR cut filter and a ZWO ASI533MC color camera (Figure 1).

Figure 1. The author preparing for the first night's crowd at the Julian StarFest

On the software side, SharpCap Pro was utilized for image acquisition and pre-processing. Designed primarily for image capture associated with astrophotography and video astronomy, SharpCap is particularly popular with those practicing EAA. It is available in the free basic version and the licensed Pro version. The Pro version offers a host of additional features, including polar alignment, a focusing assistant, a Sequencer, advanced live-stacking options, and target-tracking features. Both versions of SharpCap support all mainstream astronomical cameras. Of the many Pro features, SharpCap Pro is capable of on-the-fly application of master dark and flat files (Glover, 2022).

ImageJ is a public domain, graphical user interface package traditionally used in life science fields for general image processing. AstroImageJ (AIJ) builds on ImageJ to provide an astronomy-specific image display environment and tools for astronomy image calibration and data reduction. AIJ is streamlined for time-series differential photometry, light curve detrending and fitting, and light curve plotting. AIJ has found considerable favor with those doing exoplanet transit analysis and has features that specifically address this type of work. AIJ has developed significantly since V3.1.0 described by Collins et al. (2017). Version 5.1 was used for the real-time

demonstration at the Julian StarFest. The latest version of AIJ can be found on the AIJ web portal (AIJ Installation Packages, 2022).

PHD2 was utilized for guiding. It is another example of a highly functional, free, open-source program that is community-developed and supported. It offers easy-to-use "push here dummy" guiding for beginners and sophisticated guiding and analysis tools for experienced users. It integrates with many popular image capture packages, including SharpCap (PHD2 Guiding, 2022).

3. Real-time Demonstration

The star chosen for the demonstration at the Julian StarFest was the eclipsing binary, V796 Cep. This star was identified through the International Variable Star Index (AAVSO, 2022), which is part of the tool set available at AAVSO. Real-time light curve plots of this EW variable were displayed on a second monitor. With a period of 9.431 hours, the divergence between the light curve of V796 Cep and the comparison stars was seen in relatively short order. Gaia EDR3 reports the distance of this 12th magnitude star as 501 pc or 1633 light years.

SharpCap was configured to collect sixty-second exposures - ideal for live viewing of the chosen target. The gain of the ZWO ASI533MC camera was set to 260, ensuring the target and chosen comparison stars were operating about halfway down the linear part of the camera response. The pre-processed images were saved to a folder which was then polled by AIJ to perform differential photometry. To get to the polling function within AIJ, the user must initially select the Data Processor (DP) option on the main toolbar (Figure 2).

Figure 2. The Data Processor icon - circled red

Initiating the DP opens two windows. Enter the target name in the SIMBAD Object ID box in the DP Coordinate Convertor window, along with the geographic location of the observatory. In the DP CCD Data Processor window, enter the polling folder destination (indicated by the blue oval, Figure 3) and select the M-Ap and M-Plot checkboxes (green oval, Figure 3) and set the poll interval to something other than zero (Red oval, Figure 3).

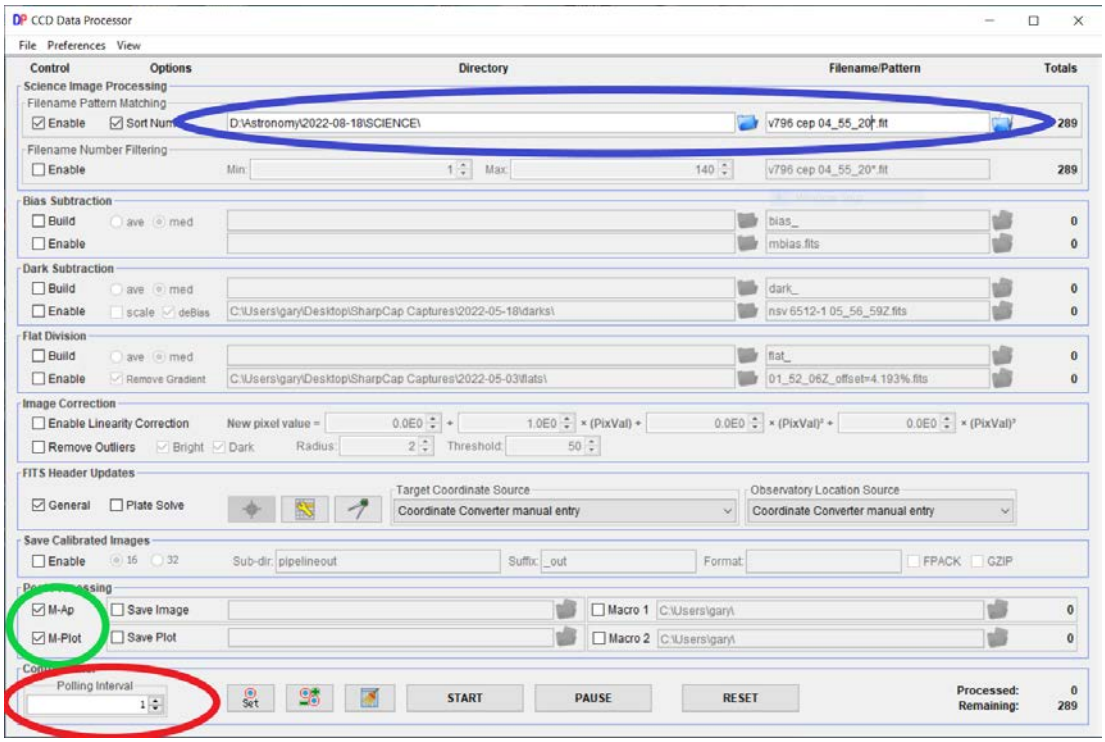

Figure 3. Setting up the DP CCD Data Processor window

Now click the START button at the bottom of the DP CCD Data Processor window. This will open several additional windows. The Multi-Aperture Measurements window allows the user to select the size of the aperture used for the differential photometry analysis (blue square, Figure 4), whether manual or auto comparison stars are used (yellow square, Figure 4), and how the photometry will proceed (green square, Figure 4).

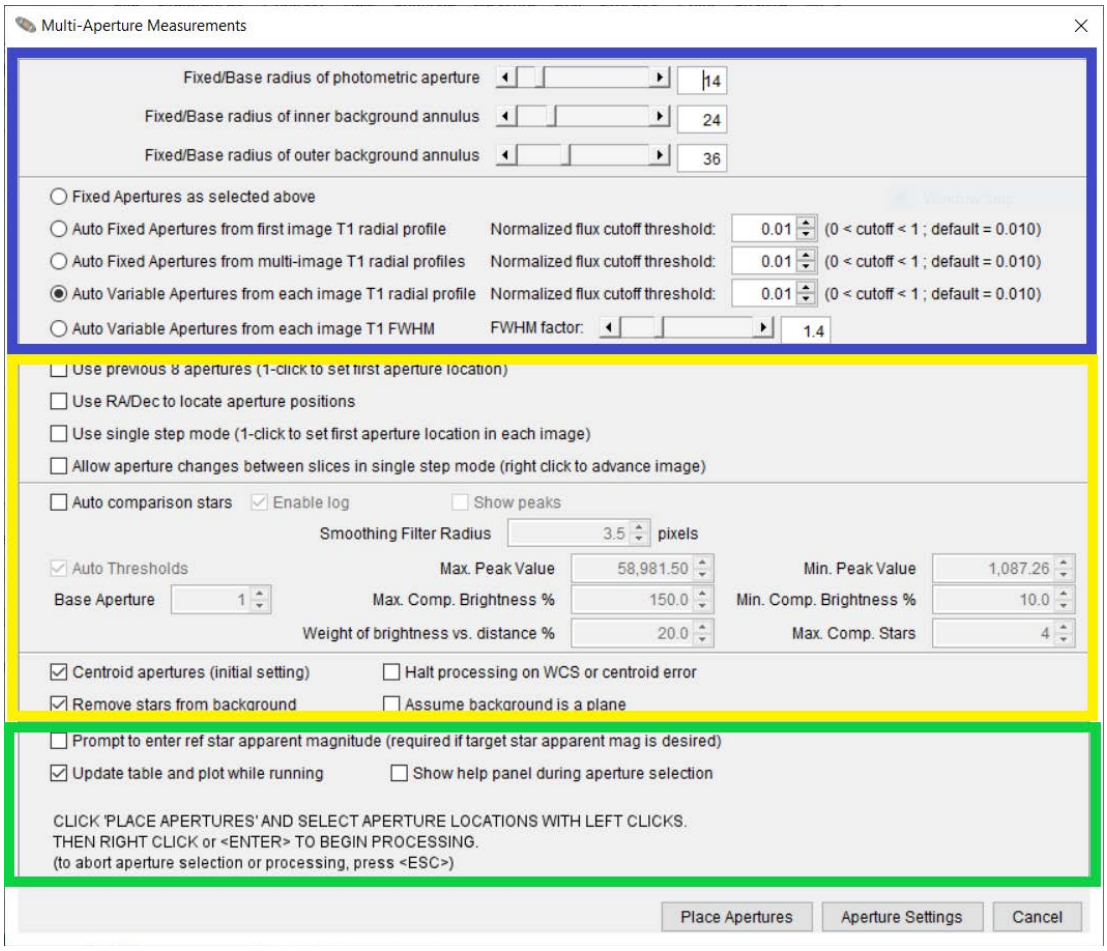

Figure 4. Selection areas within the Multi-Aperture Measurements window

The author's chosen selections for the demonstration are shown in Figure 4. Clicking the Place Apertures button allowed for the manual placement of apertures. In addition to the target star, V796 Cep (denoted by the cross-hair in Figure 5), the star labeled 121 (000-BMM-014) was selected as the comparison star, and the star labeled 129 (000-BMM-015) was selected as the check star from the AAVSO Finder Chart X28380AAD (Figure 5).

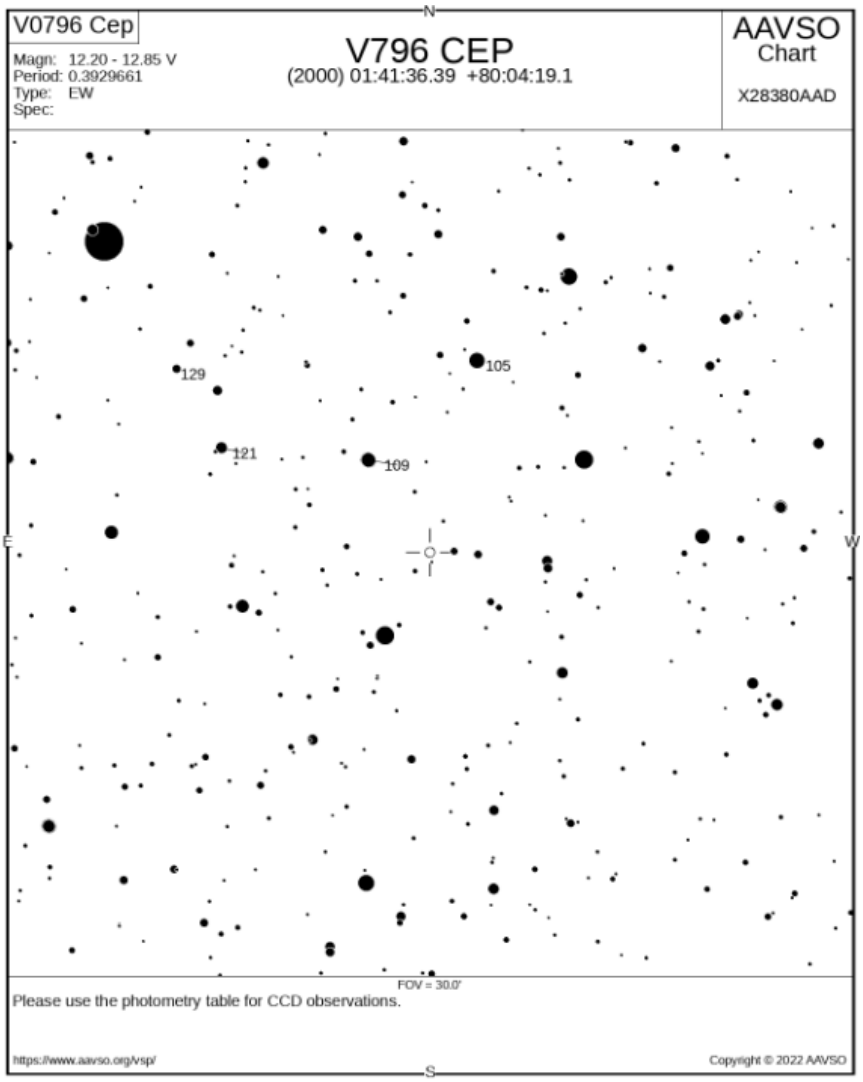

Figure 5. AAVSO Finder Chart for V796 Cep

AIJ uses its centroiding algorithm, combined with any RA/Dec information in the image FITS header, to keep the apertures accurately placed on the target, comparison, and check stars. As the calibrated FITs images consisted of tri-color data, the plot represents a total flux measurement. The Multi-plot Main window, which appears along with a host of other control windows, was used to customize the plot window. Under the File menu on the Multi-plot Main window, selecting Create AAVSO Variable Star Report brings the user to a recent and appreciated addition to AIJ's functionality. This easy-to-populate macro window developed by Dennis Conti (Conti 2022) allows for the generation of AAVSO WebObs-compatible files, greatly simplifying the submission of AIJ-derived photometry results to the AAVSO International Database (AID). A description of the workflow and an example of the display viewed by the public on the night of August 18, 2022, is provided in a YouTube video (Hawkins 2022). The complete light curves for that evening, as displayed in the Plot of Measurements window, are shown in Figure 6.

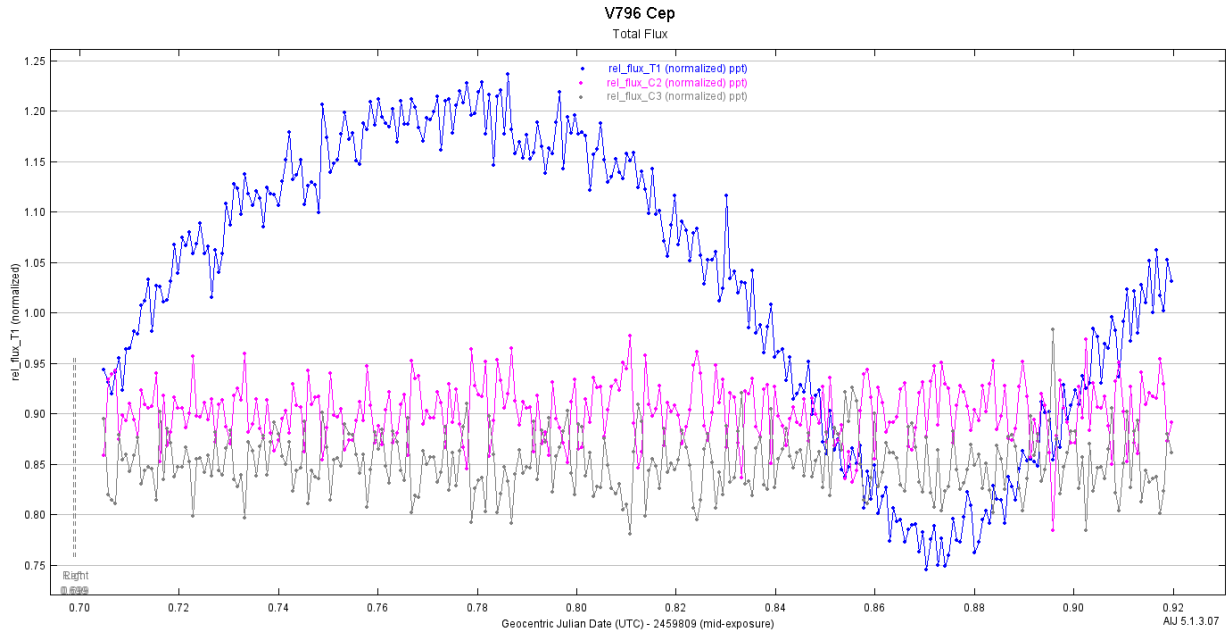

Figure 6. Light curve for V796 Cep, comparison and check stars, August 18, 2022

When doing this type of outreach, it is recommended the presenter cut between the developing real-time light curve and a presentation. This presentation should ideally contain information on the basics of photometry, equipment and software used, characteristics of the target star, and how this data will be used within the astronomical community. This additional information keeps the audience engaged and aids with the visualization of the target being measured. A sample presentation can also be found in the previously referenced YouTube video (Hawkins 2022).

3.1 Captured results and the public reaction at the Julian StarFest

When trying something new, there is uncertainty about how it will be accepted. A little to my surprise, the viewing public was fascinated by the concept of two stars orbiting around a common gravitational center. They were also thrilled to hear amateur astronomers could provide meaningful data to the scientific community, supporting the operation of telescopes like Hubble and James Webb, and providing data for analysis on exoplanets and binary stars. The event and subsequent YouTube video (Hawkins 2022) has generated much interest from fellow astronomers wishing to try photometry or perform this type of outreach.

Nearly thirteen hours of data was collected over two nights at the Julian StarFest (Figure 7). This data was subsequently post-processed with ASTAP (Astrometric STAcking Program, 2022) and AIJ. ASTAP was used to plate-solve each of the images and undertake the tri-color extraction, while AIJ handled the differential photometry. A tri-color green (TG) measurement report was formatted with the new macro in AIJ and uploaded to the AID.

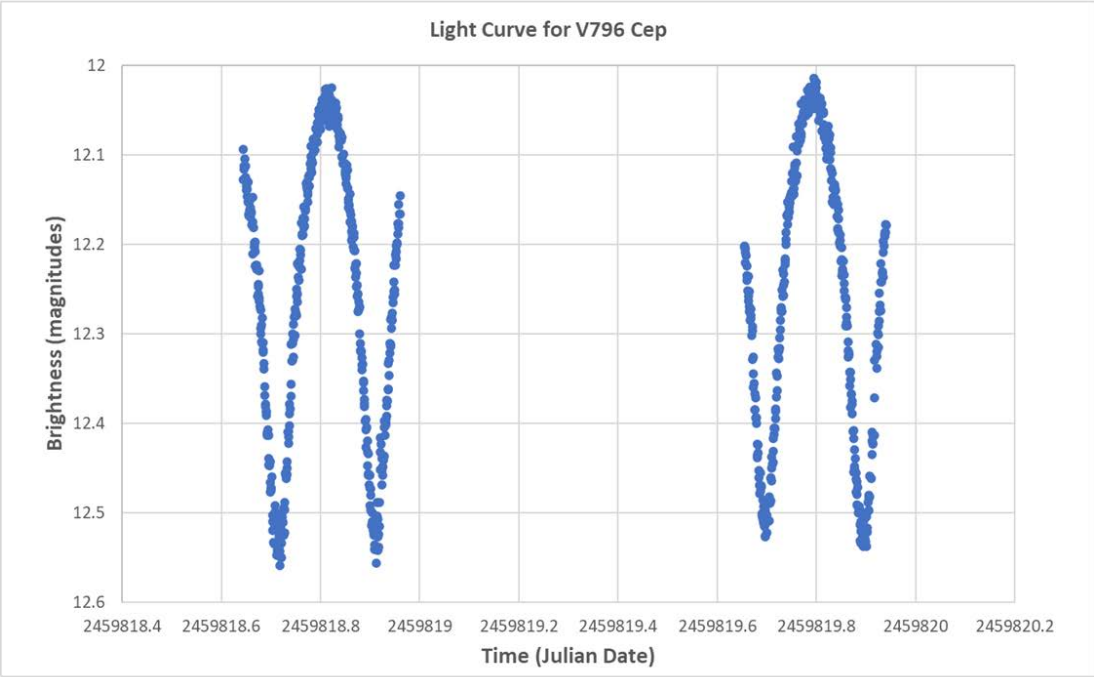

Figure 7. TG Data for V796 Cep collected on the nights of 18th and 19th August 2022

4. A Real-Time Display as Part of Photometric Image Capture

The demonstration of a real-time photometric display with AIJ convinced the author that this tool should be incorporated within his typical photometric capture workflow. Not only could a developing light curve be monitored in real-time, but it was also possible to view systematic error occurrences if the appropriate display parameters were selected. Further, real-time viewing adds a degree of anticipation when undertaking measurements, particularly when attempting to capture unpredictable stellar events. The opportunity to measure such events occurred soon after the Julian StarFest when the author joined the RedDwarf Flare Star Project (RedDwarf Flare Star Project, 2022).

The RedDwarf Flare Star Project was created in 2021. The goal of the project is "to observe stellar flares and characterize their spectroscopic properties (variations in line strength and profile vs. time) and their photometric properties (brightness vs. time)." The founders note, "it is particularly valuable to catch some flares with both photometry and spectroscopy, to correlate the spectroscopic and photometric properties as there are very few such observations reported in the literature" (RedDwarf Wiki, 2022). The team consists of prominent members of the citizen science community and James Jackman, Postdoctoral Research Scholar, School of Earth and Space Exploration, Arizona State University (Arizona State University, 2022).

Thus, I found myself on the evening of October 18, 2022, viewing the steep rise of what was to become a double flare event on M-class star EV Lac (Spectral Type: M4.0Ve; nominal V Mag: 10.26) – Figure 8. Capturing photometric data is fulfilling, but the experience of seeing an

unpredictable stellar event play out in real time made me feel a bit like Jodie Foster hearing those first rhythmic beats of an incoming alien transmission.

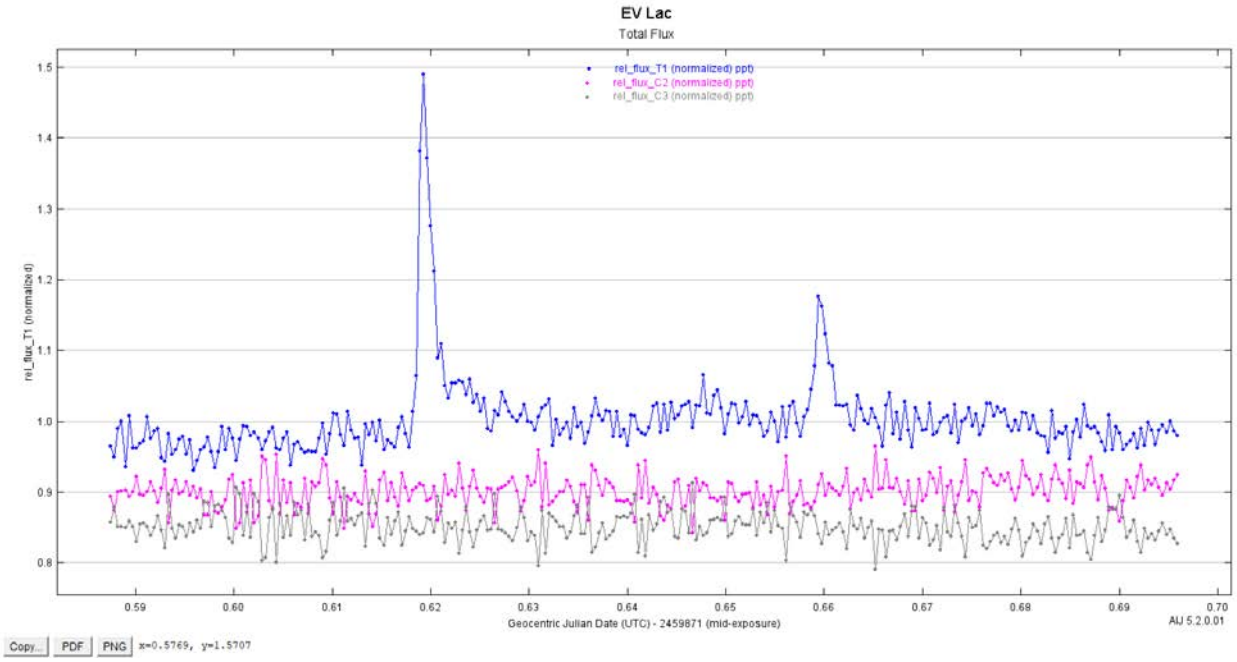

Figure 8. Screenshot of a multiple flare event occurring on EV Lac

Having expressed my excitement to the family, they came out to the telescope on the patio and gazed in wonder at the result of photons hitting the camera sensor that had just traveled 16.476 light years.

5. Discussion

Real-time photometry was successfully demonstrated over two nights at the Julian StarFest to amateur astronomers and the public. The slowly changing light curve of an eclipsing binary star system captured the imagination of many of those viewing it, greatly exceeding the author's expectations of this outreach opportunity. The author hopes this demonstration, poster, and accompanying YouTube video (Hawkins 2022) will encourage amateur astronomers to try photometry and begin their journey into citizen science.

The author has now included a real-time display of total flux results within his photometric capture workflow. The ability to view the developing light curve in real-time, along with potential systematic errors, is another step toward optimizing photometric data capture. Not only that, the anticipation of viewing unpredictable stellar events adds dramatically to the measurement experience.

Acknowledgments

I would like to acknowledge Karen Collins and her team for developing AstroImageJ; Dennis Conti for developing the *Create AAVSO Variable Star Report* macro within AIJ; Robin Glover, the developer of SharpCap and SharpCap Pro; the developers of ASTAP and PHD2; Kevin Alton for his encouragement through the AAVSO mentorship program, and the team members of the RedDwarf Flare Star Project.

References

(2022). Retrieved from PHD2 Guiding: https://openphdguiding.org/

(2022). Retrieved from Arizona State University: https://search.asu.edu/profile/3775785

(2022). Retrieved from Astrometric STAcking Program: https://www.hnsky.org/astap.htm

VSX. (2022). Retrieved from AAVSO: https://www.aavso.org/vsx/

AIJ Installation Packages. (2022). Retrieved from AstroImageJ: https://www.astro.louisville.edu/software/astroimagej/installation_packages/

Conti, D. (2022, November). Create AAVSO Variable Star Report Macro Revision 1.4. (G. Hawkins, Interviewer)

Glover, R. (2022). *SharpCap*. Retrieved from SharpCap: https://www.sharpcap.co.uk/

Hawkins, G. (2022). Retrieved from YouTube: https://www.youtube.com/watch?v=uSz5n2b6QR4

Collins, K. A., et al. (2017). AstroImageJ: Image Processing and Photometric Extraction for Ultra-Precise Astronomical Light Curves. *The Astronomical Journal*, **153**, 77.

RedDwarf Flare Star Project. (2022). Retrieved from RedDwarf Flare Star Project: https://aatel.groups.io/g/RedDwarf

RedDwarf Wiki. (2022). Retrieved from RedDwarf Flare Star Project: https://aatel.groups.io/g/RedDwarf/

Double-Pulsator 'Hidden' Binaries: New Targets for Studying Classical and Solar-like Oscillations

Anne Hedlund[1,2], Jason Jackiewicz[1], Joyce A. Guzik[2], Patrick Gaulme[3]

[1] Department of Astronomy, New Mexico State University, P.O. Box 30001, MSC 4500, Las Cruces, NM 88003-8001, USA; ahedlund@nmsu.edu, jasonj@nmsu.edu
[2] Los Alamos National Laboratory, XTD-NTA, MS T082, Los Alamos, NM 87545-2345, USA ; ahedlund@lanl.gov, joy@lanl.gov
[3] Max-Planck-Institut für Sonnensystemforschung, Justus-von-Liebig-Weg 3, 37077 Göttingen, Germany; gaulme@mps.mpg.de

Subject Keywords

JAAVSO Keywords = Spectra; Spectroscopy; Asteroseismology; Radial Velocity; Binary Stars; Delta Scuti Stars; Giants, Red; Pulsating Variables; ADS Keywords = Spectroscopic binary stars (1557); Radial Velocity (1332); Asteroseismology (73); Red giant stars (1372); Delta Scuti variable stars (2101); Gamma Doradus variable stars (370)

Abstract

Since the advent of space-based photometric missions, the field of asteroseismology has been completely transformed. Thousands of new stellar oscillators have been detected, increasing the sample of known stellar pulsators by orders of magnitude. The unprecedented precision has allowed detailed analysis of stellar pulsators, motivating updates to our classification of stellar pulsators, oscillation driving mechanisms, and the interior stellar physics our stellar models rely on. In order to fully test our understanding of stellar structure and evolution, it is necessary to find well-constrained stellar pulsators to treat as standards. A particularly advantageous place to study stellar pulsators is in detached binary star systems where stellar properties can be derived with high precision. *Kepler*'s long temporal baseline and high frequency resolution make its targets ideal candidates for study, but the number of pulsating binaries detected by *Kepler* is limited in number and biased. This work looks to find *Kepler* pulsating binaries that are 'hidden' from photometric detection methods by looking for *Kepler* targets with frequency signatures of two distinct stars and taking spectroscopic observations to detect orbital motion and determine whether they are non-eclipsing, spectroscopic binaries. 21 *Kepler* red giants that also displayed frequency signatures of classical oscillations were considered as pulsating hidden binary targets. 17 of these targets have been observed 3+ times using the ARCES spectrograph on the 3.5-meter telescope at Apache Point Observatory. Through the detection of Doppler shifts in spectral lines and the derivation of radial velocities using the broadening function technique, 14 targets have been confirmed as spectroscopic binaries with one target clearly displaying two sets of spectral lines. Future observations are scheduled in order to ensure that all targets have been observed numerous times, to confirm that target spectra have sufficient SNR such that the spectral lines of faint companions can be detected, and to obtain proper phase coverage of double-lined spectroscopic targets so that dynamical modeling can be performed.

1. **Introduction**

One of the main obstacles in stellar astronomy is the inability to directly observe stellar interiors. Asteroseismology, or the interpretation of observable stellar oscillations to study global stellar properties and probe stellar interiors, is a methodology that provides high-precision information about stellar interiors that can subsequently be used to validate stellar models. Since the advent of space-based photometry, the field of asteroseismology has flourished. With photometric precision 10-100x better than ground-based observations and long continuous temporal baselines, missions like the NASA *Kepler* space mission have discovered thousands of classically pulsating A-F type stars and tens of thousands of main-sequence, sub-giant, and giant-branch stars with solar-like oscillations (Balona 2018; Hon et al. 2019).

Asteroseismology of solar-like oscillators has progressed rapidly due to the similarities to helioseismology and the ability to apply asymptotic theory to the low-radial order stochastically excited oscillations. Relatively simple measurements of asteroseismic diagnostics, such as the large frequency separation and the frequency of maximum power, along with effective temperature, enable the use of solar-based scaling relations to determine stellar mass and radius for solar-like oscillators (Brown et al. 1991; Kjeldsen and Bedding 1995; Kallinger et al. 2018).

Asteroseismology of classical oscillators such as delta Scuti and gamma Doradus stars has progressed more slowly. These classical oscillators have complex frequency patterns that can be difficult to interpret due to rotational splitting, combination frequencies, amplitude and frequency modulation, and mismatch between observed and theoretical frequency patterns. Regardless of these difficulties, promising work with classical oscillators has still been accomplished such as determining stellar parameters for early main-sequence delta Scuti stars (Bedding et al. 2020) and using non-uniform period spacing in gamma Doradus stars to measure internal rotation rates (van Reeth et al. 2016).

One method of constraining stellar parameters in order to better understand classical oscillations is to study stellar pulsators in binary star systems. Binary star systems are often used as benchmark systems for studying stellar models due to the constraints of coevality and the ability to derive precise stellar properties such as mass and radius. Previous research studying classical pulsators in binary star systems has proven fruitful with binarity providing necessary constraints on stellar models in order to study the stellar oscillations (Streamer et al. 2018; Steindl et al. 2021).

Which stellar and orbital parameters can be derived for a binary star system depends on the detection method. Photometric detection of eclipses provides information about the relative scale of the system, yielding fractional radii and orbital parameters (P, e, ω, i). Spectroscopic detection, when the stellar lines from both components of the binary are observed, provides information about the absolute scale of the system, atmospheric parameters from disentangled spectra (T_{eff}, log(g), metallicities), the mass function, and orbital parameters (P, e, ω, asin(i)). Combined, eclipsing double-lined spectroscopic binaries allow for the derivation of absolute masses and radii, all orbital parameters, and stellar atmospheric parameters. Although follow-

up spectroscopic observations of known eclipsing binary star systems (EBs) provide the most direct path to deriving precise stellar properties for stellar models, the NASA *Kepler* Space Mission sample of EBs is limited in number and biased towards systems with low eccentricity and short orbital period (Kirk et al. 2016). Furthermore, only approximately 10% of the *Kepler* binary sample are found to have a pulsating component.

One way to increase the sample of pulsating binary star systems and expand to new regions of orbital/stellar property parameter space is to use a different detection method to look for pulsating binaries observed by *Kepler*. Beck et al. (2022) matched a spectroscopic catalog of binaries with space photometry catalogs (*Kepler*, K2, TESS, and BRITE) to find 99 systems containing an oscillating red giant component. The spectroscopically detected binaries containing a red giant star had higher orbital periods and more systems with high eccentricity in comparison to the photometrically detected red giant binaries found by *Kepler*. Furthermore, because of longer orbital periods, the spectroscopically detected binaries contained more luminous, evolved red giants that had begun core helium burning in comparison to the photometrically detected sample. In order to get a representative sample of pulsating binaries to use as benchmarks for stellar models, more than one method of finding pulsating binaries is necessary.

Finding new, non-eclipsing spectroscopic pulsating binaries in the *Kepler* database will increase the number of benchmark systems and increase the diversity of the stellar and orbital parameters included. But, without eclipses to constrain the inclination, a double-lined spectroscopic binary can only provide minimum masses for the stellar components. This degeneracy can be overcome if one of the components of the double-lined spectroscopic binary (SB2) is a red-giant star displaying solar-like oscillations. Murphy et al. (2021) illustrated this solution when they identified a *Kepler* amplitude spectrum containing signatures of red giant (RG) solar-like oscillations as well as a number of delta Scuti (dS) frequency peaks. Using a high-resolution spectrograph, they derived radial velocities (RVs) for the RG component and atmospheric parameters for both components. They used observed light arrival-time delays for the delta Scuti pulsations to determine radial velocities for the dS component (radial velocities are the time derivative of the time delays). With orbital modeling of the RVs, the modeled atmospheric parameters, and the asteroseismic mass of the red giant derived from scaling relations, Murphy et al. (2021) were able to break the degeneracy and determine inclination subsequently leading to sufficiently constrained stellar evolution and oscillation models for comparison with observations. Double-lined spectroscopic binaries that contain a solar-like oscillator and a classical oscillator provide similar constraints as an eclipsing double-lined spectroscopic binary and can be used to constrain stellar models to study classical pulsators.

2. Methodology

2.1 Initial target selection

In order to take advantage of the high frequency resolution and asteroseismic performance of *Kepler* data, potential double-pulsator `hidden' binary targets were drawn from a catalog of *Kepler* red giants presented in Gaulme et al. (2020). Gaulme et al. (2020) published a catalog of

4,465 red giant stars selected from the *Kepler* red giant catalog (Berger et al. 2018). This subsample was chosen such that all the red giants should have detectable oscillations, e.g., not limited by photon noise and a ν_{max} less than the sampling cut-off and above a minimum frequency that might be filtered out by light-curve processing. In this subsample of bright, mainstream RGs with high asteroseismic performance, 21 light curves were flagged for displaying delta Scuti or gamma Doradus pulsations in addition to RG solar-like oscillations (see Fig. 1). These 21 *Kepler* targets became the initial targets for this study–they displayed red giant and classical pulsations in the time series power spectral density, but no signs of eclipse in the light curve meaning they could be 'hidden' double-pulsator binary star system.

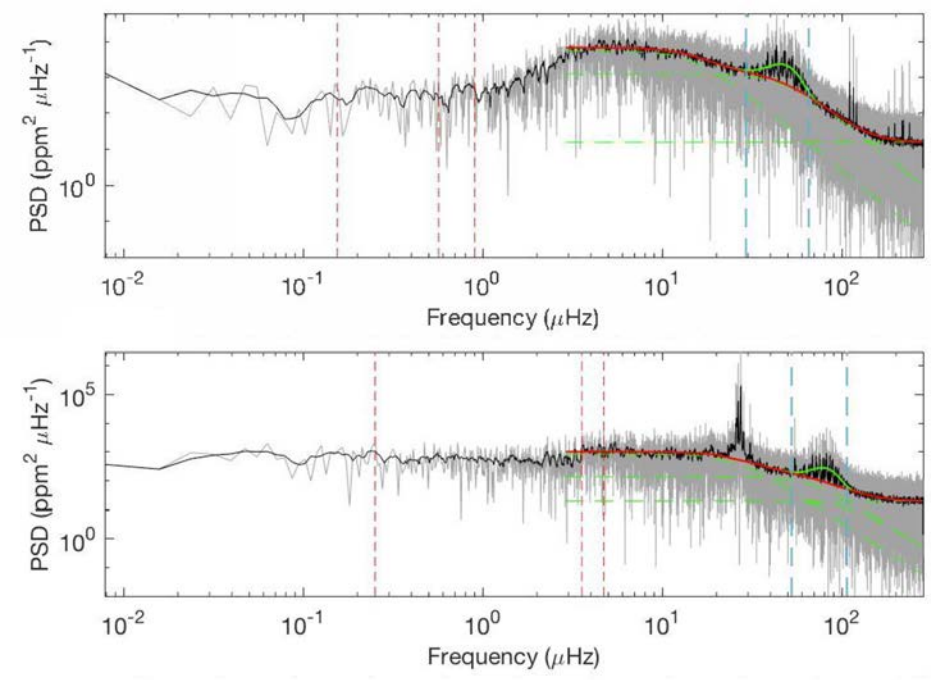

Figure 1. Top: The PSD of KIC 4951617 exhibits a solar-like acoustic mode bump as well as higher frequency peaks characteristic of a delta Scuti pulsator. Bottom: The PSD of KIC 6707691 exhibits a solar-like acoustic mode bump as well as lower frequency peaks characteristic of a gamma Doradus pulsator.

2.2 Eliminating false positives

Before obtaining spectroscopic observations in order to look for signs of binarity, attempts were made to eliminate false positives or blended sources. The 21 targets flagged for signatures of RG and classical oscillations were identified by inspecting simple aperture photometry (SAP) light curves publicly available on the Mikulski Archive for Space Telescopes (MAST). The light curves are the combination of 13+ combined quarters of data and multi-quarter SAP light curves are known to have systematic artifacts due signal falling in and out of aperture pixels in different quarters (Jenkins et al. 2017). This can lead to a false positive, e.g., a secondary pulsator falling inside an aperture pixel during a single quarter and showing up in the final result, or a bright pulsator right outside the aperture pixels leaking light into the aperture, making it appear as

though two pulsators are in the combined light curve. As the target pixel files are the least processed data available for *Kepler* targets, a randomly selected quarter of data was inspected for each of the targets. By looking at the pixel files for a single quarter of data, the light curves and power spectral density of the time series could be inspected in each pixel, as well as the combined signal of the pixels included in and excluded from the aperture for a given target during that quarter (see Fig. 2). If it did not appear that both sets of oscillations fell inside the pixels included in the aperture, the target was marked as a potential blend. KIC 3660182, KIC 4951617, KIC 9813963, KIC 10616594, and KIC 11659003 were flagged as potential blends. Additionally, a literature review of the targets was performed and the SIMBAD Astronomical database was used to look for known nearby neighbors of the targets. Of the five targets flagged as potential blends, four had nearby, <35" away, variable neighbors (e.g., rotationally variable, eclipsing binary, eruptive variable, etc.) with the exception being KIC 4951617.

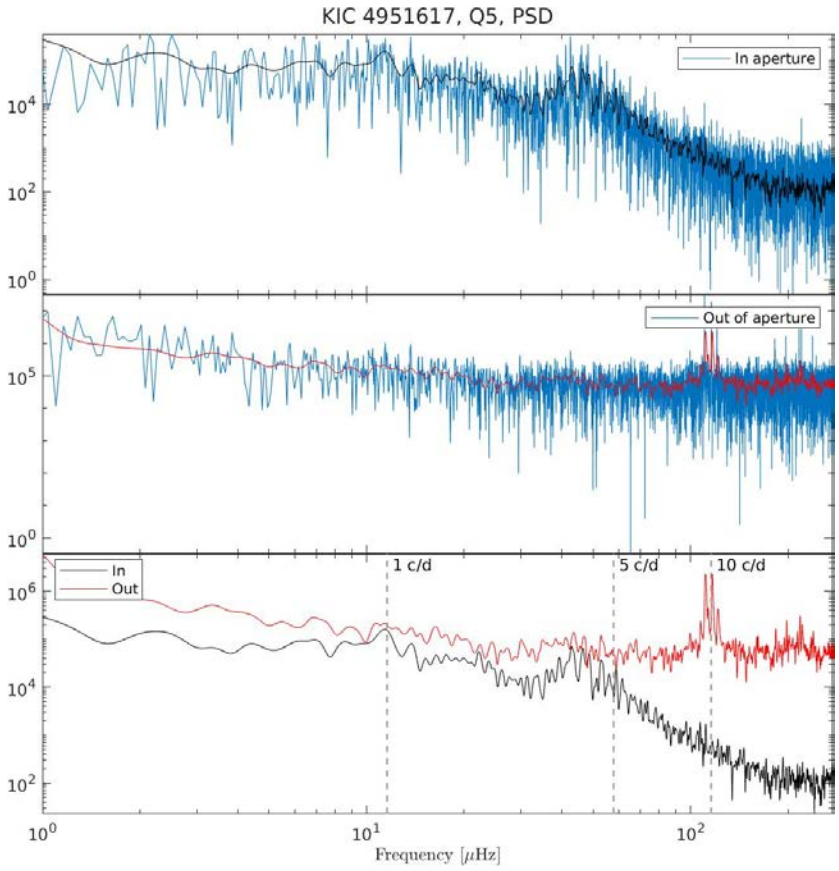

Figure 2: PSD and smoothed PSD of the mean light curves in and out of the aperture for KIC 4951617 for Q5. Acoustic mode bump is inside the aperture while the higher frequency peaks are from outside the aperture.

2.3 Spectroscopic observations

In order to determine whether the targets were in detectable binary star systems, spectroscopic follow-up observations were taken. Targets were observed multiple times in order to look for

periodic shifts in the spectral lines indicating that the target is composed of multiple orbiting components. All spectroscopic data was obtained using Apache Point Observatory's 3.5-meter telescope and the ARC echelle spectrograph (ARCES). ARCES is a high-resolution (R≈31,500) visible spectrograph that spans from 3200-10000 angstroms (Wang 2003). Observations were taken starting in October 2021 through November 2022, and currently 17 targets have been observed 3+ times. The echelle spectra were reduced using standard reduction techniques and PyRAF/IRAF packages (following the procedure of Karen Kinemuchi's ARCES reduction cookbook available at http://astronomy.nmsu.edu/apo-wiki/doku.php?id=start). The resulting spectra were 1-D, wavelength calibrated, and continuum normalized.

3. Results

3.1 Radial velocity derivations

If Doppler shifts were detected in a target's time series spectra, the broadening function (BF) technique was used to reconstruct the components' radial velocities. The BF method of deriving radial velocities is outlined in Rucinski (1992, 2002) and is generally better than traditional cross-correlation functions for extracting radial velocities. Essentially, a BF is a Doppler broadening kernel, $\boldsymbol{B}$, such that the convolution of the BF with a sharp-lined spectra, $\boldsymbol{T}$, equals the observed spectra, $\boldsymbol{O}$, (see Eq. 1). A least-squares technique or singular value decomposition is performed to solve the BF deconvolution and then the BF peaks can be fit with gaussians to obtain the radial velocities of the binary components. A Python adaptation of the Rucinski's IDL routines was used to calculate and fit the broadening function for the observed spectra. A MARCS synthetic spectrum with $\boldsymbol{T_{eff}}$= 7,000 K, log(g)=4, z=0 obtained from the Pollux database was used for the sharp-lined spectra (Gustafsson et al. 2008). A hot star template was chosen instead of a RG template for a number of reasons. As the RG luminosity dominates the spectra, it is much more difficult to detect the companion's spectral lines. Using a template similar to that of the expected companion provides a stronger secondary signal in the BF. Additionally, the atmosphere model for a RG template contains many lines which generate noise in the broadening function such that a hot star template is more successful at extracting the RG radial velocity as well as the companion velocity (Benbakoura et al. 2021).

$$\boldsymbol{O}(\boldsymbol{x}) = \int \boldsymbol{B}(\boldsymbol{x}')\boldsymbol{T}(\boldsymbol{x}-\boldsymbol{x}')\boldsymbol{dx}' \qquad (1)$$

In addition to using a hot star template to increase the chances of detecting the RG's hot star companion, the wavelength region used in the BF analysis was towards the bluer end of the observed spectra, $4300 \leq \boldsymbol{\lambda} \leq 5800$ angstroms. This region has high SNR, minimal telluric lines, and avoids excess noise found in the bluest part of the spectrum. Once the BF is solved for, it is smoothed with a Gaussian to remove uncorrelated noise and then Gaussian profiles are fit to the BF peaks. The locations of the broadening function peaks correspond to the radial velocities of the binary star components (see Fig. 3).

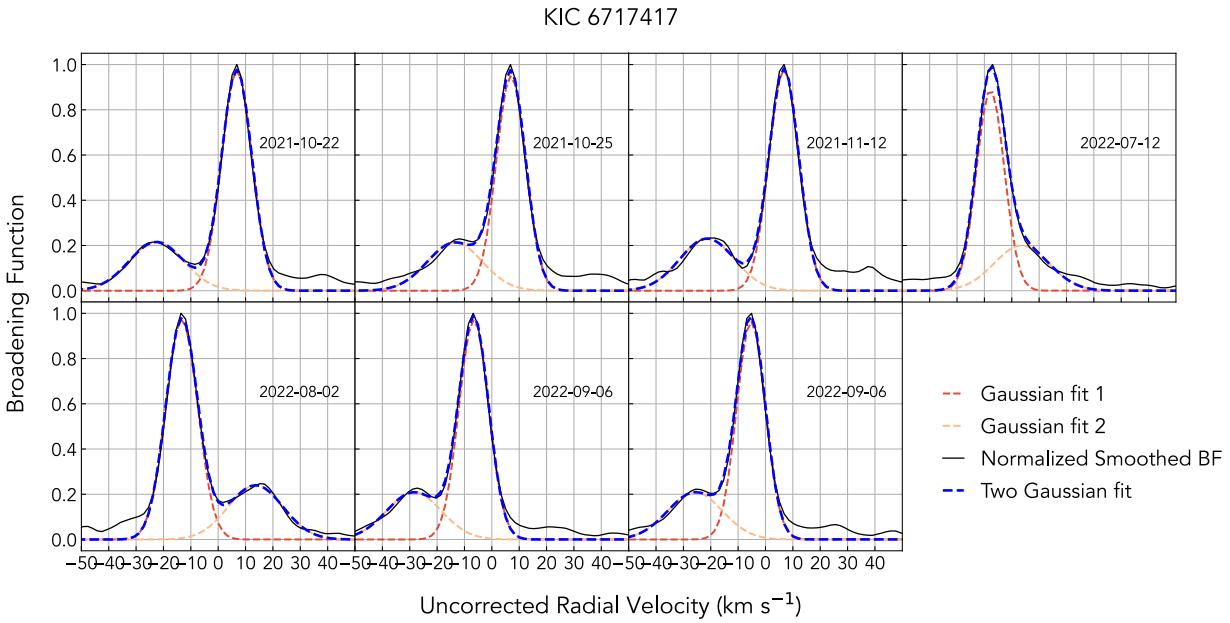

Figure 3: Broadening function for a series of observations of KIC 6717417. The double-lined nature of this spectroscopic binary is demonstrated by the two distinct peaks in the BF.

3.2 Spectroscopic binary status of observed targets

The results from the ongoing spectroscopic follow-up mission are preliminary. Of the 21 initial targets, only 17 have been observed three or more times. Although some targets have been observed up to 10 times, others have only been observed 3 times. Depending on the mass of the components and the orbital period, orbital velocities may be low and relatively undetectable with only a few observations over the span of a year. Additionally, if a binary is orientated pole-on, we would only observe very low line-of-sight velocities. That being said, Gaulme et al. (2020) determined a metric to estimate the expected amplitude of RV measurements of RGs in binaries using the ARCES instrument. Gaulme et al. (2020) used previous studies of RGs in EBs to determine a reasonable parameter space to model observable RV measurements. Systems were simulated with orbital periods 10-200 days, $\boldsymbol{M_{RG}}$=1-2.5Msol, mass ratios from 0.1 to 1, and eccentricities from 0 to 0.4. For orbits with e<0.4, the RG semi-amplitude ranges from 3-90 km/s with an average value of approximately 30 km/s. Since the observed RV is dependent on the inclination as well as the semi-amplitude, a sample of inclinations were drawn from a uniform distribution and the result was that sin(i) > 0.16 in 90% of cases. This means that with an average semi-amplitude of 30 km/s, there would be an observable RV > 4.7 km/s in 90% of randomly selected inclinations. As previous studies of RGs using ARCES have demonstrated that a typical RG spectrum with SNR ≈10-20 leads to derived RV uncertainties of $\boldsymbol{\sigma_{RV}}$ = 0.5 km/s (Rawls et al. 2016, Gaulme et al 2016), Gaulme et al. (2020) concluded that a target could be classified a spectroscopic binary if the radial velocity dispersion was greater than 2 km/s.

Although this analysis was designed for hidden binary star systems containing an active red giant, which is thought to have a shorter period and a more circularized orbit than the general RG binary population, the simulated systems largely overlap with the expected population of the targets

observed in this work. Since it is likely that spectroscopically detected RG binaries may have longer periods and higher eccentricities as shown in Beck et al. (2022), using $\boldsymbol{\sigma_{RV}} \geq$2km/s as a classification of binarity doesn't necessarily exclude targets below that threshold as binaries, but rather defines which targets' observations already display clear signs of binarity. According to this metric, 14 targets have been identified as spectroscopic binaries with one target clearly displaying two set of stellar lines (SB2). The current observational results can be seen in Table 1.

Table 1. Current observational results of pulsating hidden binary targets, including derived radial velocity dispersion and current classification of binary status.

KIC	# of observations	Radial Velocity dispersion (km/s)	Spectroscopic Binary Status
3660182	0	-	PB
4840401	11	4.66	SB1+
4951617	0	-	PB
5080290	5	47.57	SB1+
5620305	13	33.63	SB1+
5816671	7	2.22	SB1+
6468112	14	11.97	SB1+
6707691	7	3.04	SB1+
6717417	12	51.32	SB2
6791033	0	-	
7287493	4	1.52	Single*
8591738	12	4.36	SB1+
8720055	13	20.93	SB1+
9029195	6	5.89	SB1+
9612084	10	32.06	SB1+
9700679	12	6.98	SB1+
9813963	4	1.97	PB/Single*
10616594	11	6.06	SB1+
10685794	3	0.42	Single*
11559263	13	9.62	SB1+
11659003	0	-	PB
Notes: SB1+ indicates that there is significant radial velocity dispersion, but the companion's velocity has yet to be detected; Single* indicates that current analysis cannot confirm the target as a spectroscopic binary; PB indicates the target is a potential blend			

4. Conclusions

Studying stellar pulsators in binary star systems provides a unique set of constraints on stellar models that pushes forward our understanding of stellar interiors, stellar oscillations, and stellar evolution. Previous studies have looked at pulsating stars in *Kepler* eclipsing binaries, but this sample is limited in number and suffers from detection biases. Finding 'hidden' pulsating binaries in the *Kepler* catalog can expand the sample of pulsating binaries and reduce sample bias. Specifically, pulsating SB2s containing a solar-like and classical oscillator have similar constraints to that of an eclipsing SB2 and can be used to significantly constrain stellar models.

21 mainstream *Kepler* RGs with detectable solar-like oscillations which also displayed frequency signatures of classical oscillations were selected as the sample of potential hidden spectroscopic binaries. In order to look for false positives, each target was inspected for a randomly selected quarter and the light curve/PSD of pixels included in the aperture were compared to those outside of the aperture. Additionally, a literature review looked for any previous classifications as binaries or false positives. The SIMBAD Astronomical database was used to determine whether there were any known variable sources near the targets.

A spectroscopic follow-up campaign has been underway for the past year looking for time series Doppler shifts in spectral lines. Currently, 17 targets have been observed 3+ times and inspected for signs of orbital motion. Upon detection of spectral line shifts, radial velocities were derived from the observed spectra using a synthetic template and the broadening function technique. Of the 17 observed targets, 14 targets show significant RV dispersion indicative of orbital motion due to binarity and 1 of which two sets of spectral lines can clearly be measured.

Spectroscopic observations are scheduled to continue in order to observe all targets 3+ times, ensure that targets identified as SB1s have sufficient SNR to detect faint companions, and to obtain adequate phase coverage for SB2 KIC 6717417. Further refinement of the BF technique needs to be explored, e.g., varying spectral templates, using a standard star observation as a template, adjusting the considered wavelength region, etc., in order to continue optimizing the detection of spectral lines from faint companions.

Finally, once sufficient orbital phase coverage of KIC 6717417 is achieved, dynamical modeling can be performed. Using inputs from stellar atmosphere modeling of the spectra, asteroseismic scaling relations for the solar-like oscillator, and the derived radial velocity curves, dynamical modeling of the binary can be carried out. Ideally, this will provide precise stellar properties such that stellar evolution/oscillation models of the classical oscillations can be compared with the observed frequencies.

Acknowledgements

This research was sponsored by a Los Alamos National Laboratory Center for Space and Earth Sciences grant XX8P ASF2. This paper includes data collected by the *Kepler* mission and obtained from the MAST data archive at the Space Telescope Science Institute (STScI). Funding for the

Kepler mission is provided by the NASA Science Mission Directorate. STScI is operated by the Association of Universities for Research in Astronomy, Inc., under NASA contract NAS 5-26555. This research could not be possible without the observations obtained with the Apache Point Observatory 3.5-meter telescope, which is owned and operated by the Astrophysical Research Consortium. This research has made use of the SIMBAD database, operated at CDS, Strasbourg, France. This research used PyRAF, a product of the Space Telescope Science Institute which is operated by AURA for NASA, and Astropy, a community-developed core Python package for Astronomy.

References

Balona, L. A. 2018, *MNRAS*, **479**, 183
Beck, P. G., Mathur, S., Hambleton, K., et al. 2022, *A&A*, Accepted for publication
Bedding, T. R., Murphy, S. J., Hey, D. R., et al. 2020, *Nature*, **581**, 147
Benbakoura, M., Gaulme, P., McKeever, J., et al. 2021, *A&A*, **648**, A113
Berger, T. A., Huber, D., Gaidos, E., & van Saders, J. L. 2018, *ApJ*, **866**, 99,
Brown, T. M., Gilliland, R. L., Noyes, R. W., & Ramsey, L. W. 1991, *ApJ*, **368**, 599,
Gaulme, P., McKeever, J., Jackiewicz, J., et al. 2016, *ApJ*, **832**, 121
Gaulme, P., Jackiewicz, J., Spada, F., et al. 2020, *A&A*, **639**, A63
Gustafsson, B., Edvardsson, B., Eriksson, K., et al. 2008, *A&A*, **486**, 951
Hon, M., Stello, D., García, R.A., et al. 2019, *MNRAS*, **485**, 5616
Jenkins, J. M., et al. 2017, *Kepler Science Document KSCI-19081-002*
Kallinger, T., Beck, P. G., Stello, D., & García, R. A. 2018, *A&A*, **616**, A104,
Kirk, B., Conroy, K., Prša, A., et al. 2016, *AJ*, **151**, 68
Kjeldsen, H., & Bedding, T. R. 1995, *A&A*, **293**, 87.
Murphy, S. J., Li, T., Sekaran, S., et al. 2021, *MNRAS*, **505**, 2336
Rawls, M. L., Gaulme, P., McKeever, J., et al. 2016, *ApJ*, **818**, 108
Rucinski, S. 1992, *ApJ*, **104**, 1968
Rucinski, S. 2002, *ApJ*, **124**, 1746
Steindl, T., Zwintz, K., & Bowman, D. M. 2021, *A&A*, **645**, A119
Streamer, M., Ireland, M. J., Murphy, S. J., & Bento, J. 2018, *MNRAS*, **480**, 1372
Van Reeth, T., Tkachenko, A., Aerts, C. 2016, *A&A*, **593**, A120
Wang, S., Hildebrand, R. H., Hobbs, L. M., et al. 2003, *Society of Photo-Optical Instrumentation Engineers (SPIE) Conference Series*, **4841**, 1145

A Comparison of the HADS(B) Variables VZ Cnc and VY Equ

Matthias Kolb

Wuppertal, Germany; mako1997a@gmail.com

Subject Keywords

HADS(B) Stars; Photometry; Power Spectrum; individual (VZ Cnc, VY Equ)

Abstract

The two High Amplitude Delta Scuti (B) stars VZ Cnc and VY Equ were observed during fall 2021 and summer 2022 with small amateur equipment. Although both stars pulsate with nearly the same two frequencies, they show differences in their light curves. The combined effect of pulsating with two frequencies leads to amplitude and frequency modulations: Not all maxima are exactly located at phase 0 and their amplitude can vary by 0.5 mag (for VZ Cnc). Whereas VZ Cnc cycles show regular shaped light curves (steeper increase, clear maxima, sometimes shoulders), VY Equ also has cycles where the brightness does not change a lot over time. Instead of a clear maximum, a plateau-like feature appears. Based on Fourier analysis of the author's as well as the TESS light curves, this effect can be explained by the differences in the power spectrum: Whereas in VZ Cnc the first mode is clearly dominating, the pulsation in VY Equ has a significantly stronger contribution from the second pulsation mode.

1. Introduction

High Amplitude Delta Scuti (B) stars typically pulsate in two frequencies. VZ Cnc and VY Equ pulsate with first and second overtone; the fundamental frequency is missing. The ratio of those frequencies lies around 0.8. VZ Cnc was investigated in detail by Fitch (1955), Cox et al. (1984), Fu and Jiang (1999) and Boonyarak et al. (2009), whereas for VY Equ only the fundamental data are available (VSX database, Khruslov 2011). According to these data, both stars have nearly identical pulsation periods: 0.176 / 0.178 d for the first overtone and 0.142 / 0.141 d for the second overtone (VZ Cnc / VY Equ). The amplitude of the pulsation is different: VZ Cnc shows amplitudes up to 0.7 mag whereas VY Equ only shows amplitudes up to 0.3 mag.

Table 1: V and TESS magnitude ranges

	VSX	**This work**	**TESS**
VZ Cnc	7.18 – 7.91	7.19 – 7.88	7.03 – 7.48
VY Equ	10.21 – 10.51	10.11 – 10.49	9.87 – 10.07

The author's motivation for the observation of both stars was to reproduce the literature data on the frequencies / periods of the pulsations and check for potential additional pulsation modes. Additionally, no data for VY Equ were available in the AID database of the AAVSO. It was rather a surprise that some light curves of VY Equ showed an unexpected behavior: Over a significant part

of the period the brightness did not change a lot, and no clear maximum appeared. A first explanation was a defect during the measurement, but the observation could be reproduced in later cycles. The fact that the Transitioning Exoplanet Survey Satellite (TESS) observed both stars offered the opportunity to compare these high-resolution light curves with the author's measurements. A detailed analysis of the pulsation modes was carried out using Vstar from the AAVSO (Benn) to identify differences between the two stars.

2. Observations

The two stars were observed using a small refractor in combination with a DSLR camera (90 mm F5.6 / Canon D450 and D600). The green channel was evaluated by comparing the instrumental magnitude with several comparison stars from the AAVSO star plots. Error bars in the light curves below are calculated from the differences due to the use of more than one comparison star. Transformation corrections were estimated based on blue channel data, but did not significantly change brightness. Anyhow, the shape of the light curves and not the true brightness level was the topic of interest.

For both stars only a small number of cycles could be observed (14/18), some not even complete. It was not possible to observe two consecutive cycles for either star. This has a significant impact on the Fourier analysis of the light curves which is described in section 4.

TESS has also observed both stars: VZ Cnc already in 5 campaigns (2019-2021), VY Equ in one (August 2022) with an observation period of 29 days each. The TESS filter band range is 600-1000 nm; therefore, the amplitude of the variations is smaller. This is typical behavior of pulsation in stars like Cepheids but also Miras.

For VZ Cnc the time range of the TESS campaigns did not coincide with the author's observations but for VY Equ, some of the observed cycles fell into the TESS campaign.

3. Light curves

Normal delta Scuti stars with one pulsation frequency show the typical pattern of steep increases followed by slower decreases, similar to Cepheids. Maxima and minima of the brightness appear at the same phase cycle by cycle; typically phase zero defines the maximum.

Pulsators with more than one significant frequency show more complicated light curves with significant amplitude and period modulation: The time differences between maxima do not exactly match the main period (inverse of major frequency). This is shown for VZ Cnc in Fig. 1 based on the TESS data. The main period of 0.1783 days is modulated by the second frequency. The "beat" (v2-v1) generates an additional periodicity. The amplitudes vary very significantly; one out of four is typically low, and shoulders may appear. Fig. 2 shows a histogram of the brightness amplitudes for VZ Cnc based on 11 observations which included both minimum and maximum for the cycle.

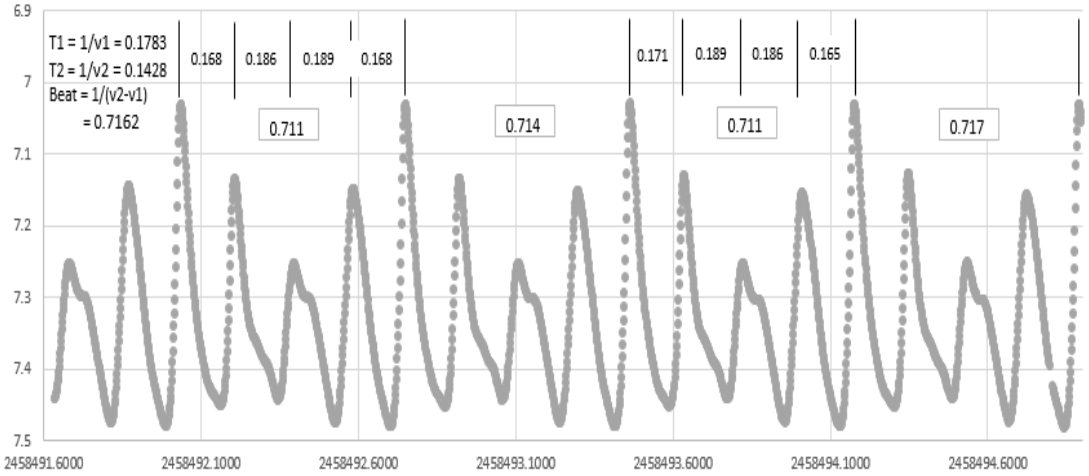

Figure 1. VZ Cnc light curve with major periods and beat

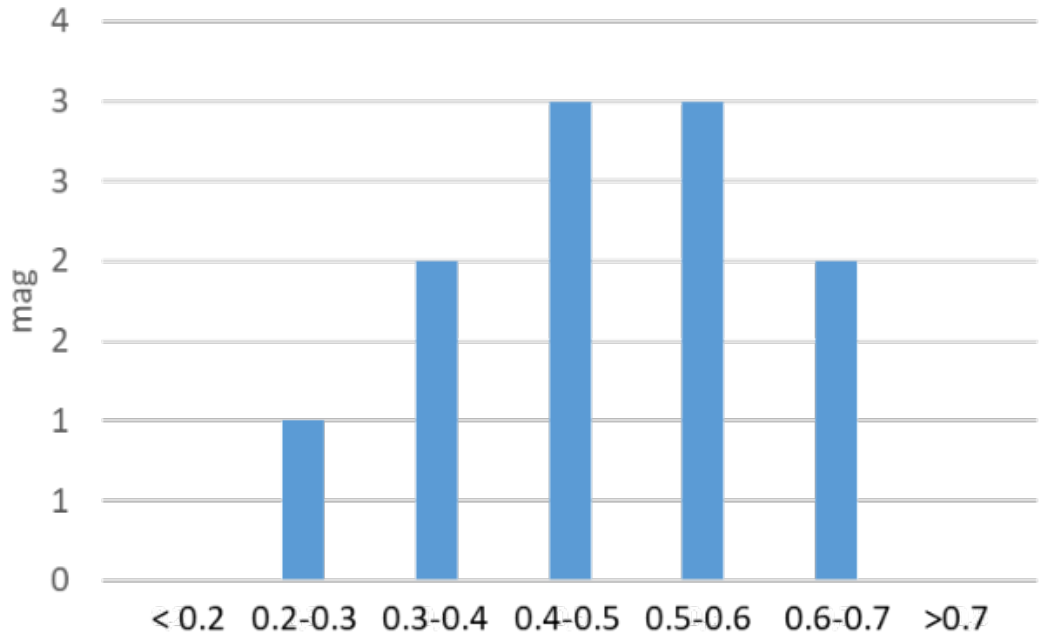

Figure 2. Histogram of amplitudes of 11 cycles of VZ Cnc

As the author did not observe VZ Cnc at same time as TESS did, the TESS measurements were used to build a Fourier model to interpolate the TESS light curves to the observation dates. Fig. 3 shows three observation cycles. For the middle one, data from the red DSLR channel are included to show that indeed the amplitude is smaller compared to the green (V) band, similar to TESS data.

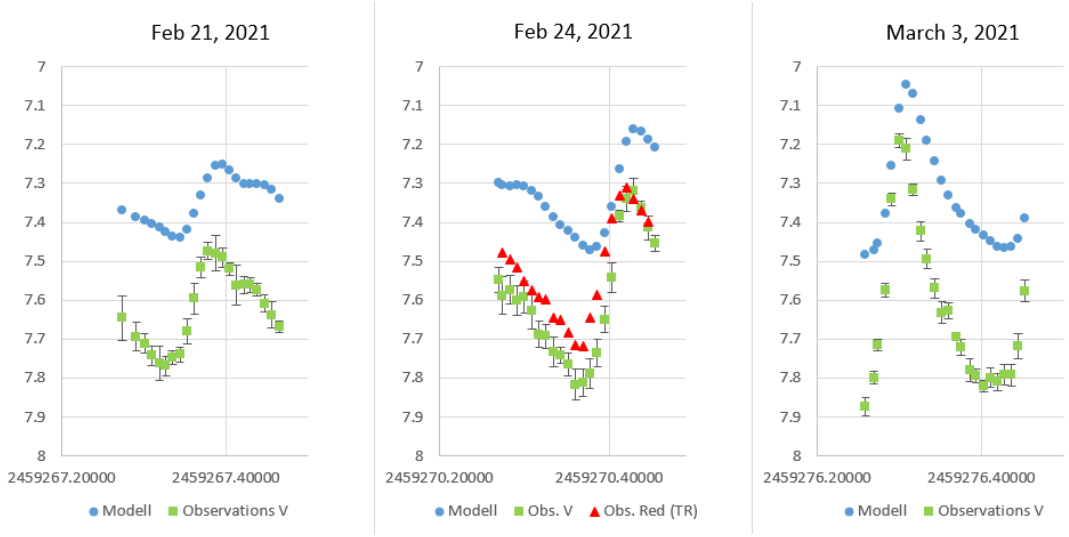

Figure 3. VZ Cnc – Own observations and TESS model

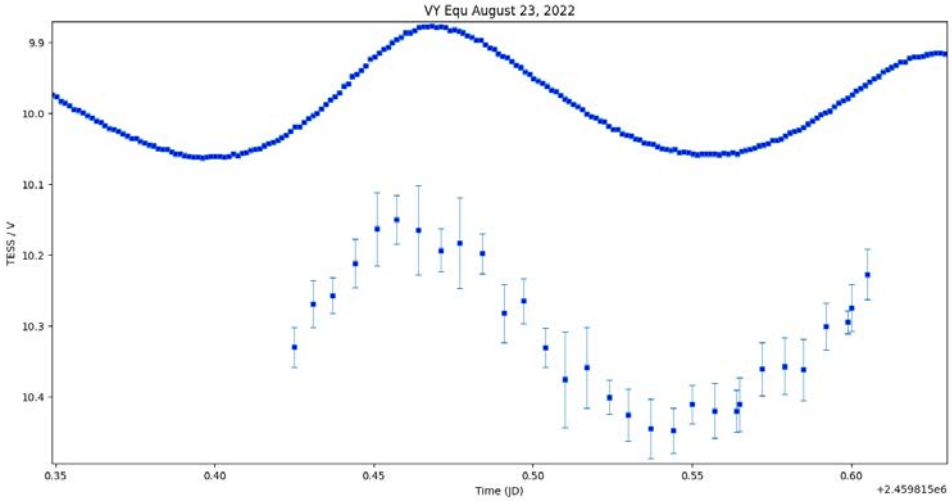

Figure 4a. Observation and TESS data for VY Equ from August 23, 2022

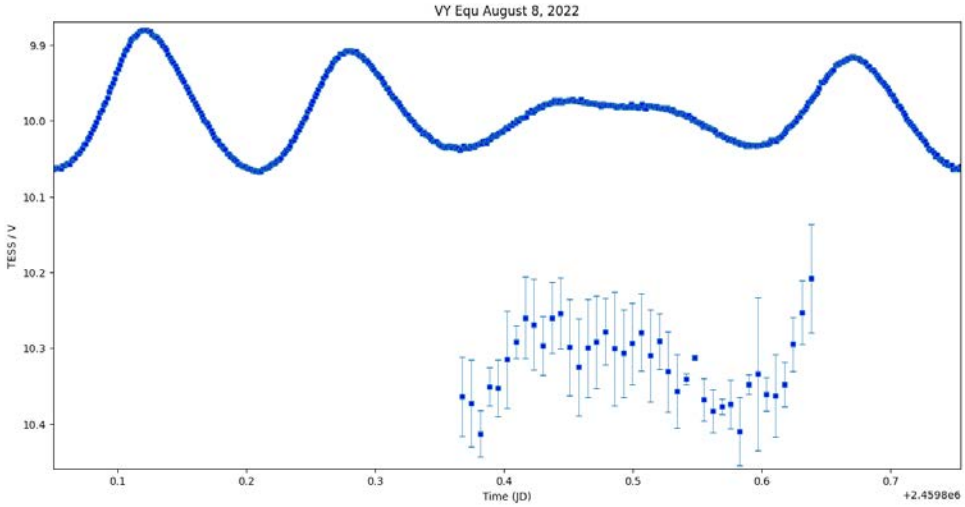

Figure 4b. Observation and TESS data for VY Equ from August 8, 2022

4. Frequency analysis of the observations and TESS data

The standard method to extract pulsation frequencies from light curves is the Discrete Fourier Transformation (DFT). The analysis was done using the program VStar (Benn 2012) from the AAVSO. The number of cycles observed is very small compared to the total number during the observation periods, and many cycles are missing between observed cycles. As a consequence, the resulting power spectra of the Fourier analysis show a significant number of *alias* peaks (left and right to the frequency with 1 d^{-1} difference). To identify the second pulsation frequency, the *pre-whitening* technique was applied: A model based on the first frequency including its harmonics was subtracted from the light curve and the residuals were analyzed with DFT. Figs. 5a and 5b show the power spectrum for VZ Cnc before and after pre-whitening.

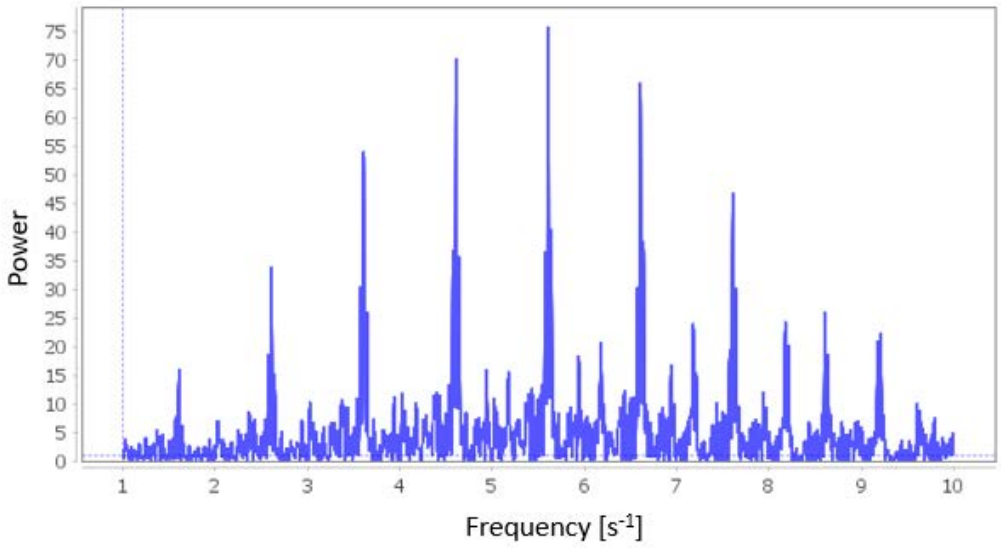

Figure 5a. Power spectrum for VZ Cnc

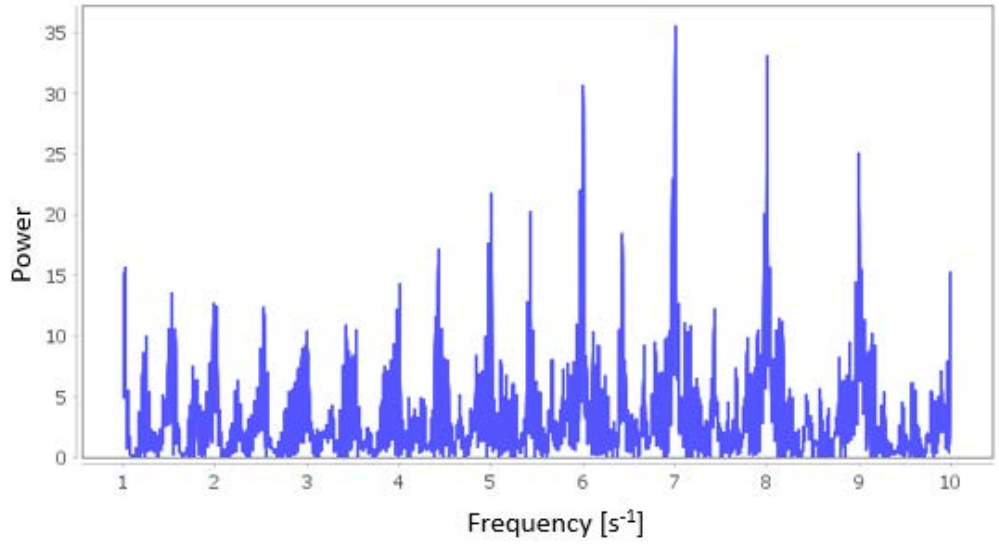

Figure 5b. Power spectrum for VZ Cnc after pre-whitening

The TESS dataset includes more than 16,000 data points per observation cycle, taken every 120 seconds. Therefore, the power spectra show very clear peaks for both the two main frequencies as well as many combinations of them, in particular their harmonics 2v, 3v, … and the "beat" v_2-v_1. Fig. 6a shows the power spectrum of VZ Cnc, identifying all peaks above the noise. No third independent frequency is visible.

In this figure the Y axis shows the semi-amplitude which identifies the amount that the frequencies contribute to the overall variation of the brightness. The main frequency at 5.61 s^{-1} and its harmonics are clearly the major contributors.

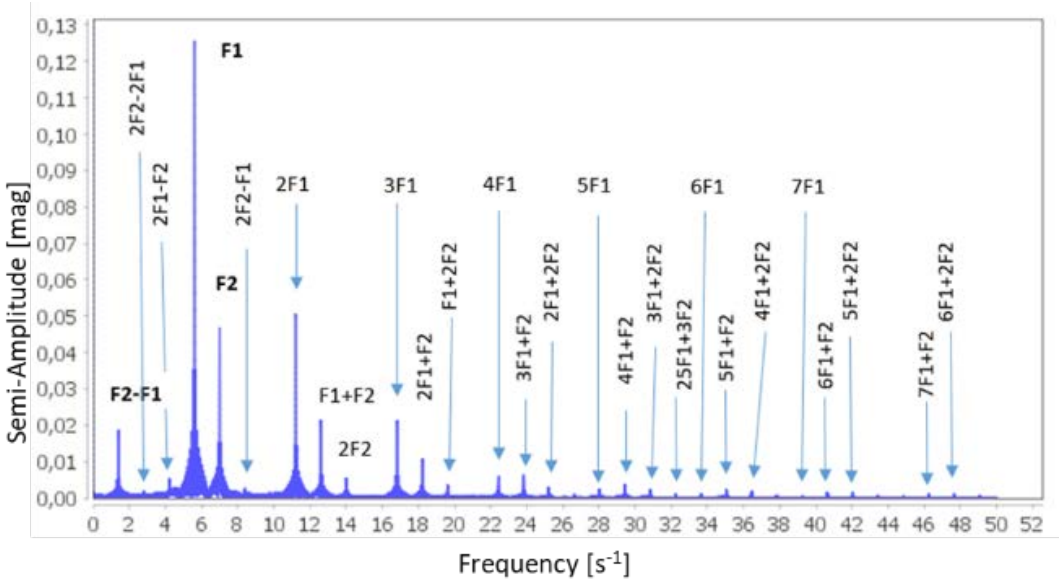

Figure 6a. Power spectrum of TESS light curves (VZ Cnc)

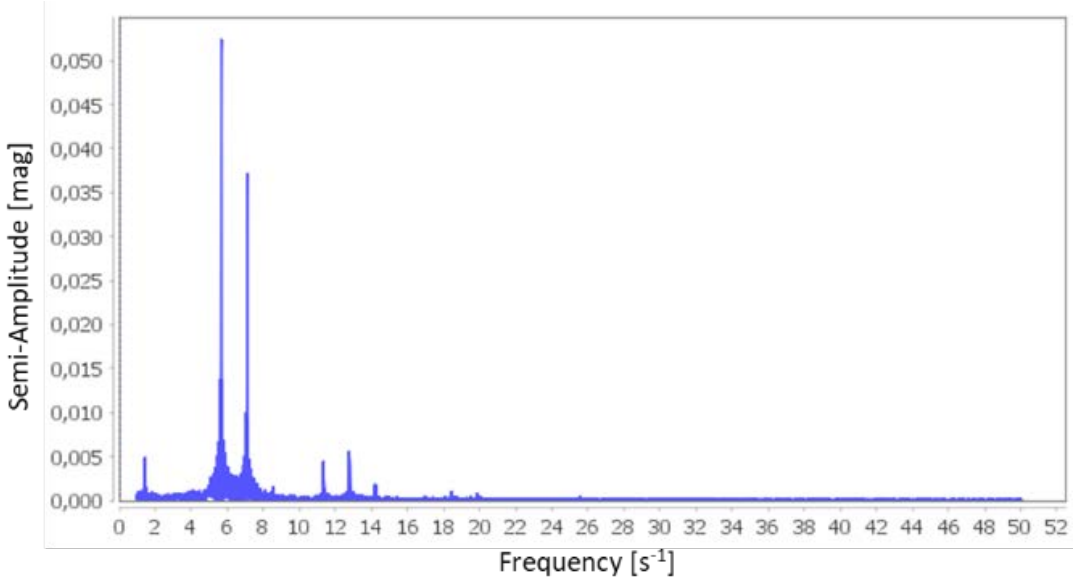

Figure 6b. Power spectrum of TESS light curves (VY Equ)

Looking at the DFT of VY Equ, it is clearly visible that the harmonics of v_1 and other combination frequencies are much smaller, but v_2 is much more pronounced vs. v_1 in comparison to VZ Cnc. As the light curve is a superposition of the frequencies, VY Equ shows a more complicates and less regular light curve than VZ Cnc. Table 2 shows the frequencies and semi-amplitudes for both stars. The periods are very similar between the two stars, but the ratio of the semi-amplitudes is approx. 2.5 for VZ Cnc but only 1.3 for VY Equ.

5. Conclusion

The calculated frequencies from the very limited number of observations match very well with previous literature and TESS data.

The unusual light curves for some cycles of VY Equ originate from a pronounced excitation of v_2. It would be very interesting to understand the underlying differences in the stellar parameters that drive the increased contribution from the second overtone of the pulsation.

Table 2: Periods (days) and semi amplitudes (mag)

		P (v_1)	**P (v_2)**
VZ Cnc	**Fu**	0.17836	0.14280
	Cox	0.17836	0.14281
	This work	0.17835	0.14279
	TESS	0.17836	0.14280
VY Equ	**Khruslov**	0.17644	0.14078
	This work	0.17644	0.14078
	TESS	0.17644	0.14079
		SA (v_1)	**SA (v_2)**
VZ Cnc	**This work**	0.180	0.060
	TESS	0.126	0.051
VY Equ	**Khruslov**	0.071	0.055
	This work	0.090	0.070
	TESS	0.052	0.037

Acknowledgements

This paper includes data collected by the TESS mission. Funding for the TESS mission is provided by the NASA's Science Mission Directorate (https://heasarc.gsfc.nasa.gov/docs/tess/). This research has made use of the International Variable Star Index (VSX) database, operated at AAVSO, Cambridge, Massachusetts, USA.

References

Benn, D. 2012, "Algorithms + Observations = VStar", *JAAVSO* **40**, 2, pp. 852-866.
VStar: https://www.aavso.org/vstar
Boonyarak, C., Khokjuntod, P., Jiang, S.-Y. 2009, *Astrophys. Space Sci.* **324**, 5-11
Cox A.N., McNamara B.J., Ryan W. 1984, *ApJ* **284**, 250
Fitch W.S. 1955, *ApJ* 1**21**, 690
Fu, J.-N. , Jiang, S.-Y. 1999, *Astrophys. Suppl. Ser.* **136**, 285-292
Khruslov, A.V. 2011, *Prilozhenie*, vol **11**, N30
Kolb, M. 2021, BAV Rundbrief 2, https://www.bav-astro.eu/rb/ rb2021 2/75.pdf

"Doing My Best to Watch Phenomenal Stars": Variable Star Astronomy in Thomas Hardy's *Two on a Tower* (1882)

Kristine Larsen

Central Connecticut State University, 1615 Stanley St., New Britain, CT, 06050, USA;
larsen@ccsu.edu

Subject Keywords

Victorian literature; variable star observing; stars: individual (Algol, eta Car, Sun)

Abstract

The science depicted in works of popular literature reflects the knowledge at the time of the work's writing. The analysis of such works therefore provides evidence for how widespread this knowledge was at the time in question, in large part thanks to popularizations of science. Using Thomas Hardy's *Two on a Tower* (1882) as an example, it is demonstrated that previous analysis by Hardy scholars of the variable star science depicted in the novel has missed numerous astronomical references. It is therefore argued that astronomers have much to offer their humanities colleagues in terms of literary analysis and historical analysis of literature.

1. Introduction

In H.G. Wells' classic 1895 novella *The Time Machine* the traveler journeys millions of years into the future, to a dying earth where the weak light of the now shrunken red dwarf sun is insufficient to warm the planet despite its now much smaller distance from us (thanks to tidal effects) (Wells 2005, 84). Wells' description reflects quite accurately the astronomical understanding of his day, when the source of the sun's energy was erroneously thought to be caused by our star shrinking itself out of existence. Literary scholars (e.g., Beare 1996, 33) have incorrectly interpreted the evolution of Wells' sun as reflecting the knowledge of the late 20th century and the sun's expansion into a red *giant* rather than a red *dwarf*. In this way we see that not only does a careful analysis of novels, short stories, and other media afford us valuable insights into the scientific knowledge and public misconceptions at the time of the media's creation (as well as the author's personal scientific knowledge), but that the examination of such texts by astronomers is likely to result in a significantly different analysis than that by literary scholars.

Pop culture references to variable stars specifically provide a snapshot of our understanding of these objects and their familiarity to the general public at a given moment in time. For example, the 1901 nova outburst of GK Persei appears in H.P. Lovecraft's 1919 short story "Beyond the Wall of Sleep," the story quoting by name a description of the event from the then popular work Garrett P. Serviss' *Astronomy with the Naked Eye* (1908). Edmond Hamilton's 1934 novella *Thundering Worlds* explores the future adventures of humanity in search of a new star once our sun begins to die. One rejected candidate is about to go nova, while another is an eclipsing binary

whose frequent eclipses by a dead companion are considered too problematic for a civilization reliant on solar energy. Gabriel Tarde's 1896 novel *Underground Man* takes an increase in sunspot activity as a sign that the sun is dying, as does Robert Heinlein's 1952 short story "The Year of the Jackpot." Olaf Stapledon's curious 1937 novel *Star Maker* depicts stars as sentient beings, with the "strange Cepheid variables" described as "the most baffling of all the stellar kinds. It seems that these and other variables of much longer period alternate mentally between fervour and quietism, in harmony with their physical rhythm. More than this it is impossible to say" (144).

Perhaps the most astronomically interesting fictional depiction of variable star astronomy has thus far largely escaped the notice of scholars beyond focused studies of its author, the 1882 Thomas Hardy romance *Two on a Tower*. Pamela Gossin (2007) has produced the most detailed survey of the astronomical references in *Two on a Tower* to date and tied them to astronomical papers of the time (especially Edward C. Pickering's 1880 seminal paper on eclipsing binaries). However, a close reading by this variable star observer has yielded additional connections that have heretofore been missed.

2. *Two on a Tower* and Variable Star Astronomy

The novel was initially serialized in *Atlantic Monthly* before being published as a complete volume, written in relative haste in order to increase Hardy's assets after recovering from a serious illness. However, it was "criticized on moral ground for certain elements of sexual innuendo and as an unfair satire on the Established Church of England" (Gossin 2007, 155). The astronomical detail in this "least known and least appreciated" (Gossin 2007, 155) of the author's works (his ninth published novel) – including observations of comets, planets, aurora, variable stars, and the sun – reflects both his personal love and knowledge of astronomy (Gossin 2007, 156) and experience with his family's "big brass telescope" (F. Hardy 1962, 2). The appearance of the novel in the year of a rare transit of Venus is no coincidence, with Hardy scholars noting the author's intention to capitalize on public interest in and knowledge of the transit (Peck 2011, 29). Indeed, Hardy's young astronomer Swithin observes the transit (off screen) as part of a scientific expedition (T. Hardy 249; 264). The eponymous observation tower itself was modelled on a column in Charborough Park in Dorset (Kim 63), and Hardy wrote to the Royal Observatory at Greenwich requesting a visit in order to get an expert opinion on the viability of his fictional observatory (Gossin 2007, 157-8).

The star-crossed love affair between Lady Vivette Constantine and younger astronomer Swithin St. Cleave begins in the titular homemade observatory with an observation of solar activity, a cyclonic "maelstrom of fire" that serves as a fitting metaphor for their ill-fated relationship (T. Hardy 1993, 11). The description of sunspots as cyclonic echoes popular astronomical works of the time; for example, in his textbook *Fourteen Weeks in Descriptive Astronomy*, J. Dornan Steele relates how "One spot was noticed which had a motion three times greater than that of clouds driven along by the most violent hurricane. Again, immense cyclones occasionally pass over the surface with fearful rapidity, producing rotation and sudden changes in the spots" (1869, 57). Popularizer of 19th century astronomy Agnes Clerke stated that "cyclonic movements are now a

recognized feature of sun-spots. They are, however, as Father Secchi concluded from his long experience, but temporary and casual…. A whirlpool phase not unfrequently accompanies their formation, and may be renewed at periods of recrudescence or dissolution" (Clerke 1902, 144). However, writing in 1902, Clerke opined that John Herschel's 1847 (434) hypothesis that sunspots are very similar to "hurricanes and tornadoes" in the atmosphere of the sun "may be said to have completely broken down" by her time (Clerke 1902, 144).

2.1 Descriptions of variable star astronomy circa 1880

Gossin (2007, 168-9) observes that Hardy was heavily influenced by the popular-level writings of English astronomer Richard Proctor, in particular, his 1872 work *Essays on Astronomy*. For example, Swithin proclaims that he hopes "to be the new Copernicus. What he was to the solar system I aim to be to the systems beyond" (T. Hardy 1993, 32), a nod to Proctor's reflection that "The Copernicus of the sidereal system is not to be expected for many generations, perhaps not for thousands of years" (1872, 240). More generally, Hardy adopts Proctor's opinion that amateur astronomers should not merely repeatedly observe showpiece objects such as Saturn, but instead "Every observation not intended as a mere relaxation from real work should be intended to ascertain some as yet unknown fact" (Proctor 1872, 44). It is therefore not surprising that chief among Swithin's astronomical observations is his work on variable stars, what he describes as "Tedious work…. Doing my best to watch phenomenal stars, as I may call them" (T. Hardy 1993, 31).

At the time of this novel's writing, there were only about 150 variable stars identified, and the reasons for their variations were the subject of open speculation, as noted in popular level astronomy books of the period (e.g., Steele 1869, 268; Sharpless & Phillips 1882, 245-6). Swithin observes variable stars every night, "while there is no moon … till about two in the morning" (T. Hardy 1993, 12). When Lady Constantine asks him to go to London on a personal errand, he initially begs off, explaining

> *I am preparing a work on variable stars. There is one of these which I have exceptionally observed for several months. And on this one my great theory is mainly based. It has been hitherto called irregular; but I have detected a periodicity in its so-called irregularities which, if proved, would add some very valuable facts to those known on this subject, one of the most interesting, perplexing, and suggestive, in the whole field of astronomy. Now to clinch my theory there should be a sudden variation this week – or at the latest next week – and I have to watch every night not to let it pass…. (T. Hardy 1993, 37).*

He ultimately relents to her request so long as she promises to observe this particular star (unnamed in the novel) every clear night about nine, and if it is cloudy at 4 AM instead (T. Hardy 1993, 37). Swithin checks in (via letter), warning that "Watching the star through an opera-glass Sunday night I fancied some change had taken place, but I could not make myself sure. Your memoranda for that night I await with impatience. Please don't neglect to write down, *at the moment*, all remarkable appearances, both as to colour and intensity; and be very exact as to time, which correct in the way I showed you" (T. Hardy 1993, 39). He is later dismayed to learn

that she had missed two nights, but nevertheless he manages to make "an amazing discovery in connection with the variable stars!... It will excite the whole astronomical world, and the world outside but little less. I had long suspected the true secret of their variability; but it was by the merest chance on earth that I hit upon a proof of my guess…. It accounts for the occasional green tint of Castor, and every difficulty" (T. Hardy 1993, 65). Unfortunately, Swithin nearly dies from pneumonia when he throws himself to the ground and lays there for hours during a rainstorm upon reading that he had been scooped by "a pamphlet by an American astronomer, in which the author announced a conclusive discovery with regard to variable stars" (T. Hardy 1993, 69).

The description of variable star observing in the novel is fairly accurate. It is done with both telescopes and binoculars, and stars that are prone to sudden changes, especially irregularly, do need to be monitored on every clear night. Careful estimation of a star's brightness and the time of observation are also required. By the time of Hardy's novel there had been a number of articles describing the methodology of estimating stellar magnitudes using comparison stars (e.g., Argelander 1855; Knott & Baxendell 1863). E.C. Pickering's famous pamphlet, *A Plan for Securing Observations of the Variable Stars*, appeared in 1882 as well, probably too late to be an influence on the novel.

While stars cannot appear green to the human eye, some observers describe Zubeneschamali in Libra as green, among others (McClure). There are numerous 19th century references to Castor appearing green (e.g., von Humbolt 1858, 131), although as Gossin correctly notes, John Herschel (1876, 621) came to attribute this to an optical effect due to "contrasted or complementary colors" in double stars. However, Gossin fails to realize that the reference to a star changing color also refers to certain variables such as Mira, which Herschel (1876, 598) noted became redder when it was near maximum, as well as discussion in the 19th century of stars that supposedly changed color over recorded history (Whittet 1999). In particular, Proctor spends a great many pages discussing star colors, and points out that two double stars that were described as white by William Herschel "now exhibit golden-yellow primaries and greenish satellites" (1872, 260). Instead, Gossin connects the reference to star colors to an eclipsing binary made of different color stars, in addition to highlighting the metaphorical usage of contrasting star colors to describe the "mutual gravitational attraction between two heavenly bodies" – Swithin and Viviette – of contrasting/complementary age and social status (2007, 178).

2. 2. Edward Pickering and Two on a Tower

Modern editors of Hardy's novel have taken as canon that the Harvard College Observatory Director Edward C. Pickering's paper "Dimensions of the Fixed Stars, with Especial Reference to Binaries and Variable of the Algol Type," presented to the American Academy of Arts and Sciences on May 25, 1880, and afterwards published in the *Proceedings*, is the real-world paper that scooped Swithin (e.g., Pinion 1975, 283; Gossin 2007, 177). As Dorrit Hoffleit (1972, 4) summarized, while an eclipsing model had been suggested for Algol as early as 1783 (by John Goodricke), Pickering provided the first "positive proof" through his detailed calculations of the stars' orbits.

While Pickering's paper is not the sole influence (see the previous discussion of star colors), Hardy scholars have made a reasonable assumption of its importance. However, there are additional facts that they have apparently missed which actually bolster their case. For example, Swithin makes it seem as though the star that he was most keenly observing has some irregularities that he seeks to explain theoretically. Similarly, Pickering (1880, 35) suggests in his paper that the well-known slight changes in the period of Algol's primary eclipses (e.g., von Humboldt 1858, 174) can be explained by the presence of a third object in the system, a possibility that is widely accepted today (GCVS Team 2005).

The question remains as to how likely is Hardy to have read this paper, or at the very least a detailed summary. Such summaries were published in at least two popular level periodicals, *The Observatory* (Anon. 1881b) and *The Astronomical Register* (Anon. 1881a), the second of which was a forerunner to the *Journal of the British Astronomical Association* (Johnson 1990, 62). The specific reference to a "pamphlet" further suggests a direct connection to these popular reviews: *The Astronomical Register* article is explicitly a review of a 37-page version of the paper "reprinted" from the *Proceedings* and published by the University Press at Harvard, in other words, a pamphlet.

2.3. The Eta Carinae connection

There is one further astronomical connection to Swithin's research that has apparently thus far escaped the notice of Hardy scholars. Not only is Swithin interested in the changes in color of his favorite variable star and its irregularities, but his fictional treatise "A New Astronomical Discovery" accounts "for the nebulous mist that surrounds some of them [variables] at their weakest time" (T. Hardy 1993, 69). This strongly suggests a connection to one of the most enigmatic variables of the 19th century, Eta Carinae (then called Eta Argus), despite the fact that it is not visible from the latitude of England. Now known to be a massive luminous blue variable (LBV), the star had its so-called Great Eruption from 1837-56, becoming one of the brightest stars in the sky. It declined for about a decade until "a small brightening or plateau occurred in 1869-71" (Frew 2004, 2).

Popular-level astronomy books as well as popular journals that Hardy would have been familiar with contain numerous references to this star's unusual activity in the 19th century. For example, Alexander Von Humboldt (1858, 135) noted that "The star η Argus, which has been rendered celebrated by Sir John Herschel's observations… is undergoing a change in color as well as in intensity of light." Indeed, John Herschel was particularly interested in the behavior of this star, writing in his *Outlines in Astronomy* (1876, 603-5) that "The alterations of brightness in the southern star η Argûs, which have been recorded, are very singular and surprising….. All at once in the beginning of 1838 it suddenly increased in lustre so as to surpass all the stars of the first magnitude except Sirius…. 'A strange field of speculation,' it has been remarked, 'is opened by this phenomenon.'" In a *MNRAS* article on the star and its "Surrounding Nebula" Herschel noted reports of changes in both the star and the so-called Keyhole Nebula associated with it in 1868, opining "There is no phenomenon in nebulous or sidereal astronomy that has yet turned up, presenting anything like the interest of this, or calculated to raise so many and such momentous

points for inquiry and speculation" (Herschel 1868, 225). In response to this renewed activity, Herschel urged that "the attention of every astronomer in the southern hemisphere provided with instruments at all competent to show… the brighter portions of the nebula, should be directed in its delineation…" (1868, 225).

Astronomers were slow to answer Herschel's call, although there was a flurry of claims of activity in 1871-2 (e.g., Russell 1871; Abbott 1873), along with an interesting pushback from some astronomers who felt the perceived activity was wishful thinking or an optical illusion. For example, Richard Proctor reportedly called these observations an "imaginary discovery" in a December 1871 article in *The English Mechanic* (cited in Abbott 1873). Given the volume of discussion, as well as Proctor's role in it, the controversy would have certainly not escaped Hardy's notice. Furthermore, Gossin argues that Proctor's description of John Herschel's astronomical accomplishments may have "played a part in developing the character of Swithin St. Cleeve" (2007, 114-5). Evidence can be seen in the novel itself, when Swithin spends time at the Cape of Good Hope for several years "with a view to his great task of surveying, charting, and theorizing on those exceptional features in the southern skies which had been but partially treated by the younger Herschel" (T. Hardy 1993, 264).

3. Conclusions

While the characterization by literary scholars and historians of science of Thomas Hardy's usage of variable star astronomy in his novel *Two on a Tower* has been technically correct, it has been far from complete. The additional references from the novel to variable star astronomy in the 19th century provided in this close reading demonstrate why astronomers have much to contribute to literary analysis.

References

Abbott, F. 1873, *Astron. Reg.*, **11**, 221.
Anon. 1881, *Astron. Reg.*, **19**, 253.
Anon. 1881, *Observ.*, **4**, 116.
Argelander, F. 1855, *Astron. J.*, **4**(8), 57.
Beare, R. 1996, *Mythlore,* **21**(3), 33.
Clerke, A. M. 1902, *A Popular History of Astronomy During the Nineteenth Century, 4th ed.*, A. & C. Black, London.
Frew, D. J. 2004, *Journal of Astronomical Data*, **10**(6), 1.
Gossin, P. 2007, *Thomas Hardy's Novel Universe,* Ashgate, Hants.
GCVS Team, 2005, International Variable Star Index, https://www.aavso.org/vsx/index.php?view=detail.top&oid=26202.
Hamilton, E. 1934, *Thundering Worlds*, http://fantasticworlds-jordan179.blogspot.com/2013/06/thundering-worlds-1934-by-edmo.html.
Hardy, F. E. 1962, *The Life of Thomas Hardy, 1840-1928*, Macmillan, London.
Hardy, T. 1993, *Two on a Tower*, ed. S. M. Ahmad, Oxford, Oxford UP.
Heinlein, R. A. 1987, *The Menace from Earth*, Baen Books, New York.

Herschel, J.F.W. 1847, *Results of Astronomical Observations Made During the Years 1834, 5, 6, 7, 8, at the Cape of Good Hope*, Smith, Elder & Co., London.
Herschel, J.F.W. 1868, *MNRAS*, **28**, 225.
Herschel, J.F.W. 1876, *Outlines of Astronomy*, New ed., D. Appleton & Co., New York.
Hoffleit, D. 1972, *J. Amer. Assoc. Var. Star Obs*., **1**, 3.
Johnson, P. 1990, *J. Brit. Astr. Assoc.,* **100**(2), 62.
Kim, D. 2012, *The Hardy Society Journal*, **8**(1), 62.
Knott, G., and Baxendell, J. 1863, *Astron. Reg*., **1**, A1.
Lovecraft, H.P. 2009, "Beyond the Wall of Sleep," https://www.hplovecraft.com/writings/texts/fiction/bws.aspx.
McClure, B., 2022, Is Zubeneschamali a green star? https://earthsky.org/brightest-stars/libras-zubeneschamali-the-only-green-star/.
Peck, G. 2011, *Pacific Coast Philology,* **46**, 28.
Pickering, E. C. 1880, *Proc. Amer. Acad. Arts and Sci.,* **16**, 1.
Pickering, E. C. 1882, *A Plan for Securing Observations of the Variable Stars, 2nd ed.,* John Wilson & Son, Cambridge.
Pinion, F.B., ed. 1975, *Two on a Tower*, Macmillan, London.
Proctor, R. A. 1872, *Essays on Astronomy*, Longmans, Green, & Co., London.
Russell, H.C. 1871, *The Astronomical Register*, **9**, 193; 212; 251.
Serviss, G.P. 1908, *Astronomy with the Naked Eye*, Harper & Brothers, New York.
Sharpless, I., and G. M. Philips. 1882, *Astronomy for Schools and General Readers, 3rd ed.,* Lippincott, Philadelphia.
Stapledon, O. 2008, *Starmaker*, Dover, Mineola.
Steele, J. D. 1869, *Fourteen Weeks in Descriptive Astronomy*, A.S. Barnes & Co., New York.
Tarde, G. 1905, *Underground Man*, transl. C. Brereton, https://www.gutenberg.org/cache/epub/33549/pg33549-images.html.
Von Humboldt, A. 1858, *Cosmos, Vol. III*, trans. E.C. Otté, Harper & Brothers, New York.
Wells, H.G. 2005 [1895], *The Time Machine*, ed. Patrick Parrinder, Penguin Books, New York.
Whittet, D. C. B. 1999, *MNRAS*, **310**(2), 355.

Detecting Unknown Asteroids using Robotic Telescopes, Open Data, and Python

Arushi Nath

Co-Founder, HotPopRobot, Toronto, Ontario, Canada; astroarushi@gmail.com

Subject Keywords

Planetary Defense, Asteroids, Python, Robotic Telescopes, Open Data, Citizen Science

Abstract

Asteroid collision risks are real and unpredictable, making them an intergenerational challenge. NASA recently concluded the DART Mission, humanity's first planetary defense test mission. Citizen scientists also have a role to play. My project strengthens planetary defense by using robotic telescopes, open data, math, and Python to find unknown asteroids. I used images from robotic telescopes located worldwide to get full sky coverage. Using Python, I created an algorithm to query GAIA and NASA Horizon sky catalogues to find all known stars and asteroids. Mean, standard deviation, and histograms were used to create masks to remove known objects. The remaining objects were classified as possible asteroid candidates. I detected three 'preliminary' asteroids. My algorithm's plate-solving ability determined its Right Ascension and Declination using the telescope's focal length and celestial location. I reported this information by creating a Minor Planet Center report for my images.

1. Introduction

Asteroids are rocky remnants left over from the early formation of our solar system. Over a million asteroids have been identified, with sizes ranging from 10 m to 530 km. Many remain undetected, or their orbits are uncertain. This presents a possibility that the asteroid's orbit can intersect with the Earth's orbit, possibly resulting in catastrophe. Some of these near-Earth asteroids (see Figure 1) may be on a collision course with the Earth. In 1908 a 30-meter asteroid entered the Earth's atmosphere and exploded above ground in Russia, knocking down around 80 million trees (Anderson & Whitt, The Tunguska Explosion, 114 Years Ago Today, 2022). In addition, in 2013, the Chelyabinsk asteroid collided with Earth, damaging buildings and injuring over 1500 people (Byrd, Chelyabinsk meteor: 9 Years Ago Today, 2022). More recently, on November 19, a 1-metre asteroid impacted the Earth in Canada. It was only the sixth time in history that an asteroid warning system noted the object before it made contact with the Earth (Westoll, Fireball lights up Toronto night sky, meteor becomes 6th to be detected pre-impact, 2022). Evidently, the risk of asteroid collision is real. Hence, detecting and tracking unknown asteroids is the key to strengthening planetary defense.

My project aimed to detect unknown asteroids using open data, middle-school math skills, and some knowledge of Python programming.

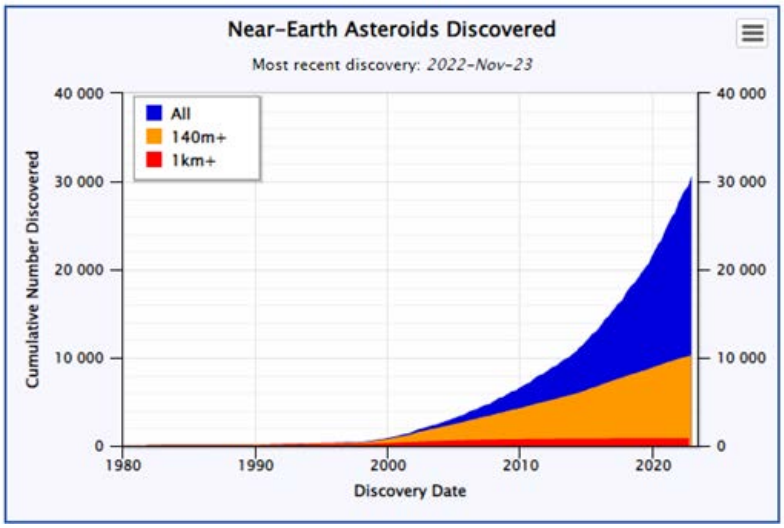

Figure 1. Near-Earth asteroids discovered to date (Data until 23 November 2022)

2. Methodology

I followed a seven-step methodology to achieve my project objective:

1. *Getting full-sky images using robotic telescopes:* I turned to robotic telescopes to get images of the night sky. Robotic telescopes can be programmed remotely to take images of the desired section of the night sky, at a particular exposure level and time. I chose four robotic telescopes in Canada, Spain, the United States, and Australia (see Figure 2), as these could be used free of charge by students and were located at different latitudes to get full sky coverage.

Figure 2. Highest aperture (2 m) robotic telescope used (Faulkes Telescope South). Image Credit: Gronk Oz - Own work

2. *Display dimmer objects:* I applied standard deviation and mean to scale the raw images to display fainter objects, as they are more likely to be unknown asteroids.
3. *Extracting sky location, telescope, and camera information:* Robotic telescopes produce images in the "Flexible Image Transport System" (FITS) format to store metadata. I wrote an algorithm to query the FITS file and gather the date and time of observation, celestial location of the image [right ascension (RA) and declination (Dec)], telescope focal length, image field of view (FOV), and the camera pixel size.
4. *Querying open data to find known objects:* To find unknown asteroids in the image, I had to remove all known objects. To do so, I turned to two open datasets. To find known stars in the field of view of the image, I queried the *GAIA Early Data Release 3* star catalogue of the European Space Agency. To find the position of all known asteroids in my image field of view at that time, I queried the *Horizons* asteroid database of the NASA Jet Propulsion Laboratory. Both datasets gave their outputs as the Right Ascension and Declination coordinates of the known objects. And in the case of asteroids, time in UTC was also provided as asteroids move across the sky at an average speed of 18 kms/s.

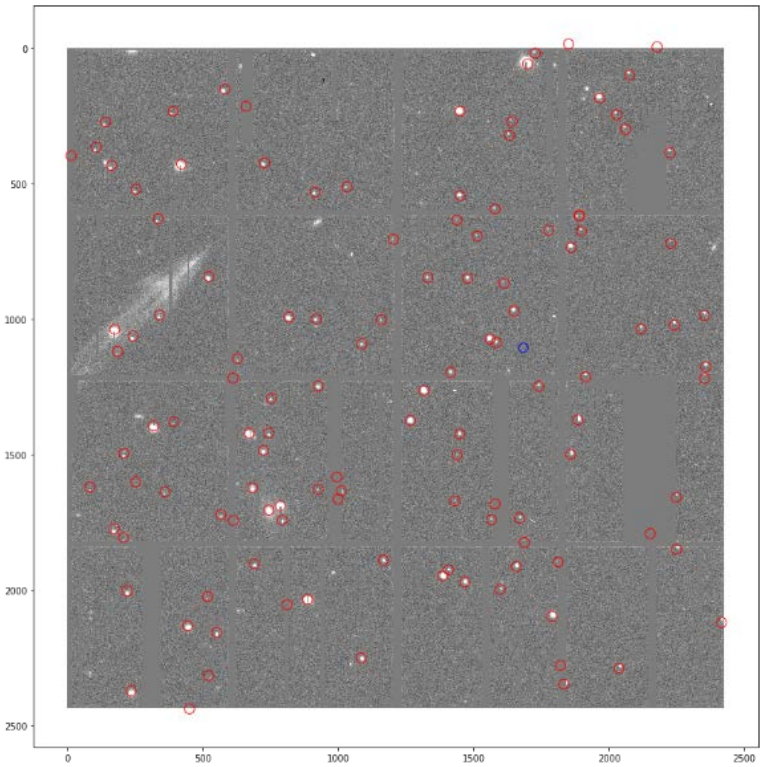

Figure 3. Sky image overlaid with all known objects

5. *Overlaying known objects on the images:* I needed to convert the celestial coordinates of the known objects to pixel coordinates. The coordinates of stars and asteroids can be expressed as positions on the celestial sphere, while my sky image is like a flat plane. I used a python code based on the gnomonic projection, which overlaid the known stars and asteroids detected onto my image (see Figure 3). To make these positions of known objects more accurate, I used a centroiding algorithm. This algorithm assumed that star

images are circular and brighter in the middle and dimmer on the outside. Using this, I found the center of all the objects overlapping with the known object positions.

6. *Creating custom-sized masks on overlaid images:* To remove known objects, I wrote an algorithm that created a custom-sized mask on all known objects. The size of the objects determined the mask radius (see Figure 4).

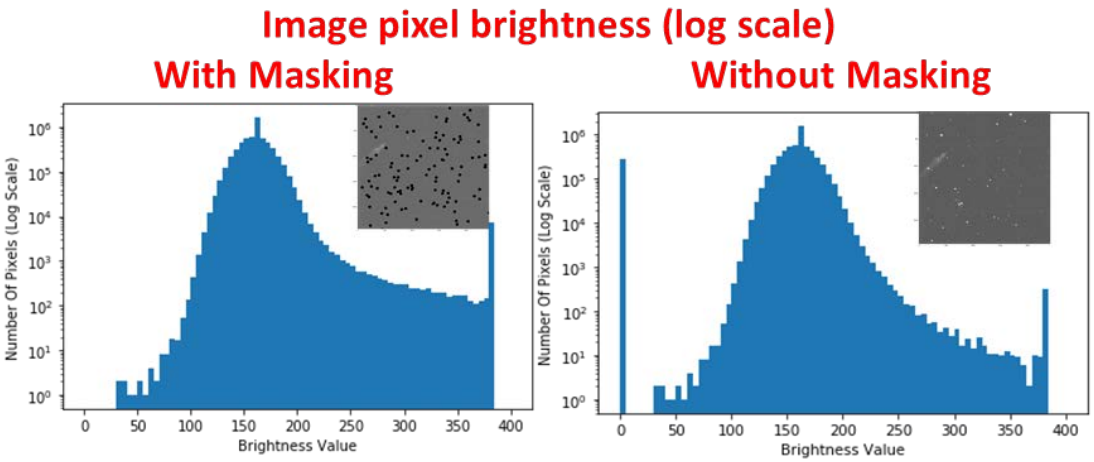

Figure 4. Change in total Image brightness with and without masking

7. *Identifying possible asteroid candidates:* To find possible asteroid candidates in my image, I had to filter out the noise. While noise is normally a few bright pixels scattered around my image, asteroids are pixels with varying brightness clumped together. My algorithm used standard deviation to get the spread of pixel brightness and eliminated objects with smaller spreads which are more likely to be noise. The remaining objects were classified as possible asteroid candidates.

All algorithms were written in Python, and Astropy, Matplotlib, and Numpy libraries were used for plotting, querying, and statistical analysis.

3. Results

It took me almost a year to learn to operate robotic telescopes and write and test my algorithm. Once my algorithm was created, it only took a few minutes to analyze each image and find possible asteroid candidates. I ended up analyzing over 20 sky images from different robotic telescopes.

3.1. Result 1: Thirty possible asteroid candidates detected

Applying my methodology, I identified over 50 possible asteroid candidates. I checked each of these candidates manually to remove noise or false positives. This left me with 30 possible asteroid candidates (see examples in Figure 5).

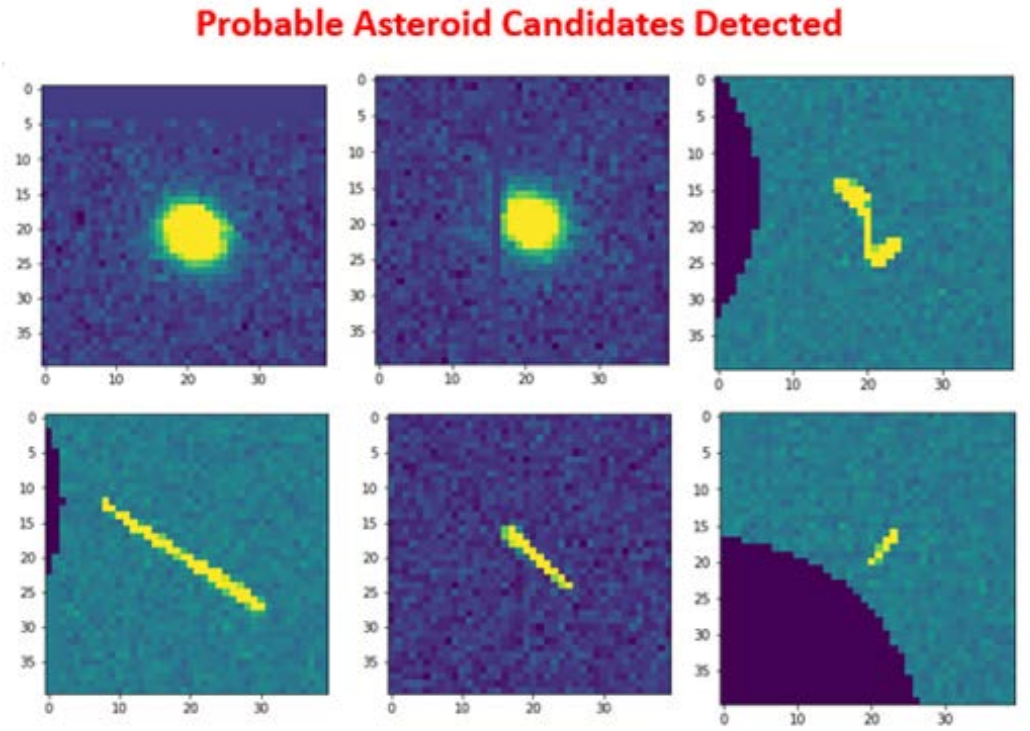

Figure 5. Six possible asteroids detected using my algorithm

3.2 Result 2: Three asteroids classified as preliminary asteroids

To validate if the possible asteroid candidates were indeed asteroids, I created Minor Planet Centre reports using Astrometrica for all 30 asteroid candidates and submitted them through the International Asteroid Search Campaign (IASC) over three months. Three of my observations were classified as preliminary asteroids as they matched the Pan-STARRS automated process and criteria set by their expert team. My remaining submissions were rejected for two reasons: either they had already been detected or their signal-to-noise ratio (SNR) was too low.

4. Discussion

4.1. Correcting the Rotation and Flip of the Images

When I was overlaying the known objects from open datasets on the images, I sometimes found that they did not match. After several attempts, I realized it was happening because the image was either rotated or flipped (see Figure 6). Once I corrected for rotation and flip through my algorithm, the match started to happen perfectly for all images.

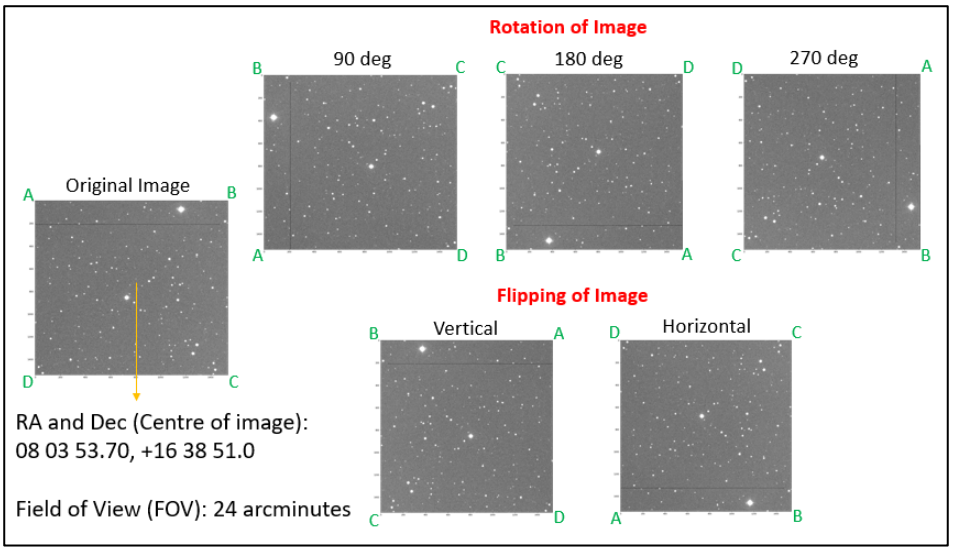

Figure 6. Possible rotation and flip of image

4.2. Newly discovered asteroids did not overlap with their expected positions

While my algorithm picked the most recently discovered asteroids, their celestial coordinates did not match the pixel coordinates of my image. This was because these asteroids' orbital path was uncertain; hence, their actual position differed from the expected position.

5. Conclusions

My open-source algorithm was able to detect three preliminary asteroids from sky images taken using free robotic telescopes. Through my year-long project, I strengthened planetary defense using open data, coding, and math skills.

Acknowledgments

Faulkes Telescope Project: Thanks to the Faulkes Telescope Project (FTP) for giving me time to control their 2-metre-wide telescope in Siding Spring, Australia. In addition to giving me sky images to test my algorithm, it helped me learn how to use robotic telescopes remotely.

Royal Astronomical Society of Canada: Thanks to the Royal Astronomical Society of Canada (RASC) for giving me my first exposure to astronomy after visiting their astronomical observatory in Collingwood and through their monthly meetings at the Ontario Science Centre. RASC has also taught me the basics of astronomy during their monthly virtual sessions.

References

Databases Used:
GAIA EDR3 Database Release: https://www.cosmos.esa.int/web/gaia/earlydr3
Horizons Database for Asteroids: https://ssd.jpl.nasa.gov/horizons/
International Asteroid Search Campaign: http://iasc.cosmosearch.org/

Software Used:
Astrometria: www.astrometrica.at
Astrometry: https://nova.astrometry.net/
Python: https://www.python.org/
Astropy: https://www.astropy.org/
NumPy: https://numpy.org/
Matplotlib: https://matplotlib.org/

Semi-Regular Yellow (SRd) Variables: New Results

John R. Percy and Yijie Wang

Department of Astronomy & Astrophysics, and Dunlap Institute of Astronomy & Astrophysics
University of Toronto, 50 St. George Street, Toronto, ON M5S 3H4, Canada;
john.percy@utoronto.ca

Abstract

SRd stars are semi-regular yellow supergiant pulsating variables, mostly low-mass stars (like the sun) in an advanced stage of evolution. They are closely related to the better-known RV Tauri (RV) variables, which are characterized by alternating deep and shallow minima.

We use V observations from the All-Sky Automated Search for Supernovae (ASAS-SN) on-line database, and the AAVSO's time-series analysis package VSTAR to investigate light curves, pulsation periods, and LSPs (long secondary periods) in several dozen stars. We use GAIA distances from the ASAS-SN variable star catalog to determine absolute magnitudes Mv. We then correct these for interstellar absorption. From these absolute magnitudes, period-luminosity relations are derived.

Contrary to previous results, we find LSPs to be quite common in SRd stars. There is considerable scatter in the P-Mv and LSP-Mv relations, but the LSP/P ratio peaks strongly at 8-10, as in pulsating red giants with LSPs.

Finally, we compare the behavior of the SRd stars with that of semi-regular red giant (SRa/SRb) variables, and also point out some unsolved problems with SRd stars – such as the cause of the variability of the pulsation amplitudes. AAVSO observations may help to solve these.

1. Introduction

SRd stars are semi-regular yellow supergiant pulsating variables of spectral type F, G, or K, mostly low-mass stars (like the sun) in an advanced (post-red-giant) stage of evolution. They have amplitudes of up to 4 magnitudes, and periods in the range of 30 to several hundred days. They are closely related to the better-known RV Tauri (RV) variables, which are characterized by alternating deep and shallow minima. Despite their abundance, interest and importance, SRd stars have been rather neglected by astronomers. AAVSO observers, however, have been productively observing both SRd and RV stars for many decades (e.g. Percy and Ursprung 2006, Percy and Haroon 2021).

A recent paper (Percy 2022) investigated the cause of the semi-regularity of SRd stars: variable pulsation amplitude (of unknown cause) in almost every case, but also period shifts and "wandering", bimodal pulsation, and "long secondary periods" (LSPs), an order of magnitude longer than the pulsation period P. See Figure 1 for a typical light curve. In the present paper, we use ASAS-SN data, and build on these results, and previous results for SRd variables based on AAVSO and other observations.

We are especially interested in the possible relation between the pulsation period and the

luminosity (P-L relation), and the relation between LSP and the luminosity (LSP-L relation). Period-luminosity relations are well-known in Cepheids and, more recently, in RV Tauri stars (Bodi and Kiss 2019).

We are also interested in the behavior and cause of the LSPs in SRd stars, which may be due to binarity – a dust-enshrouded companion (Pollard et al. 1996, Vega et al. 2021). LSPs are also found in the RVb sub-class of RV stars, and in pulsating red giants (Soszynski *et al.* 2021).

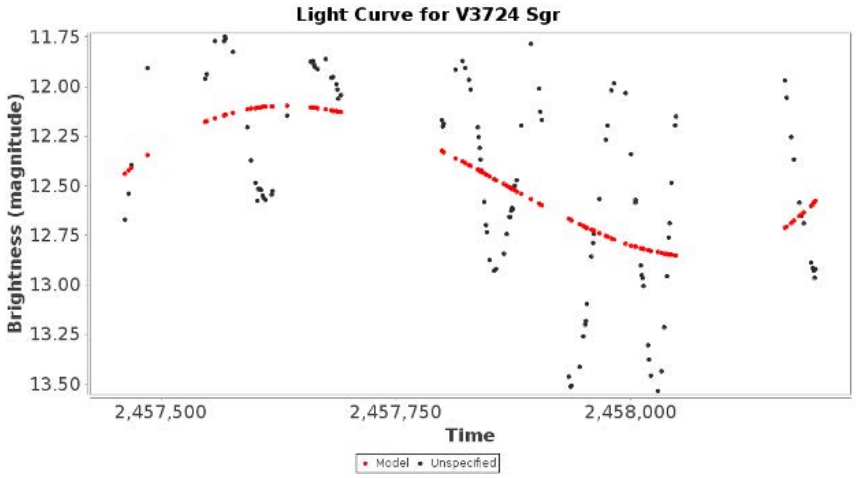

Figure 1. The ASAS-SN light curve of the SRd star V3724 Sgr, showing an LSP of about 900 days (red dotted curve), on which is superimposed a pulsation period of about 82 days, with variable amplitude.

2. Data and analysis

We use V observations from the All-Sky Automated Search for Supernovae (ASAS-SN) on-line public database (asas-sn.osu.edu), light-curve analysis, and the AAVSO's time-series analysis package VSTAR to investigate light curves, pulsation periods and LSPs and their amplitudes, in a sample of 50 stars. A very few stars showed evidence for double-mode pulsation. As emphasized by Kim and Percy (2022), it is important to first look carefully at the light curve, e.g., Figure 1, to "see what the star is doing". In some stars, the pulsation period was dominant; in others, the LSP was dominant. The pulsation periods and LSPs can first be measured from the light curve to a reasonable degree of accuracy, before using time-series analysis. We use mean V magnitudes and GAIA distances from the ASAS-SN variable star catalog to determine absolute magnitudes Mv. We then correct these for interstellar extinction, using the interstellar reddening data on the ASAS-SN catalog. From these absolute magnitudes, P-L and LSP-L relations are derived (Figure 2).

We used the LSPs in the ASAS-SN catalog. They are given to 8-10 significant figures but are probably accurate to 10 percent. We estimate that the pulsation periods, determined by us, are accurate to 5 percent. The absolute magnitudes can be in error by up to 0.5 because of the error in parallax.

3. Results and Discussion

Figure 2 shows the P-L and LSP-L relations. The points on the left (in blue) are for pulsation periods. The points on the right (in red) are for LSPs. With some imagination, you can perhaps see two "sequences" for the pulsation periods, the longer pulsation periods being fundamental mode pulsators, and the shorter ones being first overtone pulsators. The separation of the "sequences", about 0.3 in log P or a factor of two, is consistent with these modes. There is no clear sequence for the LSPs. Compare with the red giants in Figure 4 in which there are clear sequences for both. There are several possible explanations for the scatter in the P-L relation: errors in periods or Mv (see above), a simplistic approach to determining Mv, as compared with Bodi and Kiss (2019), the effect of a binary companion on the Mv, or a range of masses or metal abundances in the stars, for instance. The slopes of our "sequences" are roughly parallel to those of the RV stars (Figure 3), which is a heartening result.

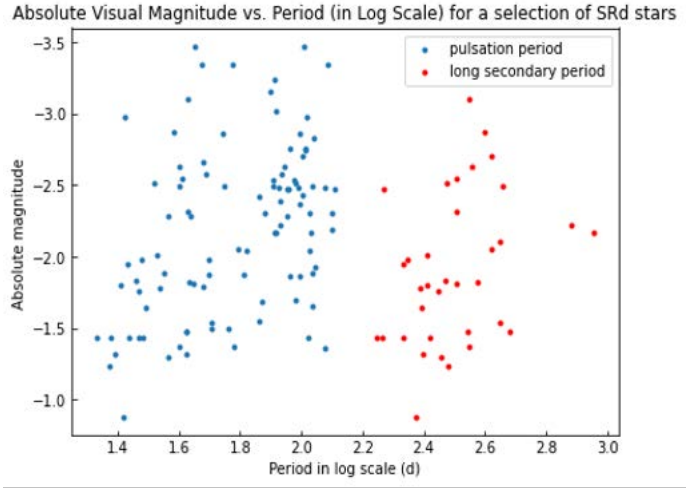

Figure 2. The period-luminosity (log P vs. Mv) relation for the SRd stars in our sample. The blue points on the left are for pulsation periods. The red points on the right are for LSPs. There is weak evidence for sequences for the pulsation periods.

Significantly, the ratio of LSP to P clusters around 8-10. Similar to the red giants, this can be interpreted as meaning that the stars are pulsating in the (shorter) first overtone mode. It also suggests that the periods that we have determined are reasonably accurate; the scatter in LSP/P is small. And, as with the red giants, it raises an interesting point: P depends on the radius of the star. LSP is an orbital period, which depends on the size of the orbit. Why should that be related to the size of the star (Kim and Percy 2022)?

Bodi and Kiss (2019) have recently used GAIA data to determine P-L relations for RV Tauri star pulsation periods and LSPs, though the latter is based on five stars only; other stars lie off the relation. Figure 3 shows, superimposed on Figure 2, the relations for the pulsation periods and the LSPs. The RV P-L relation, which is for the fundamental mode, is roughly parallel to the two "sequences" which may be present in Figure 2. However, it is offset from the longer-period SRd "sequence" – presumably the fundamental-mode sequence. This could reflect different masses or compositions, on average, for the RV and SRd stars.

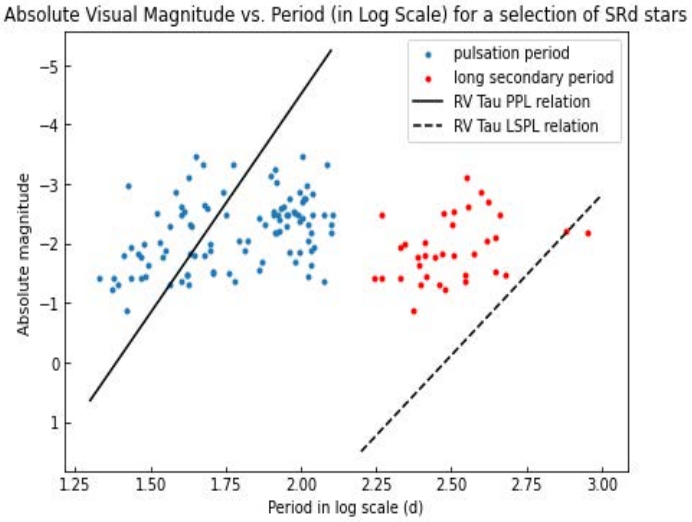

Figure 3. The same as Figure 2, but with the period-luminosity relations from RV stars superimposed. At the left is the relation for the pulsation periods. At the right is the relation for the LSPs. The latter forms an upper limit to the LSPs in the SRds.

The SRd LSPs tend to be shorter than RV LSPs, but that may be partly bias: our ASAS-SN datasets are less than 2000 days long, so longer LSPs will be harder to identify in our data. However, it does seem that SRd LSPs are somewhat shorter, implying that the companions' orbits are smaller, relative to the size of the star. Or, to put it another way, the LSP-L relation for the RVb stars is the long-period limit for the LSPs of the SRd stars in Figure 3. Certainly one of the reasons to continue the study of LSPs in SRds is to learn more about the companions and their orbits.

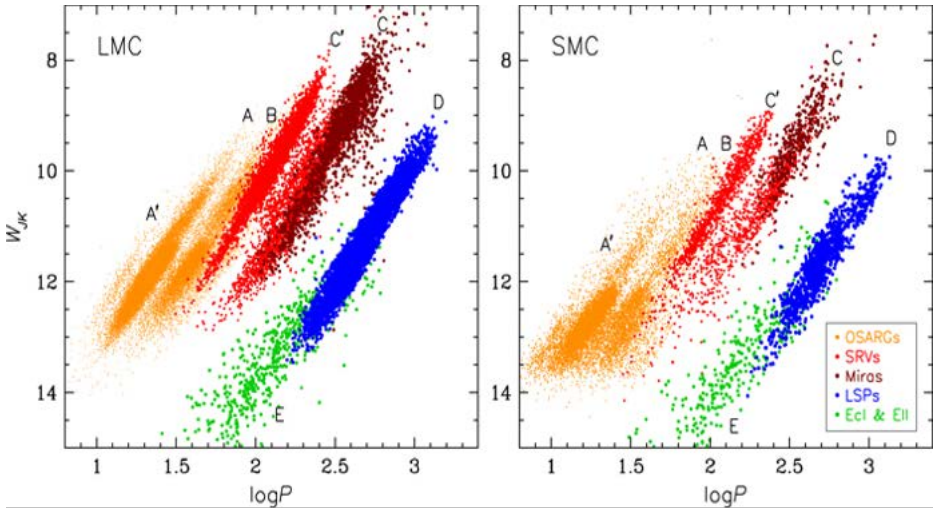

Figure 4. The period-luminosity relations for pulsating red giants in the Large and Small Magellanic Clouds. At left (yellow and red) are sequences for different pulsation modes -- fundamental and first overtone and possibly higher. At right (blue) is the sequence for LSPs (Soszynski et al. 2021).

Finally, we compare the behavior of the SRd stars with that of semi-regular red giant (SRa/SRb) variables. Figure 4 shows the period-luminosity relations for the pulsation period(s) and LSPs of red giants in the Large and Small Magellanic Clouds. Because the stars in each galaxy are at the same distance, the absolute and apparent magnitudes are directly related. In each galaxy, there are two or three pulsation sequences, presumably corresponding to different pulsation modes. What is more interesting are the well-defined LSP sequences. The pulsation period is determined by the radius of the star; the LSP is determined by the radius of the companion's orbit. As explained in Kim and Percy (2022), the existence of a LSP sequence implies that there is a relation – approximately a factor of two – between the radius of the companion's orbit and the radius of the star. It is not immediately clear why that should be. In the SRd stars, the orbital radii are less than twice the radii of the pulsating star. Perhaps it's because the atmospheres of the SRd stars are less extended than those of the red giants.

4. Concluding Remarks: SRd Stars

In our search for P-L relations for SRd stars, we have encountered the limitations of ASAS-SN data. AAVSO data may still be able to help. And we have found that LSPs are common in SRd stars, contrary to previous results using the AAVSO data. There are about a hundred SRd stars in VSX, many of them under-studied. Of the 229 SRd stars in the ASAS-SN catalogue, all those with periods greater than about 150 days are LSPs. They are not rare! Further study may help us to learn about the nature of the companion, and its dusty envelope, if any. It may also cast light on the cause of the variable pulsation amplitudes; they may be due to the finite lifetime of the pulsation modes.

5. Concluding Remarks: LSPs in Red Giants

At least a third of red giants have observable LSPs. If they are due to eclipses by dust-enshrouded, former planetary companions (Soszynski *et al*. 2021), then geometrical considerations require that half or more pulsating red giants have such companions; many will have orbits which are flat-on. But what determines the amplitude of the LSP? How does the amplitude depend – if at all – on the size of the dust-enshrouded companion, and the red giant? Does the amplitude and shape of the LSP phase curve change with time?

Acknowledgements

We thank the ASAS-SN team for making the observations available, the AAVSO for creating VSTAR and making it available, and the University of Toronto Work-Study Program and Dunlap Institute for financial support.

References

Bodi, A. and Kiss, L.L. 2019, *Astrophys. J*., **872**, 60
Kim, J.V.E. and Percy, J.R. 2022, *JAAVSO*, **50,** in press
Percy, J.R. and Ursprung, C. 2006, *JAAVSO*, **34**, 125
Percy, J.R. and Haroon, S. 2021, tspace.library.utoronto.ca/handle/1807/106550
Percy, J.R. 2022, *JAAVSO*, **50**, 1
Pollard, K.R. *et al.* 1996, *Mon. Not. Roy. Astron. Soc.*, **279**, 949

Soszynski, I. *et al*. 2021, *Astrophys. J. Letters*, **911**, L22
Vega, L.D. *et al*. 2021, *Astrophys. J*., **909,** 138

Characterizing Mass Loss in Mira and SR Variables in the LMC

Henry A. Prager[1,2], Lee Anne Willson[3], Michelle J. Creech-Eakman[1], Massimo Marengo[4,3], Joyce A. Guzik[2], and Qian Wang[5]

[1]New Mexico Institute of Mining and Technology, Department of Physics, 801 Leroy Place Socorro, NM 87801, USA; henry.prager@student.nmt.edu
[2]Los Alamos National Laboratory, Los Alamos, NM 87545, USA
[3]Iowa State University, Department of Physics and Astronomy, 2323 Osborn Drive, Ames, IA 50011, USA
[4]Florida State University, Department of Physics 77 Chieftan Way, Tallahassee, FL 32306, USA
[5]Iowa State University, Department of Food Science and Human Nutrition, 2323 Osborn Drive, Ames, IA 50011, USA

Subject Keywords

ADS Keywords: Asymptotic giant branch (108); Carbon stars (199); Evolved stars (481); Extreme carbon stars (512); Giant stars (655); Large Magellanic Cloud (903); Late-type giant stars (908); M giant stars (983); M stars (985); Mira variable stars (1066); Pulsating variable stars (1307); Pulsation modes (1309); Semi-regular variable stars (1444); Stellar mass loss (1613); Stellar pulsations (1625); Astronomy data modeling (1859); SRa variable stars (2010); Low mass stars (2050),;Asymptotic giant branch stars (2100); Theoretical models (2107)

Abstract

Asymptotic Giant Branch (AGB) stars, which make up the Mira variables and a substantial part of the semi-regular variable stars, have long been of interest to astronomers. These stars are in a crucial stage of stellar evolution, losing their mass and transitioning into planetary nebulae. Characterizing the long-term evolution of mass loss through a mass-loss formula in these stars has been elusive. To try to get a firmer grasp on this problem, we analyzed a set of AGB stars in the Large Magellanic Cloud. Going in, we knew that a reasonable mass-loss formula should create a sharp turn in luminosity-mass space. That is, they should evolve at nearly constant mass, reach a critical zone near the right edge of the strip, transition smoothly to evolving at near-constant luminosity, and then exit the bottom of the strip. Initially, we tried a linear fit of the luminosity and pulsation period to the mass-loss rates of the stars. This fit was clearly incorrect, leading us to attempt more complicated fitting methods which did not help us. We realized that the measurement errors of luminosity and mass-loss rate made standard fitting methods practically impossible as opposed to simply unreliable. Noting this, we developed a method to determine a mass-loss formula by analyzing the distribution of stars in the pulsation period-luminosity plane. This method uses a program to 'seek' a formula that minimizes the difference between measured and predicted mass-loss rates using the population's change in luminosity and pulsation period during stellar evolution. Through this, we found four mass-loss formulae for four different subsets of the AGB population. These formulae reproduce the sharp turn we expect from observations of AGB populations and from theoretical models, putting formulae from theory and observation into agreement. As a next step, we are generating grids of atmospheric models of

AGB stars to compare against the stars seen in the Large Magellanic Cloud. We examine how models with typical parameters compare to observations, and how they compare when these parameters are pushed to their expected limits. We will also investigate what details and physical processes might need to be accounted for to make these grids fit stars observed in the LMC.

1. Introduction

Mira variable stars have long been a target of interest for astronomers. Although the star Mira had been long known, periodic variability was first discovered and measured in 1638 by Johannes Howlrada. Since then, hundreds of these objects have been found inside the Milky Way and thousands more in nearby galaxies. We now understand that Mira stars and a subset of the related semi-regular variable (SRV) stars are Asymptotic Giant Branch (AGB) Stars. These are low-to-intermediate mass (about 0.8 to 6 $M_{\odot}$) stars that have reached the end of their life cycles. They are actively fusing hydrogen and helium in concentric shells around an inert core of carbon and oxygen, with extensive stellar envelopes, on the order of Earth's orbital distance in radii. These stars are only stable in the short term; over the course of a few hundred thousand to a million years, the opacity-driven pulsations and a dust-driven stellar wind remove the envelope of the star, in a process called mass loss, leaving the core as a white dwarf. Understanding how this material is removed from stars and returned to galaxies is vital for understanding the evolution of galaxies and clusters and understanding the changes from low-metallicity stars to high-metallicity stars (Willson 2000; Höfner & Olofsson 2018).

The first part of our work has primarily been motivated by the disagreement between mass-loss formulae found through observations and formulae found through models. When we model the atmospheres and mass loss in AGB stars, we generally find mass loss that is strongly dependent on stellar parameters. When we observe mass loss in AGB stars, we tend to, but not always, find a weak dependence on stellar parameters (Willson 2000; Höfner & Olofsson 2018); the dust-derived mass-loss rates tend to show significantly less luminosity dependence than spectral-line based studies (Höfner & Olofsson 2018). Clearly, only one of these options is correct. The second part of our work has been to determine the effects of changing stellar parameters, beyond those we can observe, and secondarily to check the models for consistency with observed populations. If we have AGB models correct, then they should be consistent with the population of AGB stars we observe. However, there is a known gap in our knowledge at very low metallicities, which will be of importance when we compare to the population data (Herwig 2005; Höfner & Olofsson 2018).

2. Methods

2.1 AGB stars in the LMC

The first part of this study relies on observations of AGB stars in the Large Magellanic Cloud (LMC) from Riebel et al. (2012). The data set is extensive and, importantly for our work, has information on luminosity (L), dust mass-loss rate, and pulsation period (P). We limited our analysis to stars

pulsating in the fundamental and first-overtone modes, having both oxygen-rich (M) and carbon-rich (C) composition, leaving us with 6,917 stars. This data can be seen in Figure 1.

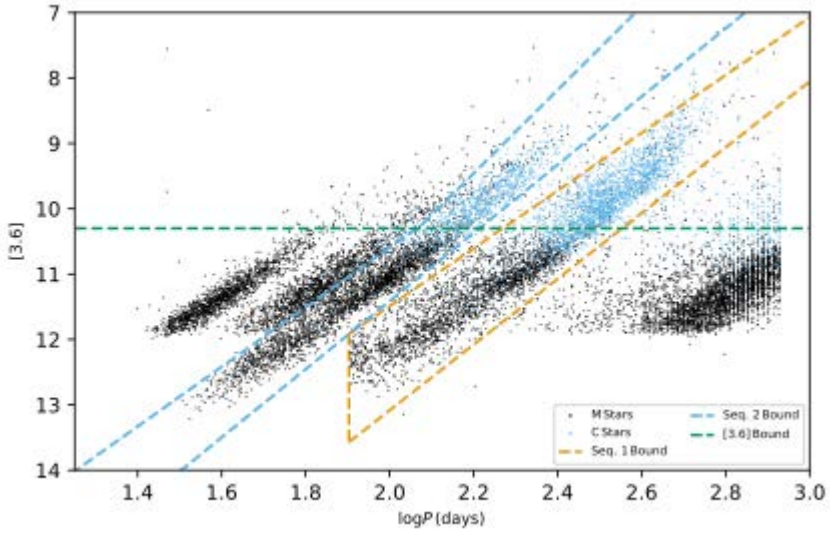

Figure 1. Plot of [3.6] vs. log P for the stars in the Riebel et al. (2012) data set. M-type stars are in black and C- type stars in blue. M stars brighter than [3.6] = 10.3 are assumed to be red supergiant stars and are excluded from the analysis. Following the naming convention established in Riebel et al. (2010), sequence 1 defines AGB stars pulsating in the fundamental mode, and sequence 2 defines AGB stars pulsating in the first-overtone mode.

Mass-loss formulae are frequently assumed to be some kind of power law, that is an equation such as

$$\frac{dM}{dt} \equiv \dot{M} = \alpha\, L^{\beta}\, P^{\gamma} \qquad (1)$$

where the rate of change of one of the variables (in this case, the mass-loss rate $\dot{M}$) is proportional to other variables raised to some exponent. In this case the variables are luminosity L and pulsation period P, but frequently stellar mass M and stellar radius R as well as other variables are used. Noting these stars have P-M-R and R-M-L relations, we can switch between the power law in equation (1) and a power law

$$\dot{M} = A\, L^{B}\, M^{-C} \qquad (2)$$

with little trouble. The first of these formulae to be published was in Reimers (1975), with numerous other formulae being published of the same form (cf., Blöcker 1995; van Loon et al. 2005; Schröder & Cuntz 2005). Most of these formulae have what we will call a weak luminosity dependence (that is, B $\lesssim$ 5). There are other formulae that are not power laws and are instead exponential functions of period, that is, some numerical value raised to a variable (cf., Vassiliadis & Wood 1993; De Beck et al. 2010). Depending on the formula, these can have either strong (B $\gtrsim$ 5) or weak luminosity dependence, once you change variables from P to L. These formulae

generally make no distinction based on the composition of the star beyond metallicity, and Reimers-like formulae generally do not distinguish stars by pulsation mode.

Our goal is to find a power law mass-loss formula for these stars that consistently predicts mass-loss rates. Through the course of our work, we determined that a standard least-squares fit was not viable, consistent with concerns raised by Riebel et al. (2012) and noted in Hofner & Olofsson (2018); formulae found through the least-squares fits were always weakly dependent on luminosity. We then developed a new method that relies on measuring the distribution of stars in P-L space; that is, we can plot the stars with those axes and measure the width and heights of the distribution. With some calculus, we can show how the exponents are related to those measurements:

$$\boldsymbol{\beta = \frac{\partial log\dot{M}}{\partial logL} \approx \frac{\Delta log\dot{M}}{\Delta logL} \quad \gamma = \frac{\partial log\dot{M}}{\partial logP} \approx \frac{\Delta log\dot{M}}{\Delta logP}} \qquad (3)$$

Now, there is the matter of fitting an appropriate strip to this data. The boundaries of the strip are uncertain because of scatter in the luminosity and mass-loss rate data due to both measurement error and intrinsic processes, such as dust-gas drift. We can work around the uncertainty by fixing the center of the strip and adjusting the bounding lines until a formula that works consistently at all ranges of mass-loss rates is found; a sample of this for the M0 stars can be found in Figure 2.

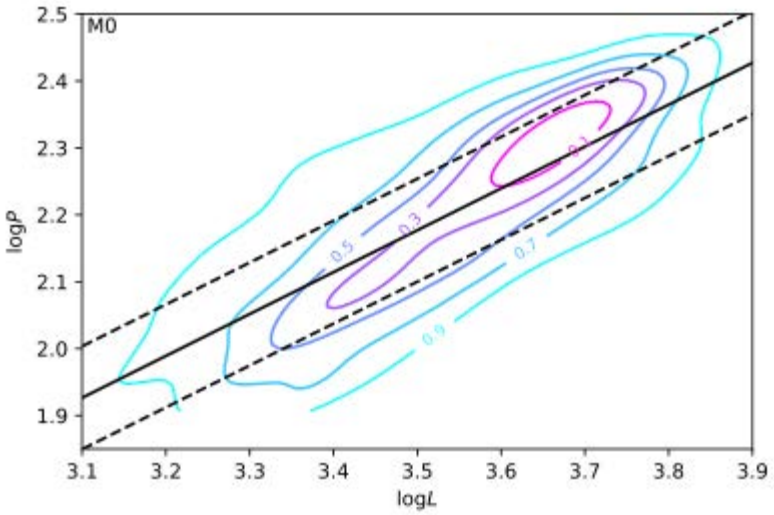

Figure 2. M0 stars in the PL strip in the Riebel et al. (2012) data set. The black solid line is the best-fit line of the data set, and the black dashed lines bound the stars in the best-fitting strip. Contours depict the fraction of stars relative to the peak density.

2.2 Atmospheric models

We have been using the atmospheric models developed by Bowen (1988) and updated with further grid-producing capability by Wang (2011). These are heavily parameterized atmospheric

models, where physical detail is traded for rapid adjustability and ease of modification, including introducing new processes. Some of the parameters of these models are simply local—they describe the star, but do not modify how physical processes happen. These would be things like stellar mass M, stellar radius R, luminosity L, or pulsation period P. Other parameters characterize the physical processes occurring in each star, and these are the ones of interest for our parameter study. They affect the opacity κ of the gas and dust, piston amplitude, dust condensation temperature, and so on. The metallicity Z is somewhere in between—it characterizes the star but has a strong influence on how much material is available to form dust. By adjusting these physical parameters in turn, we can characterize the effect they have on the location of AGB model grids in the luminosity-mass plane or the luminosity-pulsation period plane.

To begin with, we have been adjusting the dust condensation temperature T_{con}, the dust opacity κ_{dust}, and the piston power transfer efficiency ϵ. T_{con} adjusts the temperature at which the non-specified dust in the model condenses from a gas phase to a solid crystal. κ_{dust} quantifies transparency and adjusts how much light energy is transferred to the dust. ϵ describes how much of the energy from luminosity is transferred to the mechanical piston through unspecified means; this in turn increases the amplitude of pulsations and regulates how much energy is mechanically transferred to the dust. A grid of models with "typical" parameters can be seen in Figure 3.

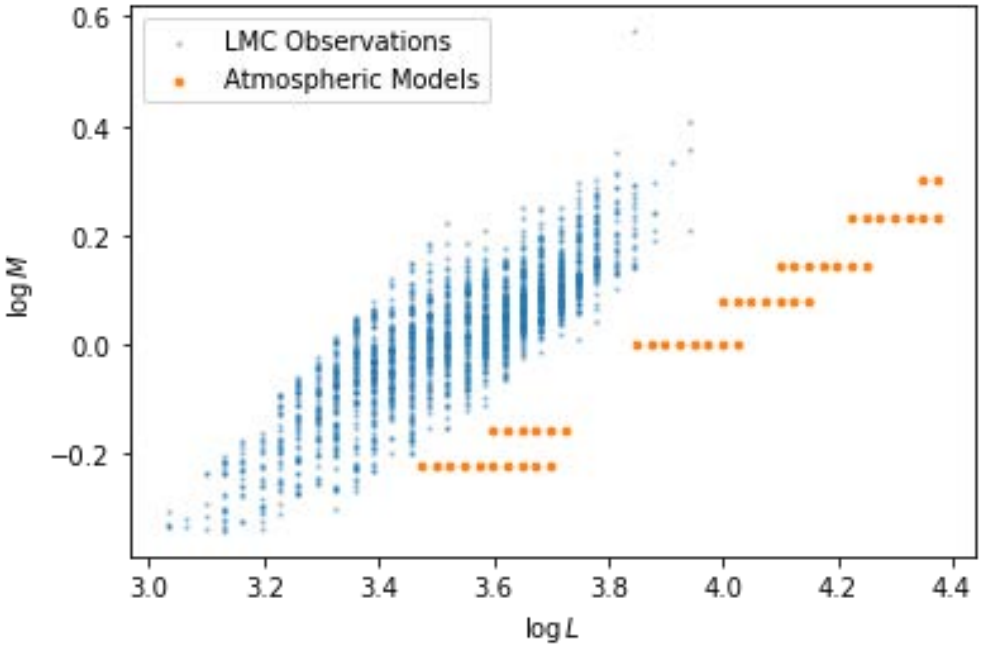

Figure 3. A grid of atmospheric models with typical parameters (Z = 0.002, Tcon. = 1450 K, κ_{dust} = 2 cm^2/g, ϵ = 0.01). Blue dots are from the Riebel et al. (2012) data set of AGB stars in the LMC, and the orange dots are a strip of stars generated from atmospheric models.

With observational data, we can also compare the location of model grids to the location of observed stars in the same plane. We know observed mass-loss rates range between 10^{-8} and roughly 10^{-5}, with the occasional star found up to around 10^{-4} at the very end of the mass-loss

process. The model grids are set to terminate when $\dot{M} > 2 \times 10^{-5}$, and we can introduce a minimum mass-loss rate for comparison. Ideally, the model grids and observed stars should overlap; that would mean theory and observation are in agreement. In the case that they don't overlap, the results from the parameter study can be used to inform us on what parameters we can adjust to bring the models into better agreement with observation. If we find that no reasonable adjustment does this, we can see what extreme adjustments may work or look into what physics is not included in the models that may help.

3. Results

3.1 AGB stars in the LMC

Through our LP-strip analysis, we found a strong dependence of mass loss on luminosity. We also found that there is no evidence of a universal mass-loss formula; stars lose mass somewhat differently depending on atmospheric composition and pulsation mode. However, the ratio of these exponents is fairly similar for stars of the same composition. The formulae we found all have luminosity exponents B > 5, with three of the four having B > 8. This is consistent with the exponential formulae (Vassiliadis & Wood 1993; De Beck et al. 2010), the results of Danilovich et al. (2015) who found B ∼ 5, and the results of Kamath et al. (2010) who found we need strong luminosity dependence to replicate the evolution of stellar clusters. Now we can search for agreement between observation and theory by approaching the problem from a new direction. The coefficients and exponents we determined for equation (2) can be found in Table 1.

Table 1. Determined exponents and coefficients for equation (2)

Subset	*log A*	*B*	*C*	*|B/C|*
M0	-35.2	8.24	-13.7	0.59
M1	-42.8	10.2	-20.5	0.50
C0	-41.0	9.62	-13.9	0.69
C1	-27.8	5.89	-9.44	0.62

3.2 Atmospheric models

We are currently working on the best way to present these results, but we can give a qualitative description. For the piston efficiency ϵ, we have examined a range of values from 0.005 to 0.1, with 0.01 being a standard and reasonable value. Increasing the efficiency tends to increase the mass-loss rates of low-luminosity models while holding the right edge of a strip in position.

Models that yield gas opacity in this environment are relatively settled, so we have left that fixed at 0.002 cm^2/g. The dust opacity, κ_{dust}, is likely a few cm^2/g, but we have explored a range from 2 cm^2/g to 500 cm^2/g because of the large effect it has in placing the LM strip. Adjusting κ_{dust} shifts the LM strip left as it increases and narrows the strip from the left side. This means adjusting κ_{dust} both changes the total mass-loss rate and adjusts the range over which significant mass loss occurs.

The condensation temperature T_{con} is a chemical property of each species, so with a single parameter we are effectively adjusting the average dust condensation temperature. Given the dust species that exist in these stars, we expect an average condensation temperature around 1450 K; we explored 150 K above and below this value, approximating a weak break from local thermal equilibrium when increased. Increasing T_{con} makes dust production easier, and we find higher mass-loss rates at lower luminosities.

A grid that shows the effects of changing various values can be seen in Figure 4.

4. Discussion and Conclusions

4.1 AGB stars in the LMC

The formulae we have found for AGB stars in the LMC bring formulae derived from theoretical models and observations into significantly better agreement.

Historically, observationally derived mass-loss formulae have tended to have a small luminosity exponent (i.e., Reimers 1975; van Loon et al. 2005; Schröder & Cuntz 2005). This disagrees with theoretical models (i.e., Bowen 1988; Höfner et al. 2003; Bladh et al. 2019a,b) and more recent observational studies (i.e., Kamath et al. 2010; Danilovich et al. 2015), which predict larger exponents. During our analysis, we concluded that this discrepancy was likely caused by regression dilution, a statistical error that occurs when data analyzed through a linear least-squares fit has excessive spread, which we know is the case in the data set of Riebel et al. (2012). Our new method works around this by measuring the exponents directly from the distributions of AGB stars. The full results of this work are available in Prager et al. (2022).

4.2 Atmospheric Models

So far, we have examined the effects of adjusting T_{con}, κ_{dust}, and ϵ, and are in the process of finding a way to best quantify these changes. We thought that adjustments to some combination of these parameters would yield a model grid that well replicates the fundamental-mode, oxygen-rich stars in the LMC, but this does not appear to be the case.

The next step will be to adjust model parameters that we thought we had settled—for example, the solar metallicity models of Bladh et al. (2019a,b) replicate Milky Way AGB stars very well. This would be interpreted as the low metallicity AGB stars having atmospheres enriched in metals due to either dredge-ups, envelopment of planetesimals, or some other manner. We also need to consider recent results regarding the dust formation process such as those of Boyer et al. (2019), who find that including quantum processes and breaking local thermodynamic equilibrium results in faster dust nucleation and the formation of larger dust. We plan to release the full results of this work in H. A. Prager, J. A. Guzik, L. A. Willson, M. J. Creech-Eakman, and Q. Wang (2023, in preparation).

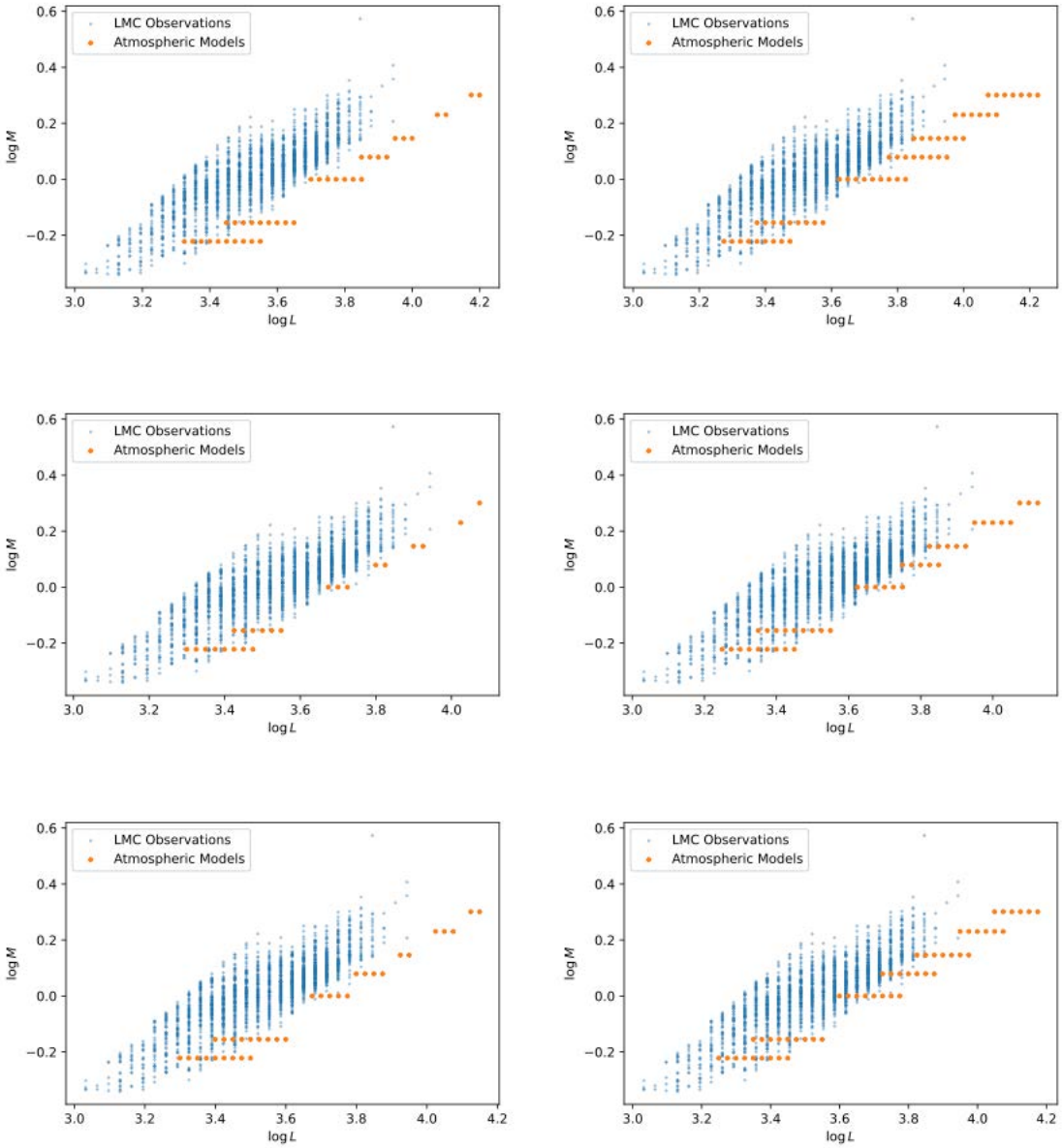

Figure 4. A comparison of model grids to the fundamental-mode oxygen-rich AGB stars in the LMC. The model grids in first column all have ϵ = 0.01 and those in the second column all have ϵ = 0.05. Model grids in the first row have T_{con} = 1450 K and κ_{dust} = 100 cm^2/g. Model grids in the second row have T_{con} = 1450 K and κ_{dust} = 200 cm^2/g. Model grids in the third row have T_{con} = 1525 K and κ_{dust} = 100 cm^2/g.

Acknowledgements

This work has made use of the NumPy library (Harris et al. 2020), the SciPy library (Virtanen et al. 2020), IPython software package (Pérez & Granger 2007), the matplotlib library for publication quality graphics (Hunter 2007), and the Scikit-learn library (Pedregosa et al. 2011). Funding for this work has been provided by the New Mexico Space Grant Consortium. Henry Prager

acknowledges support from LANL, managed by Triad National Security, LLC for the U.S. DOE's NNSA, Contract # 89233218CNA000001.

References

Bladh, S., Eriksson, K., Marigo, P., Liljegren, S., & Aringer, B. 2019a, *A&A*, **623**, A119, doi: 10.1051/0004-6361/201834778

Bladh, S., Liljegren, S., Hofner, S., Aringer, B., & Marigo, P. 2019b, *A&A*, **626**, A100, doi: 10.1051/0004-6361/201935366

Blocker, T. 1995, *A&A*, **297**, 727

Bowen, G. H. 1988, *ApJ*, **329**, 299, doi: 10.1086/166378

Boyer, M. L., Williams, B. F., Aringer, B., et al. 2019, *ApJ*, **879**, 109, doi: 10.3847/1538-4357/ab24e2

Danilovich, T., Teyssier, D., Justtanont, K., et al. 2015, *A&A*, **581**, A60, doi: 10.1051/0004-6361/201526705

De Beck, E., Decin, L., de Koter, A., et al. 2010, *A&A*, **523**, A18, doi: 10.1051/0004-6361/200913771

Harris, C. R., Millman, K. J., van der Walt, S. J., et al. 2020, *Nature*, **585**, 357, doi: 10.1038/s41586-020-2649-2

Herwig, F. 2005, *ARA&A,* **43**, 435, doi: 10.1146/annurev.astro.43.072103.150600

Höfner, S., Gautschy-Loidl, R., Aringer, B., & Jørgensen, U. G. 2003, *A&A*, **399**, 589, doi: 10.1051/0004-6361:20021757

Höfner, S., & Olofsson, H. 2018, *A&A Rv*, **26**, 1, doi: 10.1007/s00159-017-0106-5

Hunter, J. D. 2007, *Computing in Science & Engineering*, **9**, 90

Kamath, D., Wood, P. R., Soszyn´ski, I., & Lebzelter, T. 2010, *MNRAS*, **408**, 522, doi: 10.1111/j.1365-2966.2010.17137.x

Pedregosa, F., Varoquaux, G., Gramfort, A., et al. 2011, *Journal of Machine Learning Research*, **12**, 2825

Pérez, F., & Granger, B. E. 2007, *Computing in Science and Engineering*, **9**, 21, doi: 10.1109/MCSE.2007.53

Prager, H. A., Willson, L. A., Marengo, M., & Creech-Eakman, M. J. 2022, ApJ, **941**,1, doi: 10.3847/1538-4357/ac9e5

Reimers, D. 1975, *Circumstellar envelopes and mass loss of red giant stars* (Springer-Verlag New York, Inc.), 229–256

Riebel, D., Meixner, M., Fraser, O., et al. 2010, *ApJ*, **723**, 1195, doi: 10.1088/0004-637X/723/2/1195

Riebel, D., Srinivasan, S., Sargent, B., & Meixner, M. 2012, *ApJ*, **753**, 71, doi: 10.1088/0004-637X/753/1/71

Schr¨oder, K.-P., & Cuntz, M. 2005, *ApJL*, **630**, L73, doi: 10.1086/491579

van Loon, J. T., Cioni, M. R. L., Zijlstra, A. A., & Loup, C. 2005, *A&A*, **438**, 273, doi: 10.1051/0004-6361:20042555

Vassiliadis, E., & Wood, P. R. 1993, *ApJ*, **413**, 641, doi: 10.1086/173033

Virtanen, P., Gommers, R., Oliphant, T. E., et al. 2020, *Nature Methods*, **17**, 261, doi: 10.1038/s41592-019-0686-2

Wang, Q. 2011, PhD thesis, Iowa State University
Willson, L. A. 2000, *ARA&A*, **38**, 573, doi: 10.1146/annurev.astro.38.1.573

Methods for Transforming Photometric Observations to a Standard System

Mark L. Spearman

Factory Physics, Inc., 505 Church Avenue, College Station, TX 77840

Subject Keywords

Photometry, CCD; Transformation Coefficients

Abstract

The Transform Generator offered by AAVSO has made it easy to compute transformation coefficients that convert raw observations into a standard system. However, this method ignores second order extinction coefficients that are important for low altitude observations with high air mass. Moreover, changes to the system caused by modifications to the optical train, changing filters, the accumulation of dust, or other such variations require repeating the process of determining the transformation coefficients. This paper presents an alternative means of estimating these coefficients using comparison stars in the target image which obviates the need for repeated TC estimation.

1. Introduction

The advent of the CCD and other linear astronomical cameras has made it easy for amateur astronomers to obtain good and useful data about variable stars. However, to make the most use of the data it is necessary to transform them into a standard photometric system to facilitate the accumulation of data from many observers. AAVSO has made this easy with the Transform Generator (AAVSO 2022). This software is used to determine transformation coefficients that convert raw observations into a standard system.

However, this method ignores second order extinction coefficients that are important for low altitude observations with high air mass. Moreover, changes to the imaging system caused by modifications to the optical train, changing filters, the accumulation of dust, or other such variations can induce errors requiring the generation of new transformation coefficients.

This study explores several alternative means of estimating these coefficients using comparison stars in the target image. Clearly, such coefficients will be using the most current setup of the imaging system so the focus of this study is to determine whether such (non-standard) comparison stars are accurate enough to produce good transformation coefficients. This concern is mitigated by two factors: (1) as more data have been gathered, the magnitudes of the comparison stars of a given field have become more accurate, and (2) with the larger fields that are available with today's cameras, there are more comparison stars, allowing for statistical variance reduction methods.

2. Background

The basic magnitude equation is measured in terms of a reference star, M_0, is

$$M = M_0 - 2.5 \log 10 \left(\frac{F}{F_0}\right)$$

where F is the flux of the star. The "instrumental magnitude" is related to this flux via,

$$M - 2.5 \log 10(F) = M_0 - 2.5 \log 10(F_0) \ .$$

The instrumental magnitude for a B filter is given by $b = 2.5 \log 10(F_B)$, so that

$$M - b = M_0 - b = Z_b \ .$$

Where Z_b is the "zero point" for the B standard. In this study, we will focus on V and B standards only. However, the techniques presented here are applicable to filters of any standard photometric system.

Adding atmospheric extinction and color correction terms yields the following relationship between instrumental magnitudes and standard magnitudes (see, e.g., Henden and Kaitchuk 1982; Boyd 2012):

$$B = b - k'_b X - k''_{bbv} X(B - V) + T_{bbv}(B - V) + Z_b$$

$$V = v - k'_v X - k''_{vbv} X(B - V) + T_{vbv}(B - V) + Z_v$$

where k' and k" represents the first and second order extinction coefficients, X is the air mass of the star, T is the instrumental transformation coefficients for the (B-V) color index, and Z represents the B and V image zero points. Combining terms yields

$$B = b - (Z_b - k'_b X) + (T_{bbv} - k''_{bbv} X)(B - V)$$

$$V = v - (Z_v - k'_v X) + (T_{vbv} - k''_{vbv} X)\ (B - V) \ .$$

Note that the air mass and the zero points are the same for all stars in a given image (as long as the image size is not too large, say, less than 1 degree). This allows us to derive the "differential photometry method."

Consider an estimation of the V magnitude of a target star, V_t, by comparing it with a star with a known magnitude, V_c.

$$V_c = v_c - k'_v X - k''_{vbv} X(B_c - V_c) + T_{vbv}(B_c - V_c) + Z_v$$

$$V_t = v_t - k'_v X - k''_{vbv} X(B_t - V_t) + T_{vbv}(B_t - V_t) + Z_v \qquad (1)$$

Subtracting the first equation from the second and solving for V_t yields

$$V_t = V_c + v_t - v_c + (T_{vbv} - k''_{vbv}X)\big((B_t - V_t) - (B_c - V_c)\big) \quad . \qquad (2)$$

Note that the first order extinction coefficients and the zero points have subtracted out and do not appear in the above equation. Using the shorthand, $\Delta(x) = x_t - x_c$, we can write

$$\Delta V = \Delta v + (T_{vbv} - k''_{vbv}X) \cdot \Delta(B - V) \qquad (3)$$

so that, $V_t = V_c + \Delta V$. There are similar equations for B and other standard filters as well, e.g.,

$$\Delta B = \Delta b + (T_{bbv} - k''_{bbv}X) \cdot \Delta(B - V) \quad . \qquad (4)$$

Typical values for k'' are around 0.02-0.04 for B and 0.002 for V. So, if the field is not too low when imaged and the comparison star is close to the same color as the target, the difference in magnitude due to extinction is very small. Ignoring the second order extinction coefficient, we obtain

$$\Delta B = \Delta b + T_{bbv}\,\Delta(B - V) \quad . \qquad (5)$$

The *AAVSO Guide to CCD/CMOS Photometry with Monochrome Cameras* (AAVSO 2022) has an excellent chapter on how to obtain these transformation coefficients. This is accomplished by computing slopes of different magnitude estimates. First, we compute the slope of a set of points with $\Delta(B - V)$ on the x-axis and $\Delta(b - v)$ on the y-axis. The inverse of this slope is identified as T_{bv}, the primary transformation coefficient:

$$T_{bv} = \frac{\Delta(B - V)}{\Delta(b - v)}$$

Multiplying by T_{bv} allows one to convert $\Delta(b - v)$, what we observe, to $\Delta(B - V)$, what we need to estimate magnitudes. Other coefficients are also computed as the slopes of,

$$T_{bbv} = \frac{\Delta(B - b)}{\Delta(B - V)} \text{ and } T_{vbv} = \frac{\Delta(V - v)}{\Delta(B - V)}$$

Applying these to (5) yields

$$\Delta\mathrm{B} = \Delta\mathrm{b} + \; T_{bv} \cdot T_{bbv}\Delta(b - v) \quad . \qquad (6)$$

Substituting the slopes for the coefficients may yield some insight:

$$\Delta\mathrm{B} = \Delta\mathrm{b} + \frac{\Delta(B - V)}{\Delta(b - v)} \cdot \frac{\Delta(B - b)}{\Delta(B - V)}\,\Delta(b - v)$$

Or,

$$\Delta B = \Delta B$$

3. Transformation Coefficients

This study considers three different types of transformation coefficients. The first is the "Null" coefficient which is, essentially, no transformation. The "Static" coefficient is determined by measuring a field of standard stars, performing the various regressions, and determining a set of coefficients for the given optical system. AAVSO has provided outstanding software (the Transformation Generator) and documentation to facilitate this procedure. The "Dynamic" coefficient uses comparison stars within a given image to produce transformation coefficients for each image. The advantage of Dynamic is that it is immune to extinction (provided the field is not too large) and is always considering current conditions. The disadvantage is that most "comparison" stars are not "standard" and so are less accurate. Another disadvantage occurs in areas where there are insufficient comparison stars to make an accurate estimate.

3.1 Null Transformation Coefficients

We must also consider what we will call the "Null" coefficient, in which $T_{bv} = 1$ and $T_{bbv} = T_{vbv} = 0$. In other words, no transformation. If the Null coefficient works as well as any other, it is certainly preferable because it is trivially easy to use.

3.2 Static Transformation Coefficients

The procedure for determining a set of static transformation coefficients is given in the Transformation Generator User's Guide. There the procedure is summarized as:

1. Identify telescope (enter telescope name and description the first time used)
2. Select standard star field used (M67, NGC 7790, M11, NGC 1252, NGC 3532, Melotte 111 or Landolt Fields.)
3. Load user-provided file(s) containing instrumental magnitudes of standard field stars
4. Compute transforms using the Transformation Generator software
5. Review plots of individual transforms, deactivating any invalid observations
6. Save transform set
7. Repeat the above steps if multiple sets of observations are available
8. Compare different sets of transforms
9. Select sets to be averaged
10. Average selected observation sets to create a final "master" transform set
11. Export a file containing the final transform values for printing and for input into "Transform Applier" (TA) or the "Two Color Transform" on VPhot

The Transform Applier in Vphot (Klingenberg et al. 2016) and the "Two Color" Transform use the transformation coefficients to create a "transformed" data set for uploading into the AAVSO data base.

3.3 Dynamic Transformation Coefficients

A third type of coefficient is the "Dynamic" coefficient, in which we compute the product of $T_{bv} \cdot T_{bbv}$ (and other similar products) from the set of comparison stars used to estimate magnitudes of the target. Since, when performing differential photometry, one never sees a coefficient such as T_{bbv} by itself, we need only compute an estimate of the product, viz.,

$$\alpha_b = T_{bv} \cdot T_{bbv} \text{ and } \alpha_v = T_{bv} \cdot T_{vbv} \ .$$

One then searches for α that minimizes the following:

$$\chi^2(\alpha_v) = \sum_{c \neq t}(V_c + \Delta v + \alpha_v(b_c - v_c) - V_t)^2 \ ,$$

where c indicates a comparison star and t labels the target star.

This parameter is used to provide estimates of the magnitude of the target star:

$$\hat{V}_{tc} = V_c + \Delta v + \alpha_v(b_c - v_c) \ .$$

The final estimate is determined by using a, possibly weighted, average of these estimates. Of course, one can discard any comparison star that yields poor performance in estimating the values of the other comparison stars.

A different set of dynamic coefficients can be developed by performing regression on a set of comparison stars. Rewriting (1) with T_{bv} inserted and collecting terms yields

$$V = v + (T_{bv} \cdot T_{vbv} - k''_{vbv}X)(b - v) + Z_v - k'_vX$$

$$V - v = \alpha_v(b - v) + C_v \quad . \tag{7}$$

Setting $Y_j = V_j - v_j$ and $X_j = b_j - v_j$ and applying regression yields an estimate of the slope, α_v, and the intercept, C_v. Plotting the values allows one to discard "outliers" as is done in the Coefficient Generator. With the estimate of α, the target star magnitude is estimated in the usual way:

$$\hat{V}_t = v + \alpha_v(b - v) + C_v \quad . \tag{8}$$

It turns out that these two methods are equivalent if the weights in the first method are all equal. In other words, the α values are the same and

$$\hat{C}_v = \overline{(V - v)} - \alpha\left(\overline{b - v}\right),$$

where $\overline{x - y}$ indicates the average of the differences.

4. Comparison of the Methods

The equipment used to evaluate the performance was an Astro-Tech 10" f/8 RC scope with an SBIG ST-10XME camera using Astrodon B and V filters. With single binning this setup results in an image scale of 0.701 arc seconds per pixel.

To compare the performance of the different coefficients we perform the following experiment:

1. Using the AAVSO transform generator (TG), estimate the transforms using standard fields, NGC 7990 and M67. Then take the average of these coefficients to form our static transform coefficients for this study.
    a. All images were processed with flat, bias, and dark frames. The flats were produced at twilight separately for each filter.
    b. The NGC 7990 images were a combination of four 90-second B images and five 50 -second V images taken on 2021-02-03 with nominal altitudes of around 36 degrees with an air mass of around 1.7.
    c. The M67 images were a combination of 24 images of 60 seconds for B and 23 images of 90 seconds for V with nominal altitudes around 45 degrees and an air mass of 1.4.
    d. Both fields are quite crowded so, to improve the estimates, we deleted any comparison star that overlapped with another, usually keeping the brighter star (see **Error! Reference source not found.** for M67).

2. The derived coefficients are given below:

	NGC 7790	M67	Average
Tbv	1.024	1.028	1.026
Tb_bv	0.050	0.022	0.036
Tv_bv	0.003	-0.010	-0.004
r2(Tbv)	0.996	1.000	0.998
r2(Tb_bv)	0.447	0.664	0.556
r2(Tv_bv)	0.051	0.352	0.202
No. Stars	34	30	30

It is important to note the Tv_bv for NGC 7790 is not meaningful as there is an approximately 20% chance of having a squared correlation coefficient with this value or higher when there is none. The statistical test employs a t-statistic given by

$$t_{n-2} = \sqrt{\frac{r^2(n-1)}{1-r^2}}$$

where n is the number of data and r^2 is the squared correlation coefficient. The value of this statistic for the NGC 7790 V coefficient is 1.31 for which

$$P\{t_{32} > 1.31|\text{no correlation}\} = 0.20$$

The same coefficient for M67 is meaningful, but the coefficient itself is almost zero (-0.010). Furthermore, after some experience with measuring these coefficients, the squared correlation coefficients for the Tv_bv coefficient are typically not significant. This means that there is no statistical reason to reject the null hypothesis that there is zero correlation between B-V and V-v meaning that Tv_bv is not statistically significantly different from zero. Nonetheless, we will use the average of these coefficients in the following analysis. The regression plots are presented in the Appendix.

3. We then compare the resulting error for the Null, Static and Dynamic coefficients by estimating the magnitude of three target stars using eight comparison stars in an image of M67 taken almost a year later.

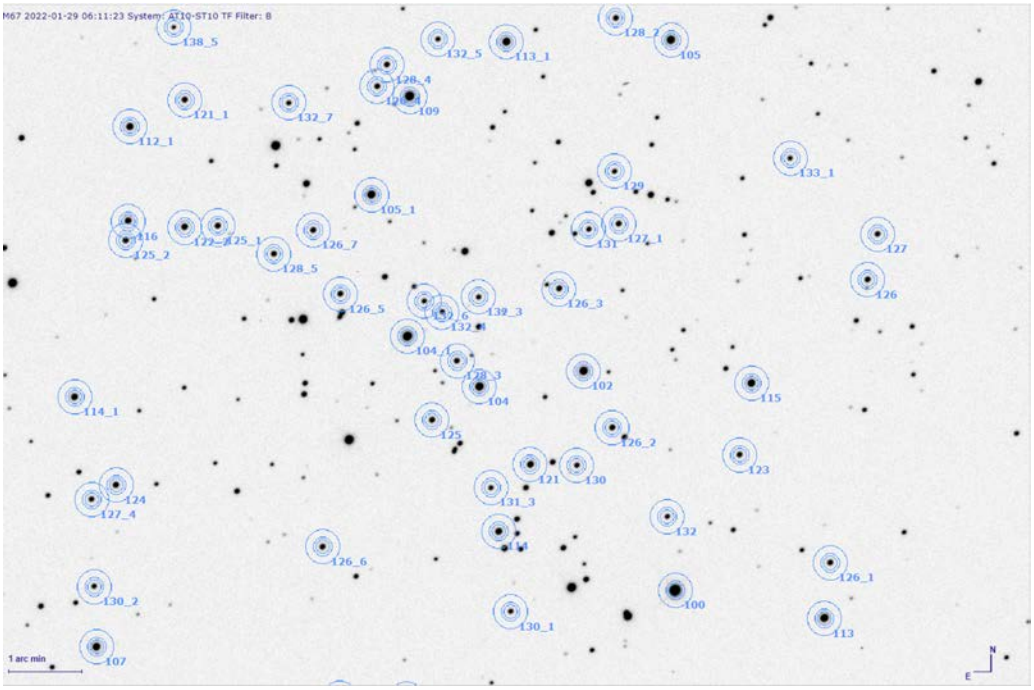

Figure 1. Comparison stars in M67 in a Vphot image

We use data from three images taken during a period of almost four hours 2022-01-29 UT. The early image, with an altitude of 26.5 degrees, had an airmass of 2.24 while the second image, at 70.6 degrees, had an airmass of 1.06. This data allows us to see the effects of airmass on the magnitude estimates.

In both cases we used eight comparison stars to estimate the magnitudes of three target stars. The comparison stars ranged in B-V index from 0.405 to 1.123. The target stars were also chosen to represent a broad range of color with B-V values of 0.128, 0.606 and 1.264. These stars are listed in the table below.

Table 1. Target and comparison stars in M67

Targets	AUID	B	B-V
112	000-BLG-895	11.391 (0.019)10	0.128 (0.025)
126_3	000-BLG-917	13.246 (0.022)10	0.606 (0.029)
102	000-BLG-886	11.553 (0.023)10	1.264 (0.028)

Comps	AUID	B	B-V
115	000-BLG-901	11.949 (0.017)10	0.405 (0.022)
121	000-BLG-903	12.572 (0.016)10	0.456 (0.021)
122_2	000-BLG-906	12.808 (0.016)10	0.562 (0.021)
116	000-BLG-902	12.686 (0.017)10	1.050 (0.021)
114_1	000-BLG-900	12.546 (0.016)10	1.052 (0.019)
112_1	000-BLG-896	12.342 (0.016)10	1.076 (0.020)
104	000-BLG-887	11.562 (0.018)10	1.109 (0.023)
105_1	000-BLG-890	11.656 (0.018)10	1.123 (0.022)

We estimate the dynamic coefficients using only the comparison stars. For the 1.06 airmass case, we estimate the value of the dynamic coefficients as $\alpha_b =$ 0.0285 and $\alpha_v =$ -0.0049. We also performed a new regression using the same method as that used in the Static procedure to obtain

$$\begin{aligned} T_{bv} &= \quad 1.0335 \\ T_{b\_bv} &= \quad 0.0276 \\ T_{v\_bv} &= -0.0048 \end{aligned}$$

Multiplying T_{bv} by the other coefficients yields, essentially, the same values as α_B and α_v. Note also that the first two Static values are the same, to two decimal places, as the average we computed with the TC generator using the data from the year before while T_{v_bv} remains essentially zero. This suggests that the TCs are quite robust over time.

For the 2.24 airmass case, we estimate the dynamic coefficients as $\alpha_B = 0.0742$ and $\alpha_V = 0.0093$. The new regression yielded

$$\begin{aligned} T_{bv} &= \ 1.0662 \\ T_{b_{bv}} &= 0.0702 \\ T_{v_{bv}} &= 0.0081 \end{aligned}$$

Multiplying the T_{bv} by the other two coefficients yields, 0.0749 and 0.0086, which are, again, very close to the values of α_B and α_V but significantly different from the static coefficients.

So, we use each comparison star to estimate the target star and then average these estimates. Again, the estimation equation is

$$\hat{B}_{ij} = B_j + \Delta b + c\,\Delta(b - v)$$

where c is zero for the Null case, the usual Static transformation coefficient (i.e., $T_{bv} \cdot T_{b\_bv}$ or $T_{bv} \cdot T_{v\_bv}$) and the Dynamic coefficient (i.e., α_b or α_v). Then, the estimate is given by

$$\hat{B}_i = \frac{1}{N}\sum_{j=1}^{N} \hat{B}_{ij}$$

For the low airmass targets, the error in the estimate was essentially the same for all three coefficients including Null. This results from the fact that, when we multiply the transformation coefficients from the previous year, we obtain an equivalent α_B of 0.0367 and essentially zero for α_V. Consequently, the estimates using the Static and Dynamic are close.

The B errors were almost the same for low air mass with Dynamic performing somewhat better then Null and Static. However, for high air mass, the difference was dramatic. Null was almost twice as high as Static which was more than twice as high than Dynamic. The large difference in the B estimates may be due to the fact that B filtered light is scattered more due to Raleigh scattering than V light. These results are summarized in below.

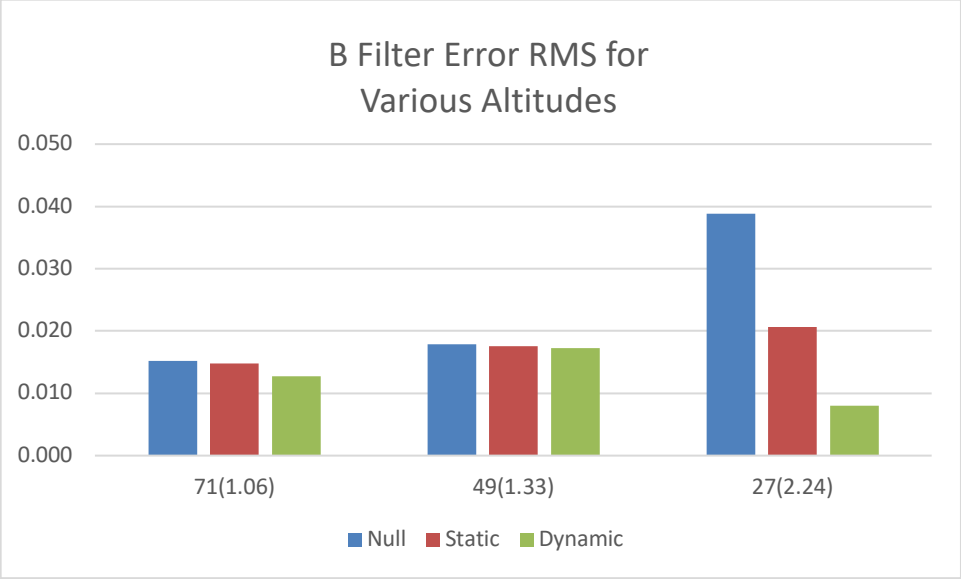

Figure 2. RMS errors using the B filter for various air masses

For the V filter, there was not much difference with all three performing essentially the same for 1.06 and 1.33 and with Dynamic performing slightly better at 2.24. We believe the reason for this is that there is very little correction necessary in the V band as the color coefficient is very small.

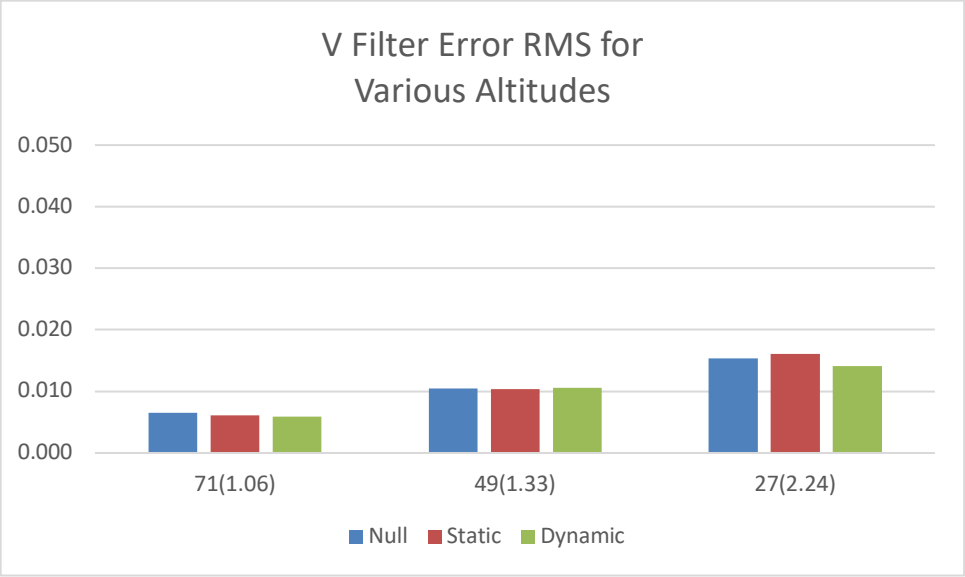

Figure 3. RMS errors using the V filter for various air masses

4. Conclusions and Recommendations

The analysis performed here is only a start but suggests a possible improvement over the methods applied by standard software such as VPHOT and Maxim DL.

VPHOT apparently uses comparison stars to estimate the zero point, Z, and then adds this to the instrumental magnitude to estimate the target magnitude, viz.,

$$\hat{B}_t = b_t + Z_b \tag{9}$$

where

$$Z_b = \frac{\sum_c B_c - b_c}{n}$$

Maxim DL does something similar but appears to use some weighting of the estimates based, perhaps, on the SNR or estimated error.

An alternative approach would be to:

1. Estimate the magnitudes of check stars using existing transformation coefficients (if there are any) and equation (6).
2. Perform a regression using the comparison stars to determine α and Z.
    a. Discard any star that is outside a set bound (e.g., 2 sigma) and redo the regression. This can be done by considering how far the star is from the regression line or by considering the error in a given star's predictions of the

other comparison star magnitudes. However, this should not be repeated once a new regression is done.

b. Determine whether there is a correlation using the t-statistic described in the text.
c. If α is significant, estimate the magnitudes of the comparison stars using (8).
d. Otherwise, use (9).

3. Choose method 1 or 2 from which has the least error in predicting the magnitude of the check stars.
4. Estimate the magnitudes of the target star(s) using the chosen method.

Such a procedure should be easily implemented in existing software and using available comparison stars. However, since it will (obviously) not work with only one color, it could be confusing to beginning users.

Acknowledgements

We acknowledge with thanks the variable star observations from the AAVSO International Database contributed by observers worldwide and used in this research. We especially like to acknowledge the late Arlo Landolt and his colleagues who painstakingly worked to provide fields of standard stars with excellent magnitude estimates.

The author would also like to thank Dr. Joyce Guzik who encouraged the dissemination of this work and Ms. Lindsay Ward who patiently worked with the author in order to make the original presentation better.

References

AAVSO. 2022, *AAVSO Guide to CCD/CMOS Photometry with Monochrome Cameras.* Cambridge, MA: AAVSO.

—. 2022., *Transform Generator User's Guide (version 6.8).* March 3. https://www.aavso.org/tg#introduction.

Boyd, D. 2012, "A Practical Approach to Transforming Magnitudes onto a Standard Photometric System," *JAAVSO* 990-1002.

Henden, A. A., and Kaitchuk, R. H. 1982, *Astronomical Photometry,* New York: Van Nostrand Reinhold Company.

Klingenberg, G., Mogil, K., Simonsen, M., Menzies, K. 2016, *VPHOT User's Guide, Version 3.2.* Cambridge, MA: AAVSO.

Appendix: Regression plots from the Transform Generator for M67 stars

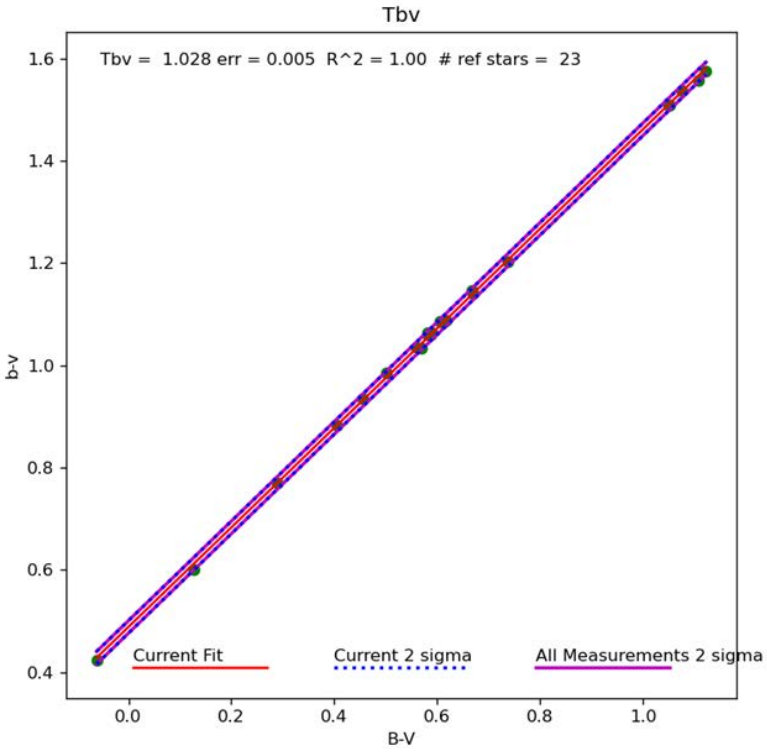

Figure A1. Plot of b-v versus B-V for 23 stars in M67

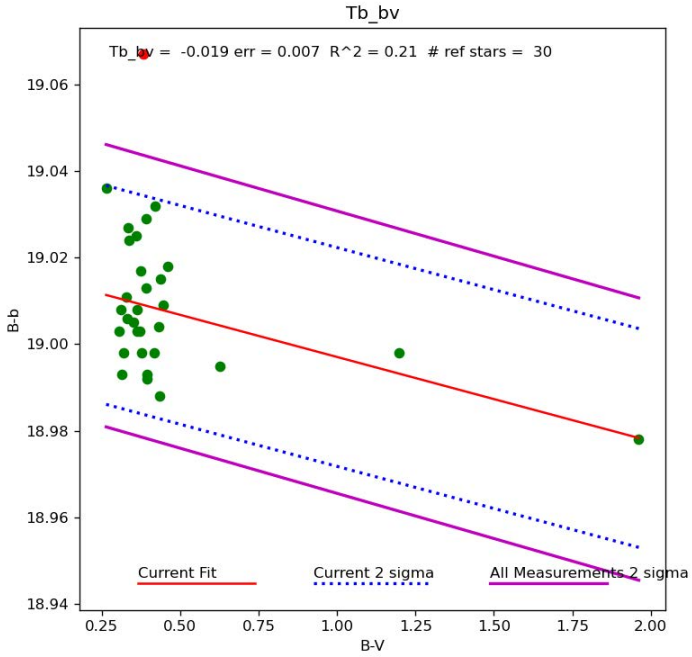

Figure A2. Plot of B-b versus B-V for 30 stars in M67

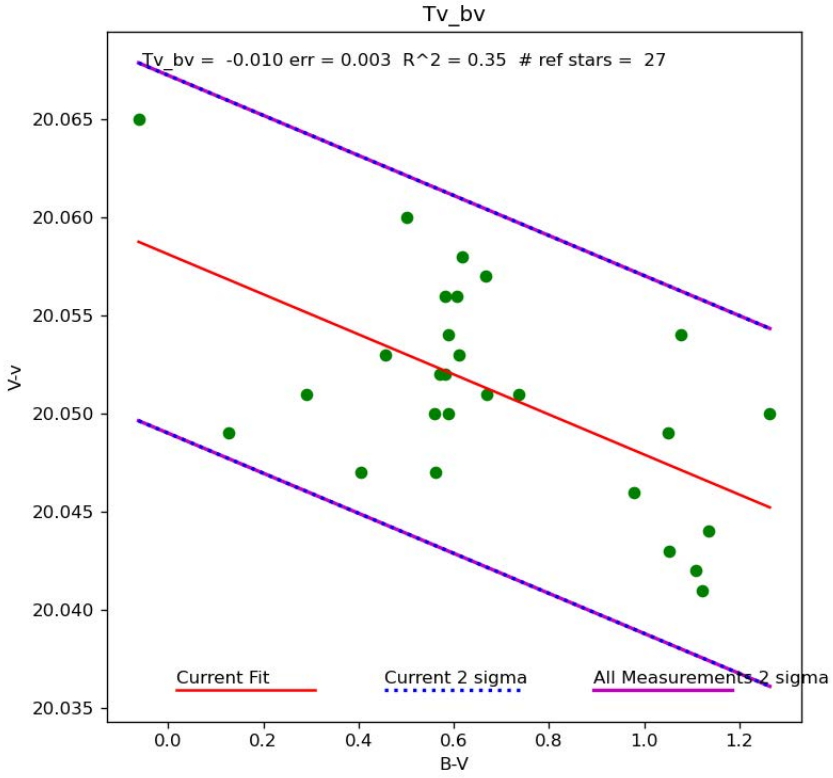

Figure A3. Plot of V-v versus B-V for 23 stars in M67

The Ultraviolet Follow-on Observatory (UFO)

Douglas Walker
Prime Solutions Group, Inc., 1300 S Litchfield Rd, Goodyear, AZ, 85338, USA;
dougwalker@psg-inc.net

Kevin France
Department of Astrophysical and Planetary Sciences, University of Colorado, UCB 391, Boulder, CO, 80309, USA; kevin.france@colorado.edu

John Martin
Department of Astronomy-Physics, University of Illinois, Springfield, Ill, 62703, USA;
jmart5@uis.edu

Ken Spencer
Astronomy Association of Arizona, 485 Watson Rd Suite 103-247, Buckeye, AZ, 85326, USA;
astronomyassociationarizona@gmail.com

Dirk Terrell
Department of Spaces Studies, Southwest Research Institute, 1050 Walnut Street Suite 400, Boulder, CO 80302, USA; terrell@boulder.swri.edu

Subject Keywords

Ultraviolet; optical; time-domain astronomy; CubeSat, SmallSat; Large UV/Optical/IR Surveyor; 12U

Abstract

Prime Solutions Group, Inc. (PSG), in partnerships with Southwest Research Institute (SwRI), the University of Colorado at Boulder, the University of Illinois, and the Astronomy Association of Arizona (AAA), are proposing the development, launch and operation of stellar observatory mission which will consist of a space-based UV/optical telescope system designated as the Ultraviolet Follow-on Observatory (UFO). This proposed CubeSat will be a 12U system housing a 125mm telescope and designed for a four-year plus mission timeline in high Earth orbit. Imaging detectors capturing simultaneous UV/optical observations will first be developed and tested on a ground-based telescope before being designed and integrated into the CubeSat. UFO will follow in the footsteps of the successful launch and operation of the University of Colorado Ultraviolet Transit Experiment (CUTE) and the planned launch of the Arizona State University Star-Planet Activity Research CubeSat (SPARCS). These systems are paving the way for this new era in CubeSat space-based astronomy. The operation of UFO in the UV (240nm to 390nm (UVC, UVB, UVA)) and optical (400nm to 750nm) will expand on these missions. UFO is being specifically designed for providing important scientific data to the university-level and amateur astronomical

community such as American Association of Variable Star Observers (AAVSO). This project will demonstrate that small telescope observations in the ultraviolet frequency can provide valuable data to the astronomical science community and will help fill a critical need in the observational ultraviolet astronomy gap until NASA's Large UV/Optical/IR Surveyor (LUVOIR) mission launches in the early 2040s timeframe.

1. Introduction

Astronomical photometry covers the range of the electromagnetic spectrum from the ultraviolet (UV) at 200 nanometers (nm) through the visible portion into the near infrared (NIR) at 1500 nm. The UV portion of astronomy research reveals a wealth of information about hot and energetic processes in astronomical objects contributing valuable information to the scientific community. Due to atmospheric absorption, UV astronomy can only be successfully conducted outside the atmosphere in the space environment; thus it is not the focus of many current or past astronomical investigations. Only a few current large space missions, such as the Hubble Space Telescope (HST) and the Neil Gehrels Swift Observatory cover the UV spectral range, some of them only in the near-UV (NUV). This UV research field is currently sparsely addressed but is of scientific interest for the larger scientific community. With the growth rate of the use of small satellites such as SmallSats and CubeSats, the opportunity to provide means of research for UV astronomy are now becoming possible. With HST and Swift currently approaching end-of-life, we are beginning to enter a period without any good UV satellites in orbit (Yatsu et al. 2019). This proposed UV/Optical CubeSat project can provide good UV photometry in a very "general purpose" orbiting observatory. While this CubeSat is a prototype, a major goal is to keep it inexpensive and, as such, it can easily be replicated to create a serial constellation of UV observing satellites that will help fill a critical need in the observational UV astronomy gap until NASA's Large UV/Optical/IR Surveyor (LUVOIR) mission launches in the early 2040s timeframe.

2. Background

As a review, CubeSats are a class of research spacecraft called nanosatellites. CubeSats are built to standard dimensions (Units or "U") of 10 cm x 10 cm x 10 cm. CubeSats can be configured in 1U, 2U, 3U, or 6U, and weigh typically less than 1.33 kg (3 lbs.) per U (Loff, 2018). Typical CubeSat sizes ranges are shown in Figure 1. The boundary between CubeSats and the next size SmallSat is normally 27U. In 1999, California Polytechnic State University (Cal Poly) Professor Jordi Puig-Suari and Stanford University Space Systems Development Laboratory Professor Bob Twiggs, developed the CubeSat specifications to promote and develop the skills necessary for the design, manufacture, and testing of small size satellites intended for Low Earth Orbit (LEO) applications. Academia accounted for the majority of CubeSat launches until around the 2013 timeframe, when more than half of launches were for non-academic purposes, and by 2014 most newly deployed CubeSats were for commercial or amateur projects (CubeSat Database, 2022).

The CubeSat Design Specification Rev.14.1 has been developed to help guide CubeSat construction (CubeSat Design Specification, 2020). The CubeSat specification accomplishes several high-level goals (Call for CubeSat Proposals, 2008). The main reason for miniaturizing

satellites is to reduce the cost of deployment using the excess capacity of larger launch vehicles or a "ride share" option. The CubeSat design specifically minimizes risk to the rest of the launch vehicle and payloads, making rideshare possible. Encapsulation of the launcher–payload interface takes away the work that would previously be required for mating a satellite with its launcher. Unification among payloads and launchers enables quick exchanges of payloads and utilization of launch opportunities on short notice.

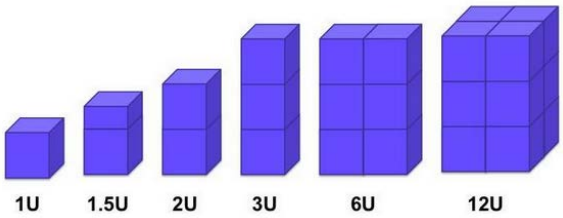

Figure 1. Buildup of CubeSat sizes utilizing 1U components (1U = 10cm x 10cm x 10cm).

2.1 Colorado Ultraviolet Transit Experiment

The Colorado Ultraviolet Transit Experiment (CUTE) is a 4-year, NASA-funded project to design, build, integrate, test, and operate a 6-unit CubeSat (30 cm x 20 cm x 10 cm). A cut-away is shown in Figure 2. CUTE is planned to have a 1-year nominal mission lifetime and was successfully launched in late September 2021 (Launch of CUTE, 2022). It has completed the commissioning processes and is now in scientific data operations (Egan et al., 2022). Using near-ultraviolet (NUV) transmission spectroscopy in the 255 nm to 330 nm range, CUTE is focusing on characterizing the composition and mass-loss rates of exoplanet atmospheres. This is accomplished by measuring how the NUV light from the host star is changed as the exoplanet transits in front of the star and passes through the planet's atmosphere. Transit light curves created from CUTE observations will provide constraints on the composition and escape rates of these atmospheres and may provide the first concrete evidence for magnetic fields on extrasolar planets.

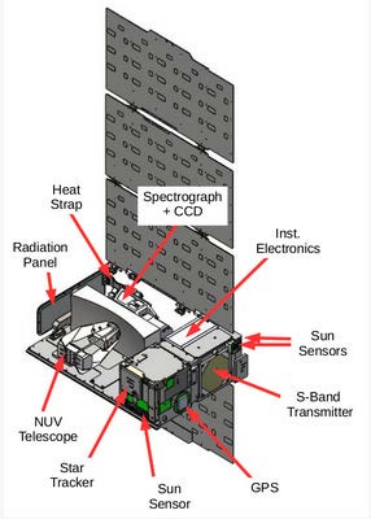

Figure 2. Cut-away CAD rendering of CUTE, with transparent top and sides to display the telescope and spectrograph. (Credit UC LASP)

CUTE is designed to follow exoplanet systems of interest for several orbital periods to provide low-resolution spectroscopy of critical atmospheric tracers (Fe II, Mg II, Mg I, OH) that are inaccessible from the ground.

CUTE was designed at the University of Colorado, Boulder, and the Laboratory for Atmospheric and Space Physics (LASP) and built by Blue Canyon Technologies. Dr. Kevin France (co-author) is the Principal Investigator of the CUTE mission at LASP.

2.2 Star-Planet Activity Research CubeSat (SPARCS)

Arizona State University's Star-Planet Activity Research CubeSat (SPARCS) is a NASA-funded astrophysics mission, devoted to the study of the UV time-domain behavior in low-mass stars (ASU SPARCS, 2022). It is a 6U spacecraft where the solar power panels extend like wings from one end. The deployed on-orbit configuration is shown in Figure 3.

Low-mass stars are important targets in the search for exoplanets residing in the habitable-zone. Over its scheduled 1-year mission, SPARCS will stare at approximately 10 stars in order to measure short term- (minutes) and long term- (months) variability simultaneously in the near-UV and far-UV. The SPARCS scientific payload consists of a 90mm reflector telescope and two high-sensitivity 2D-doped CCDs. The payload will be placed on a Sun-synchronous terminator orbit, allowing for long observing stares for all targets. Launch is expected to occur in the 2023 timeframe.

Figure 3. Illustration of SPARCS in orbit and operational parameters. (Credit ASU School of Earth and Space Exploration)

SPARCS will also be capable of "target-of-opportunity" ultraviolet observations for the rocky planets in M-dwarf habitable zones. This will provide the needed ultraviolet information context for the first habitable planets that the James Webb Space Telescope will characterize.

2.3 Ultraviolet Follow-on Observatory

A search of the literature shows that, in addition to the missions above, there are several Earth orbiting UV CubeSat telescopes in the discussion stage but no funded projects. To help bridge the

observing gap between the end-of-life of the CUTE and SPARCS missions and the launch of LUVOIR, a follow-on CubeSat mission is being proposed, the Ultraviolet Follow-on Observatory or UFO. This proposed CubeSat will be a 12U system housing a 125mm telescope. Our initial proposal is calling for a pair of CubeSats to be place in Earth orbit to provide simultaneous time-domain observing of high energetic objects of interest. If the initial prototype mission is successful, a follow-on proposal will be for a series of three CubeSat pairs where each is designed for a four-year plus mission timeline in high Earth orbit. The continuation of the CubeSats observing timeline will fill the approximate 15-year observing gap described above. A camera capturing simultaneous UV/optical observations will first be developed and tested on a ground-based telescope before being designed and integrated into the CubeSat. A dichroic beam splitter or mirror has been selected for separating out the UV from the optical wavelength. Separate duplicate cameras will then be used for image capture.

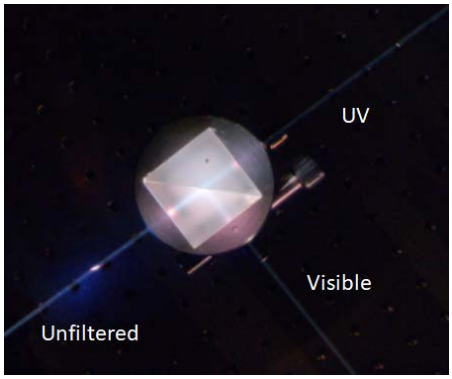

Figure 4. Dichroic beam splitter for separating UV and optical wavelengths.

The operation of UFO will expand on the previous missions and demonstrate that small telescope observations in the ultraviolet can provide valuable data to the astronomical science community and will help fill a critical need in the observational ultraviolet astronomy gap until LUVOIR becomes operational, NASA GSFC (2022).

3. Program Objectives

The primary science objective is to provide simultaneous time-domain observational data in the UV wavelength range of 240nm to 390nm (UVC, UVB, UVA) and the optical wavelength range of 400nm to 750nm. Because it is small aperture, it can handle “bright” objects and events that are beyond the bright limit of larger satellites. This science data is useful in a variety of professional observing programs.

The secondary objective is to provide synergy with ground-based university and amateur-level science programs and observatories. Systems at this level can provide excellent time-series photometry and spectroscopy of bright targets that are out of range for larger observatories. Science mission objectives are broken out by the following areas.

3.1 Science objectives

Scientific objectives for observing in the UV for stellar/galactic regions include:

- Bright transient sources (supernovae) (Welsh et al., 2011; Wils et al., 2010; Ganot et al., 2016)
- Active Galactic Nuclei (Wang et al., 2019)
- Flare stars (Welsh et al., 2007)
- Gravitational wave counterparts (Ridden-Harper et al., 2017)

For Solar System observations:

- Venus – observations help fill gaps between NASA missions (Limaye et al., 2018)
- Pluto – observations of atmosphere via stellar occultations (Kammer et al., 2020)
- Asteroids (Xing and Bodewits, 2021)
- Trans-Neptunian Objects (Tan et al., 2021)

For exoplanets:

- Planetary eclipses
- Atmospheric detections (Lopez et al., 2022)

For the general astronomical community:

- Provide access for advanced amateur, university faculty and professional astronomers to conduct follow-up observations of objects of interest.
- Allow astronomers to conduct original research.
- Provide opportunities for graduate students to perform original research.

3.2 Benefits/Cost ratio (BCR)

The Benefit-Cost Ratio (BCR) is an indicator used in industry that shows the relationship between the relative costs and benefits of a proposed project. An analysis was conducted to determine the benefit of the UFO project in relation to other observatory type systems.

3.2.1 Science BCR

The science results and benefits of any observational system are difficult to quantitively measure. An approach taken here is to determine the cost of a published paper in a peer-reviewed journal as the ratio of cost of system operations over the number of papers. Table I shows the results of comparing the HST and the Las Cumbres Observatory (LCO) against the estimated cost for the UFO project.

Table 1. Benefit-Cost Ratio of UFO compared to other observatory systems.

System	Operations Cost ($M)	No. Peer Review Articles	Cost/Paper Ratio ($K)
Hubble Space Telescope	$16,000	18,000	$888.89
Las Cumbres Observatory	$44.37	431	$102.95
UFO	$11.14	323	$46.44

Table 1 is based on the assumptions that the UFO total project cost is approximately $15M for initial prototype system development and operation over the 4-year target lifespan and that the number of published papers is 75% of what has been accomplished with the LCO system. This preliminary analysis shows a very good potential payback for science results for funds invested.

3.2.2 Education BCR

A similar analysis was carried out for estimating the cost for reaching students at the high school, college, and university level. The AAA will be taking the lead in developing the educational and public outreach events.

Table 2. Benefit-Cost Ratio of Educational Aspects of UFO.

Event	Cost per Event	No. Students Reached	Cost/Student Ratio ($)
High School Seminar	$3,000	14,000	$4.50
University	$3,000	1,400	$15.00

For a relatively small amount of funds, high school and university students can be reached with the introduction of STEM-related activities.

3.3 Engineering objectives

Model-based Systems Engineering (MBSE) is a formalized methodology that has been developed over the past 10 years is to support the requirements, design, analysis, verification, and validation associated with the development of very complex systems. In contrast to the more traditional engineering approach, MBSE puts models at the center of system design for each design phase. The increased adoption of digital-modeling environments during the past few years has led to increased adoption of MBSE. In January 2020, NASA noted this trend by reporting that MBSE, “has been increasingly embraced by both industry and government as a means to keep track of system complexity.” (Shevchenko 2020).

A model support tool which supports this MBSE approach has been selected for the UFO project. The Innoslate modeling environment offers a full lifecycle software for model-based systems

engineering, requirements management, verification, and validation, plus DoDAF with a powerful ontology at its core, Innoslate MBSE Tool (2022).

3.4 Education objectives

As first introduced above, education is a major emphasis for this project. Education objectives include the following:

- Provide education opportunities to AAA members and the general public regardless of ethnic origin, cultural beliefs, or socioeconomic status.
- Provide opportunities for high school, community college and university students to become involved in a multi-year project which can lead to high school science projects, community college special project courses and university level Capstone projects.
- Provide observational data to university faculty and professional astronomers to conduct original research in their areas of expertise.
- Provide observational data and guidance to amateur astronomers and students to conduct original research and publish their findings.
- Provide synergy between UV satellite data and ground-based data that is achievable with college and semi-professional observatories.
- Provide synergy of satellite UV photometry observations with ground-based spectroscopy.

The AAA will take the lead in emphasizing the importance and interaction of education and public outreach.

4. CubeSat Design

The CubeSat Design Specification Rev.14.1 specifies the basic design and major components for CubeSats. A basic design of the UFO CubeSat consists of the 12U bus structure, deployable solar panels for power generation and containing the 125mm optical telescope. An example configuration is shown in Figure 5.

As shown in the cutaway diagram, the typical CubeSat bus consists of about 1/3 bus electronics, Attitude Determination and Control System (ADCS) and payload assembly respectively. The 12U size of the UFO is driven by the 125mm telescope.

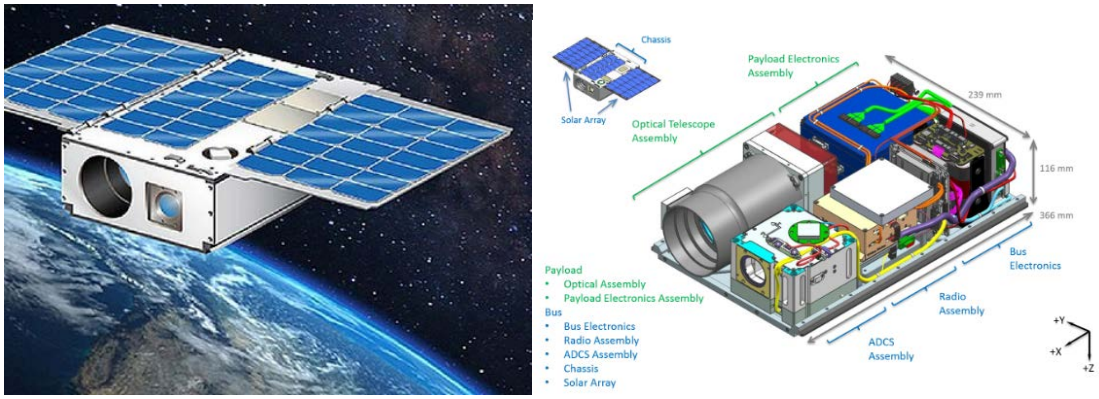

Figure 5. CubeSat with solar panels deployed. (Credit Knapp 2019)

4.1 Satellite bus

Defining a standard bus and developing standard hardware components using commercial off-the-shelf components and a standard spacecraft frame simplifies the development of picosatellites. The CubeSat development will provide a standard spacecraft frame, a spacecraft controller, radio transceiver, attitude determination and control, solar cells, batteries, and an interface for a payload.

As a subsidiary of Raytheon Technologies, Blue Canyon Technologies is a complete end-to-end spacecraft company and a leading provider of turnkey small satellite solutions, including nanosatellites, microsatellites, and ESPA-class satellites. Initial discussions have taken place with Blue Canyon technologies for the development of the bus assembly. Discussions have also taken place with other vendors such as Pumpkin CubeSat Kits. Currently, the SwRI Boulder facility is the lead facility for UFO construction, integration, and testing.

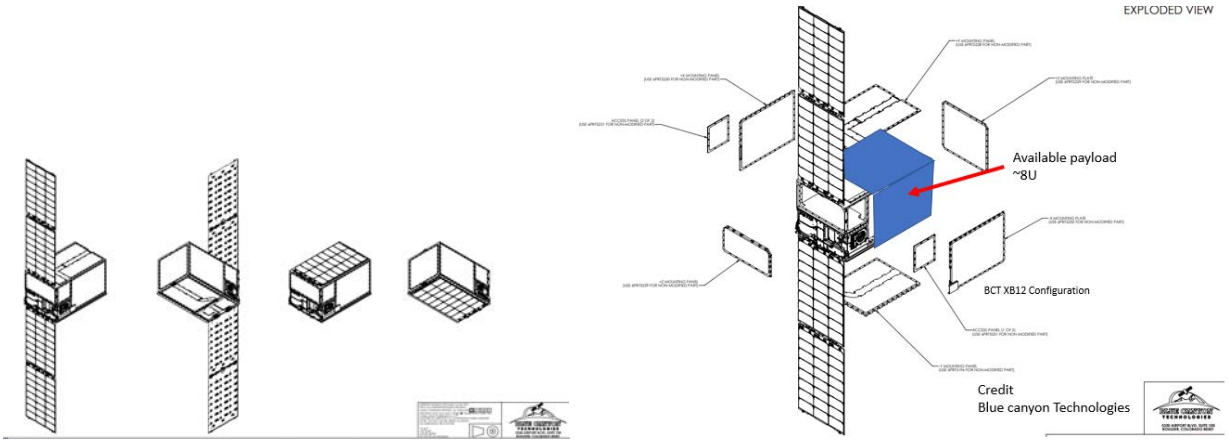

Figure 6. Blue Canyon Technologies is one possible CubeSat bus manufacturer.

4.2 Optical telescope

The main scientific instrument on UFO is the telescope system. Aperture Optical Sciences (AOS) designs, develops and manufactures optics for satellite imaging and communications systems (AOS, 2022). AOS develops aspheric mirrors for high-energy lasers and specializes in the use of Silicon Carbide materials for extreme performance applications.

The AOS CC series is the new generation of high-performance telescopes for CubeSats, supporting 3U, 6U and 12U applications. Extensive use of Silicon Carbide (SiC) provides a telescope that is inherently athermal and low mass, ensuring consistent imaging performance and lowering launch costs. Custom solutions with apertures to 250 mm are available.

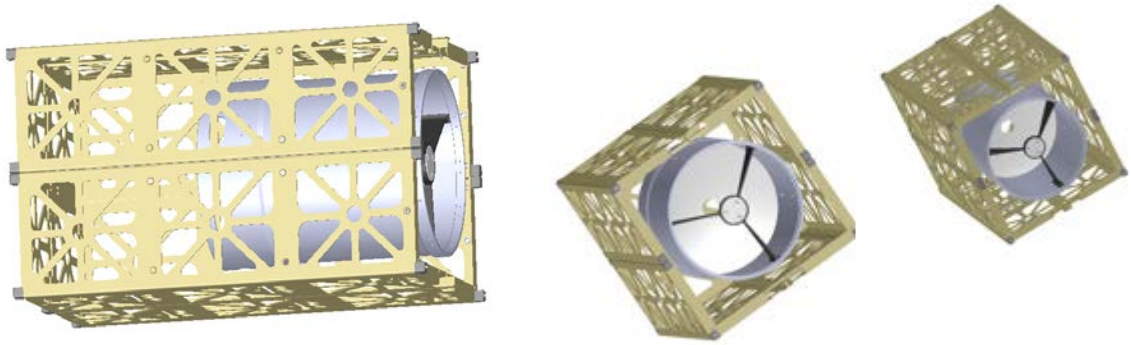

Figure 7. Aperture Optical Sciences 250mm CC Series telescope.

The CC Series telescope system is designed for simplicity and economy – but with its all-ceramic construction it can outperform more typical refractive designs by providing broadband, thermally insensitive performance. The standardized architecture with generalized specifications is intended to define baseline performance specifications. CC series telescopes require only minimal customization to meet customer defined mission requirements.

5. Ground Station Support

The Amazon Web Services (AWS) Ground Station is a fully managed service that lets you control satellite communications, process data, and scale your operations without having to worry about building or managing your own ground station infrastructure. Satellites are used for a wide variety of use cases, including weather forecasting, surface imaging, communications, and video broadcasts. Ground stations form the core of global satellite networks. The AWS Ground Station allows direct access to AWS services and associated infrastructure including a low-latency global fiber network. Satellite command and telemetry will be provided by the AWS Ground Station network.

Figure 8. AWS ground station services will provide UFO command and telemetry.

5.1 Target querying and prioritization

The spread of telescopes around the world has greatly increased the opportunities to observe all astronomical events. The light from celestial objects can be sampled with greater frequency and for longer durations when observations are passed from one telescope to the next. The Las Cumbres Observatory has been developed to provide access to astronomical telescopes located around the world to enable both amateur and professional astronomers to take advantage of transients which are astronomical phenomena whose duration can range from seconds to several years.

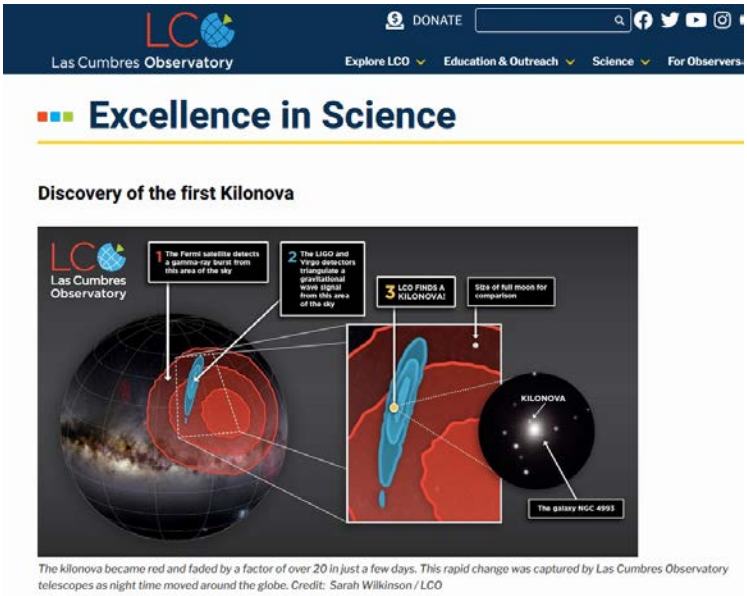

Figure 9. The Las Cumbres Observatory provides a system of fully automatic target querying, observing and image distribution.

The heart of LCO operations is its dynamic observation scheduling system. Working without human intervention, LCO's internet-based scheduler takes requests for observations from scientists and observers, deconflicts competing requests and conditions at each telescope site, directs individual telescopes to make the desired observations, and compiles the results. Scientists can make requests for observations at any time as the scheduler updates the entire network plan about every 5 minutes.

Figure 10. LCO's automated system allows internet sign-on, request of targets for observation, querying and deconflicting of targets, imaging, and distribution of results.

The network operates around-the-clock where calibration observations are made during daytime. Observing schedules are stored at site, so telescopes can continue observing even when an external link is interrupted. Within minutes of the camera shutter closing at the telescope, the science data are calibrated and sent to the science archive for retrieval by the scientists.

The LCO system is being investigated as to whether UFO can integrate into the current LCO infrastructure and take advantage of synergism between the two systems. Target querying and prioritization lists would be transferred to the LCO system with the observing specifications routed from LCO to the AWS ground station system. Discussions with the LCO team are being initiated.

6. Launch Support

The CubeSat Launch Initiative (also known and rideshares) provides opportunities for small satellite payloads built by universities, high schools and non-profit organizations to fly on upcoming launches, NASA CubeSat Launch Initiative (2022). However, with PSG being a for profit company, NASA rideshare is not available. NASA does provide some launch support for their funded missions as this avenue is being investigated. Other launch providers are being considered including SpaceRyde, Spaceflight, SpaceX and RocketLab. CubeSat rideshares are generally constrained to CubeSats 12U and smaller. The plans for UFO are to take advantage of the rideshare thus the sizing of UFO being restricted to size 12U.

7. Pro-Am Science

Astronomy is one field of science where amateur astronomers can perform cutting-edge science research. These activities are usually in the form of partnering with professional astronomers in pro-am collaborations. Amateur astronomers have the ability to move and observe when and where they choose and are often better at tracking asteroids or hunting for new supernovae than many pros. Amateurs are also branching into the field of spectroscopy, splitting starlight into its constituent wavelengths to study the composition of stars and other celestial objects.

7.1 Partnerships with universities

This UFO project is designed with pro-am astronomy research as one of the primary objectives. As the system becomes operational and knowledge of research opportunities becomes widely known, it is anticipated that many professional-amateur relationships will be established and flourish. The primary mission of the AAA is to seek out and develop these relationships with educational institutions from high school through the university level.

7.2 Availability to AAVSO members

This UFO project is designed with pro-am astronomy research as one of the primary objectives. As the system becomes operational, members of the AAVSO will be able to submit proposals for observing runs and extended observing campaigns. Imaging of selected variable stars in the UV frequency range coupled with space- and ground-based optical imagery will enhance the opportunities for AAVSO members to perform original scientific research and produce publications.

8. Project Team Organization

In order to execute this program, a series of partnerships have been established with a select set of engineering and science organizations. This mix of expertise ensures that the probability of mission development and execution is maximized. This partnership organization includes the following profession organizations.

8.1 Prime Solutions Group, Inc. https://psg-inc.net/

PSG is a professional engineering services company with a legacy in Intelligence, Surveillance & Reconnaissance (ISR) technology. Leveraging deep experience and expertise in synthetic aperture radar (SAR) processing, core skills in complex system-of-systems engineering, and cutting-edge applied research and development in image-based machine learning, PSG helps solve the 21st century challenges faced by both private industry and government organizations. PSG is the prime contractor and system integrator for the UFO project. Its staff includes multiple decades of experience in project management and mission execution.

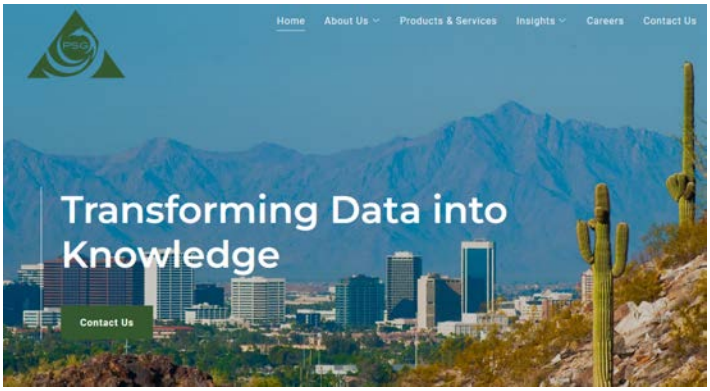

Figure 11. Prime Solutions Group is located in Goodyear, Arizona.

8.2 Southwest Research Institute. https://www.swri.org/

Southwest Research Institute (SwRI), headquartered in San Antonio, Texas, is an independent, nonprofit, applied engineering and physical science research and development organization with over 3000 employees. The Institute's Planetary Science Directorate has over 100 employees and is located in the Exeter Building at 11th and Walnut in downtown Boulder, Colorado.

The Space Science and Engineering Division's goals are excellence in space research and the expansion and deepening of SwRI's space research efforts. SwRI has successfully executed space missions such as the New Horizon fly-by of Pluto, Areas of research and development include:

- Space Studies
- Planetary Physics
- Planetary Atmospheres and Surfaces
- Lunar Origin and Evolution
- Solar Physics
- Solar System Dynamics
- Astronomy
- Computer Systems
- Space Operations
- Space Technologies
- Mission Operations

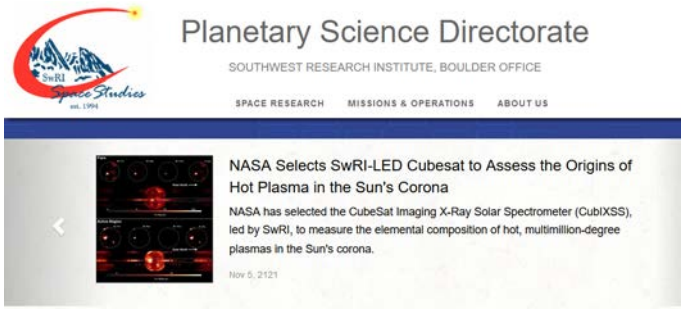

Figure 12. SwRI Planetary Science Directorate.

8.3 University of Colorado. https://lasp.colorado.edu/home/

The Laboratory for Atmospheric and Space Physics (LASP) at the University of Colorado Boulder (CU) began in 1948. UC is the world's only research institute to have sent instruments to all eight planets and Pluto.

LASP seeks to maintain and improve the capability to pursue key science questions using experimental, laboratory, theoretical, and information systems approaches. LASP is dedicated to building and maintaining a unique synergism of expertise in space science, engineering, and spacecraft operations. The progressive development and use of innovative technologies and continuing participation in new research initiatives will help ensure a strong leadership role for LASP into the future.

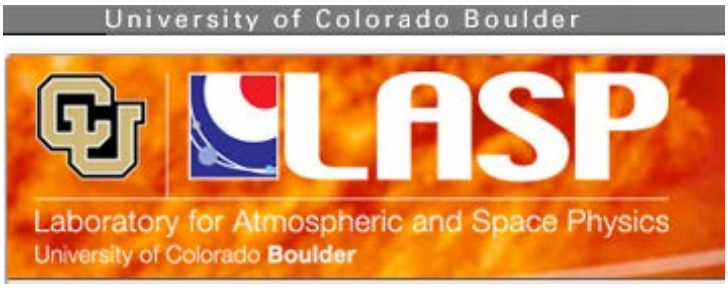

Figure 13. University of Colorado Laboratory for Atmospheric and Space Physics

8.4 University of Illinois. https://www.uis.edu/astronomy-physics

The goal of the University of Illinois Astronomy-Physics group in the Chemistry Department is to enhance society's ability to understand the Universe through the application of scientific problem solving. The university provides opportunities to learn about the universe through the courses which are offered, the scholarship of the faculty, star parties, disability-friendly support, and community updates of upcoming astronomical phenomena.

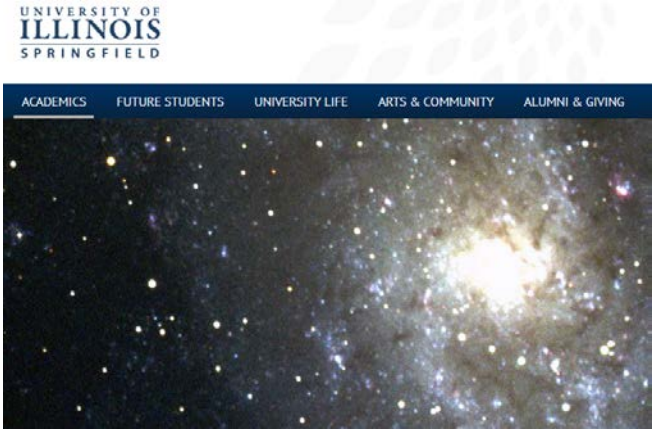

Figure 14. University of Illinois at Springfield.

8.5 Astronomy Association of Arizona. https://astronomyassociationarizona.org/

The Astronomy Association of Arizona is a nonprofit 501(c)3 organization. Their vision is to create an environment where anyone, regardless of ethnic origin, cultural belief or socioeconomic status, succeeds in meeting their personal astronomical and education goals through state-of-the-art learning activities and unsurpassed membership benefits. Mission statements include the following:

- To engage and educate those of all interest levels and to provide the highest quality of astronomical science to our community and beyond.
- Provide formal and informal education programs for both beginners and experienced astronomers.
- Encourage member participation regardless of their level of interest.
- Create and support programs to increase skills, broaden knowledge and focus on studies and research in specialized astronomical sciences.

The Association is located in Buckeye, Arizona.

Figure 15. The Astronomy Association of Arizona is a 501(c)3 nonprofit organization dedicated to bringing astronomy and space science to the general public.

9. Project Funding

The Astrophysics Research and Analysis Program (APRA) under the NASA Research Opportunities in Space and Earth Sciences (ROSES) solicits basic research proposals for investigations that are relevant to NASA's programs in astronomy and astrophysics and includes research over the entire range of photons, gravitational waves, and particle astrophysics. Awards may be for up to four years' duration. APRA investigations may advance technologies anywhere along the full line of readiness levels, from Technology Readiness Level (TRL) 1 through 9.

Proposals relevant to the APRA program are those that address the best possible (i) state-of-the-art detector technology development that is directly applicable to incorporation in future space astrophysics missions; (ii) science and/or technology investigations that can be carried out with

instruments flown as suborbital-class payloads on balloon-borne, sounding rocket, CubeSat, or other platforms; or (iii) supporting technology or laboratory research that are directly applicable to space astrophysics missions.

The APRA funding mechanism is the source being investigated to develop the UFO program. Active proposals to the NASA APRA program will be targeted for the 2023 calendar year.

10. Conclusion

A 12U CubeSat containing a UV telescope is being proposed as a follow-on mission to both the current CUTE and SPARCS satellites. This CubeSat, designated as UFO, is being designed to have a mission timeline of at least 4 years after achieving science commission operations. A pair of satellites will provide continuous time-domain observations of highly energetic objects of interest. With the success of the prototype mission, a series of CubeSat satellites with an overlap in observing operations will be deployed to fill the UV observational gap until LUVOIR is launched in the early 2040s timeframe.

Acknowledgements

D.W. would like thank Joe Marvin, president of Prime Solutions Group, for allowing me to pursue the area of CubeSat research and development, an area currently outside of PSG's area of expertise. D.W. would also like to thank the executive committee of the AAA for support in developing the aspects of the project and the involvement necessary to get the project concept defined.

References

Aperture Optical Sciences. 2022. Retrieved from https://apertureos.com

Arizona State University Star-Planet Activity Research CubeSat. 2022. Retrieved from https://sparcs.asu.edu/

CubeSat Design Specification. 2020. Retrieved from https://www.cubesat.org/cubesatinfo?msclkid=e895ce69bdb111ec972040c67bc2069b

CubeSatShop, Retrieved from https://www.cubesatshop.com/

Educational Payload on the Vega Maiden Flight – Call for CubeSat Proposals. 2008. Retrieved from: Microsoft Word - CubeSat CFP issue 1 rev 1.doc.

Egan, E., et al. 2022, "The Colorado Ultraviolet Transit Experiment: Integration, Testing, and Lessons Leaned on a NASA Astrophysics CubeSat," 36th Annual Small Satellite Conference, SSC22-WKII-02.

Ganot, N., Gal-Yam, A., Ofek, E. O., et al. 2016, "The Detection Rate of Early UV Emission from Supernovae: A Dedicated Galex/PTF Survey and Calibrated Theoretical Estimates," *Astrophys. J.,* **820**, 57.

Innoslate MBSE Tool. 2022. Retrieved from https://www.innoslate.com/

Kammer, J., Gladstone, G., Young, L., et al. 2020, "New Horizons Observations of an Ultraviolet Stellar Occultation and Appulse by Pluto's Atmosphere," *Astron. J.,* **159**, 26.

Launch of CUTE. eoPortal Directory 2022. Retrieved from https://eoportal.org/web/eoportal/satellite-missions/content/-/article/cute?msclkid=c5b06b8bbdab11ec953e9b87e8b2352b

Limaye, S., Mogul, R., Smith, D., Ansari, A., Slowik, G., Vaishampayan, P. 2018, *Astrobiology*, Vol. **18**, No. 9.

Loff, S. 2018, February 14. CubeSat Overview. NASA CubeSat Fact Sheet. Retrieved from: https://www.nasa.gov/mission_pages/cubesats/overview

Lopez, E., LUVOIR Team, 2022, "Exoplanet Transit Spectroscopy with a Future Large UV to IR Flagship Observatory," *Bulletin of the AAS,* Vol. **54**, Issue 5.

LUVOIR, NASA GSFC, 2022. Retrieved from https://asd.gsfc.nasa.gov/luvoir/

NASA CubeSat Launch Initiative. 2022. Retrieved from https://www.nasa.gov/directorates/heo/home/CubeSats_initiative

Ridden-Harper, R., Tucker, B. E., Sharp, R., Gilbert, J., & Petkovic, M. 2017, "Capability of detecting ultraviolet counterparts of gravitational waves with GLUV," *Mon. Not. R. Astron. Soc.*, **472**, 4521.

Shevchenko, N. 2020, "An Introduction to Model-Based Systems Engineering (MBSE)," retrieved from https://insights.sei.cmu.edu/blog/introduction-model-based-systems-engineering-mbse/

Tan, N., Bannister, M., Fraser, W., et al., 2021, "Initial results from the near-ultraviolet survey of Col-OSSOS trans-Neptunian objects," *Bulletin of the AAS,* Vol. **53**, Issue 7.

Wang, J., Xu, D. W., Wang, Y., et al. 2019, *Astrophys. J.,* **887**, 15. doi:10.3847/1538-4357/ab4d90

Welsh, B. Y., Wheatley, J. M., & Neil, J. D. 2011, *Astron. Astrophys.,* **527**, A15. doi:10.1051/0004-6361/201015865

Welsh, B. Y., Wheatley, J. M., Seibert, M., et al. 2007, *Astrophys. J. Suppl.,* **173**, 673. doi:10.1086/516640

Wils, P., Gansicke, B. T., Drake, A. J. et al. 2010, *Mon. Not. R Astron. Soc.,* **402**, 436. doi:10.1111/j.1365-2966.2009.15894.x

Xing, Z., Bodewits, D. 2021, "Ultraviolet spectral reflectance of asteroids," *Bulletin of the AAS*, Vol. **53**, Issue 7.

Yatsu, Y. et al. 2019, "6U CubeSat for ultraviolet time-domain astronomy," 33rd Annual AIAA/USU Conference on Small Satellites, SSC19-WKVII-08.